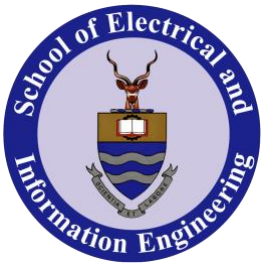

School of Electrical and Information Engineering

University of the Witwatersrand

Private Bag 3, 2050, Johannesburg, South Africa

Overall vehicle stability for a non-linear multi-varied suspension aimed at disturbance attenuation, energy efficiency and robustness
September 2020

Student: Lihle Immaculate Nkomo
549809@students.wits.ac.za

Supervisor: Dr. Otis Nyandoro

A dissertation submitted to the Faculty of Engineering and the Built Environment, University of the Witwatersrand, Johannesburg, in fulfilment of the requirements for the degree of Master of Science in Engineering.

Declaration

I declare that this dissertation is my own, unaided work, except where otherwise acknowledged. It is being submitted for the degree of Master of Science in Engineering to the University of the Witwatersrand, Johannesburg. It has not been submitted before for any degree or examination to any other university.

Signed this 28 day of September 2020

Lihle Immaculate Nkomo

Abstract

This dissertation presents the design and implementation of a half-car active suspension system with a pre-disturbance detection algorithm that aims at reducing driver experienced vibrations. The first research contribution is slack-based state constrained optimal control which is used to address the limitations of the penalty function methodology. The performance index is designed so that it optimises for the control actuation energy and the driver's ride comfort. The optimal control results demonstrate displacement attenuation of 97.5 % and acceleration of up to 80 %, which is practically feasible if high performance sensors and actuators are utilised to enable a fast and efficient response of the active suspension system. The second research contribution is derived from extending the slack variable state constrained optimal control to the linearised half-car suspension system by addressing the limitations of input output feedback linearisation as the state transformation often results in hidden state dynamics. The results from the completely linearised controller show a displacement attenuation of up to 81.82 %. The third research contribution is through the application of an adaptive sliding backstepping controller to the constructed test-rig, that ensures robust control on non-smooth road surfaces consisting of white noise. The results from the adaptive sliding backstepping demonstrate improved attenuated displacement and smoother accelerations of up to 71.3 % and 60 % respectively. Although the adaptive sliding backstepping trade-offs disturbance attenuation performance, it demonstrates adaptive properties when tested on rough road surfaces. To achieve overall vehicle stability, the use of these controllers can be integrated to benefit from the targeted performances such as robustness.

To God who created everything ...

Acknowledgements

I would like to thank my family and friends who showed support throughout this research work. I would also like to thank God for giving me the strength to seek this knowledge. Also, I would like to thank my research supervisor for providing guidance throughout this research work.

Contents

List of Figures

List of Tables

List of Symbols

The principal symbols used in this thesis are summarised below,

M_{sf}	front spring mass
M_{sr}	rear spring mass
X_{sf}	front spring mass displacement
$\dot{X}_{sf}$	front spring mass velocity
$\dot{X}_{sr}$	rear spring mass velocity
X_{uf}	front unsprung mass displacement
$\dot{X}_{uf}$	front unsprung mass velocity
U_r	rear control actuation input
U_f	front control actuation input
v	input of the transformed system
B_f	front linear damping coefficient
B_{fnl}	front non-linear damping coefficient
B_r	rear linear damping coefficient
B_{rnl}	rear non-linear damping coefficient
K_f	front spring coefficient
K_{fnl}	front non-linear spring coefficient
K_r	rear linear spring coefficient
K_{rnl}	rear non-linear spring coefficient
K_{tr}	rear tire stiffness
K_{tf}	front tire stiffness
y	suspension system output
u	suspension system input
n	number of original non-linear states
r	relative degree of transformed system
ψ	controllable new states
ϕ	hidden states
$IOFBL$	Input Output Feedback Linearisation
$ISFBL$	Input State Feedback Linearisation

Chapter 1

Introduction

An Active Vehicle Suspension System (AVSS) is a critical component of automotives as it aims to improve the passenger's road comfort and the vehicle's road handling capabilities [1]. This work focuses on the design and construction of the half-car suspension system test-bed and developing controller techniques that deal with non-linearities, energy efficiency and robustness properties. Therefore the purpose of this document is to present the design and application of high performance controllers that address vehicle stability for non-linear multi-varied suspension systems with non-parametric uncertainties.

1.1 Introduction to suspension systems

An AVSS consists of a physical suspension system comprising of springs, dampers, and actuators, which are assembled between the vehicle's wheels and body. This design arrangement is such that the vibrations resulting from road surface irregularities do not perturbate to the vehicle's body. In AVSS, the design of a high performance controller is significant to the performance of the system as the controller receives mass displacement signals from the mechanical system and computes the required actuation force to ensure the desired performance measure. The challenge with these systems is the response time as the control signal only receives the road disturbance as it is being experienced by the vehicle. This does not give the actuation mechanism adequate response time to ensure maximum efficiency of the active suspension system. If the future information of the disturbance is available, then the performance of the transient responses can be greatly improved [1]. Suspension systems are used for eliminating disturbance actuation in vehicular bodies by counteracting these road disturbances.

Suspension system types vary, depending on the injected actuation energy. Depending on the actuation energy a suspension can either be passive, semi-active or active. Passive systems do not have a controller computed input for actuation [2], whereas active systems have active actuators that control the energy in the system [3].

1.2 Performance criteria

The performance of suspension systems is analysed through indicators such as ride comfort, vehicle road handling capabilities, shock absorption, vehicular body movement and dynamics [4]. The suspension system performance indicators have trade-offs, therefore the control design can only optimise for the indicators chosen by the designer. Research work has been conducted to improve on the elimination of vibrations induced by road surface irregularities, aerodynamics forces, engine vibration, and irregular tire structure [5]. In addition to suspension systems, control researchers have also gained interest in other active chassis systems like braking mechanism, vehicle steering and propulsion systems [6, 7]. Yet suspension systems have been extensively studied, integrated vehicle dynamic performance brings new challenges for AVSS control which is relevant in the new age of self-driving vehicles as in addition to their basic functionality. Suspension systems can be incorporated in the Integrated Vehicle Dynamic System and this makes it significant to analyse practical challenges within the suspension system.

1.3 Structure

This dissertation is structured as follows: Chapter 2 presents the literature review on vehicle suspension systems, suspension system test-rigs, review of linear and non-linear control techniques. Chapter 3 discusses the research details for the active vehicle control for the multi-varied, non-linear half-car suspension system. Chapter 4 shows the constructed mechanical test rig and its system dynamics model. Chapters 5, 6 and 7 show the limitations and solutions to traditional control techniques such as state constrained optimal control on non-linear systems, feedback linearisation for constrained optimal control and backstepping controller designs. Chapter 8 shows the comparison and critique of the application and performance of the different controllers and the conclusion.

1.4 Publications of this work

The outputs of this research work have been published $(1, 2, 3)$ and accepted by (4):

1. 20^{th} International Federation of Automatic Control world congress in Toulouse France, (IFAC2017) detailed: Nkomo, L.I., Nyandoro, O.T. and Dove, A., 2017. Comparison of backstepping and sliding mode control techiniques for a high performance active vehicle suspension System. IFAC-PapersOnLine, 50(1), pp.12604-12610.

2. Conference Control Africa in South Africa (CCA2017) detailed: Nkomo, L.I., Dove, A., Ngwako, M.T. and Nyandoro, O.T., 2017. Heaviside based optimal control for ride comfort and actuation energy optimisation in half-car suspension systems. IFAC-PapersOnLine, 50(2), pp.259-264.

3. 18^{th} IFAC Symposium on Control, Optimisation and Automation in Mining, Minerals and Metal Processing (MMM2019) detailed: Nkomo, L.I. and Nyandoro, O.T., 2019. Conditions for complete feedback lin- earisation on active suspension systems for mining trucks. IFAC-PapersOnLine, 52(14), pp.189-194.

4. Acceptance for a Backstepping Control of Nonlinear Dynamical Systems chapter in an Elsevier book entitled: A novel design approach to Adaptive Sliding Backstepping control techniques for a high performance active vehicle suspension system.

Chapter 2

Literature review

This chapter discusses the different applications of suspension systems, suspension test-beds, performance parameters, braking and challenges in suspension control design systems. Controller designs have limitations when addressing challenges with practical application of AVSS such as addressing non-linearities, Multiple Input Multiple Output (MIMO) systems and robustness. The literature review on controller designs focuses on major control techniques applied in this research work: state constrained optimal control, completely linearised optimal control through feedback linearisation, backstepping and sliding mode control techniques. The literature review aims to contextualise and to analyse the existing solutions and their limitations within this research field.

2.1 Application of suspension systems

Suspension systems are used in automotives such as cars, trains, planes and motor bikes. They are used for mitigating road disturbance impact to ensure ride comfort for the driver and the passengers. Suspension systems are utilised for vertical displacement control to eliminate vibrations that can pose harm to both the passenger and the lifespan of the vehicles. These systems have been used in other applications outside of automotive industry such as vibration control of motors and generators. [8].

Vehicles require an active suspension system since passive systems do not have a controller input to the actuator that attempts to isolate the sprung load from the vehicle tyres. The applied actuation force aims at reducing the vehicles' vertical displacement and acceleration. The limitations to this reduction are characterized

by the physical constraints in the constructed vehicle suspension system. In [9], a semi-active train suspension vibration control using magnetorheological dampers is implemented. This system consists of a nine degree-of-freedom model which comprises the car's body, two trucks and four wheels. This model considers the vertical pitch and roll motions of the body. A Linear Quadratic Gaussian (LQG) controller is used to analyse the effectiveness of the controlled dampers on the railway system, whereby the state variables are estimated with a Kalman estimator. The simulation results indicated that the train suspension system with semi-active control is feasible and effective [9], but to improve these results the use of a full active suspension is recommended.

2.2 Energy efficiency in suspension systems

Various approaches can be implemented to satisfy the constraint of energy efficiency within mechanical systems. Energy regenerative techniques can be employed, such as using an electromagnetic damper to consume active vibration energy which is referred to as active vibration control and is widely applied in the control industry [10]. Electromagnetic dampers can also be used as an active suspension as it is controlled to obtain desired vertical car body travel while regenerating energy [11]. [12] proposes a zero-energy self-powered active suspension for active energy absorption instead of using an electric generator or a motor. These techniques are aimed at mechanically regenerating energy that is typically dissipated in shock absorbers [13], this energy is then used to re-power the active suspension actuator [14].

2.3 Suspension system test-beds

In automotive control engineering, suspension system test-beds and high performance controllers are frequently used for analysing performance parameters such as ride comfort, road handling and suspension deflection concepts [15], [16], [17]. The frequently used model and constructed active suspension system test-bed is a quarter-car as it is simpler to construct and model when compared to a half-car or full-car test-bed [18]. This is due to quarter-car models only considering vertical motion dynamics without incorporating pitch, roll or yaw dynamics. Although half-car test-beds are more costly and time-consuming to construct they are used to achieve a more practical and accurate model for testing implemented controllers. Compared

to quarter cars, half-car models have higher degrees of freedom and also represent the pitch motion dynamics of the vehicle [19].

In [20], a quarter-car test bed is constructed with the road disturbance modelled as a hydraulic power source and the actuation force produced by an electric motor. The electric motors convert electrical energy to linear mechanical motion that ensures that the car's body experiences reduced displacement [20]. The use of controllers in suspension system test-rigs is such that instructions are sent to the actuators on the force requirements to achieve improved ride comfort. In [3], a quarter car suspension design test-bed is used to analyse passenger discomfort, suspension deflection and varying tyre load for the semi-active and fully-active system using a linear optimal controller. Although the analysed semi-active system derives control laws that are formulated from the fully active systems, it has the ability of dissipating energy, so that the semi-active model turns off the case where the active system would be supplying energy [3].

2.4 Performance parameters

Specifically with cars and other road-based vehicles such as motor bikes and trucks, control techniques have been developed to focus on ride comfort and road handling capabilities [21]. As the vehicle encounters a disturbance that leads to vibrations and vehicle discomfort, the suspension system attempts to minimise the impact of these vibrations onto the vehicle. While monitoring the displacement of the vehicle's body, it is important to also track the other performance indicators such as road handling capabilities and the rattle space. The rattle space, which is the maximum allowable suspension travel is the key design constraints for the development of an AVSS. Other key constraints are imposed by the systems' robustness and road-handling capabilities [22].

The suspension system design should consider traction on various road surfaces such as snow, tar, concrete, mud, dirt and gravel. The different types of road inputs can be classified into shock or vibration. Heavy vehicles such as a trucks have a high load variation by a wide margin when comparing an empty to a full load. The actuation effort or energy required to maintain a minimal vertical movement will vary depending on the load and the road disturbance. With a shock disturbance, the fully active suspension system will significantly consume power that can be optimised by an optimisation technique [12].

2.5 Braking and cornering

The advancement in suspension system research has led to suspension systems being integrated with other vehicle systems such as braking and cornering systems. An Anti-lock Braking System (ABS) aims to enhance vehicle steerability and increase braking force while avoiding skidding [23]. This is achieved through monitoring the difference between the wheel speed, braking pressure and distance. In ABS, weight is the normal vertical reaction with vertical motion and dynamics. In recent research projects, the actuation of the AVSS is analysed together with the ABS in order to enhance the normal reaction thereby increasing the braking forces and improving the braking system [23]. Similar to ABS, traction control also applies during vehicle take-off acceleration which is the reverse of braking resulting in longitudinal motion.

Cornering traction results in transversal motion; it is a combination of the braking and suspension system control [24]. In [25], an analysis of an electric vehicle drive indicated that the torque coordinated control can improve the cornering ability limit, the manoeuvrability and the balance of the vehicle. The study utilised a Neural Network Proportional Integral Derivative (NNPID) control strategy on a seven degrees-of-freedom model. Simulations conducted for the step, steady-state cornering and the sinusoidal input yielded positive results [25].

2.6 Challenges in suspension control design systems

Regarding the application of vehicle body stability, most vehicles have AVSS per wheel where the actuation is integrated for the full vehicle. AVSS research has not only focused on driver comfort but has also joined the fray of automatic and particularly integrated vehicle control. An integrated system will typically have numerous performance criteria and multiple inputs and outputs. The control design for such systems can be challenging as it is complex. Additionally once a controller is designed, wear and tear will affect the parameters of the system thereby resulting in stochastic elements. Therefore integrated dynamic performance measure becomes a necessity in vehicle dynamics control.

2.6.1 Robustness within AVSS

Over and above ABS and cornering, the system is supposed to result in smooth control for complicated road conditions. In cases where the vehicle swerves, resulting in the set of wheels being exposed to different road surfaces, the suspension system is required to balance the vehicle stability. Other road conditions are acceleration and turning or the combination of braking and turning. Another case can be if one of the wheels goes over a rock, the suspension system has to balance the level of the car. To have one AVSS to deal with all the integration of these vehicle dynamics and controls implies an extremely robust AVSS. Even then the limits of robustness, are likely to be exceeded. Additionally the sensitivity of the integrated approach to suspension system parameter variations will change the control design and dynamics. Robustness control techniques are necessary to deal with uncertainties due to unknown variations however robustness has limits [22]. Additionally, robustness in linear systems is relatively easy whereas robustness in non-linear systems can be challenging. Control techniques are further implemented on a digital platform introducing discrete analysis on the integrated components.

2.6.2 Multiple-Input Multiple-Output (MIMO) AVSS

Suspension system models for half-car and full-car designs have multiple inputs as each wheel typically has its own suspension system, therefore the control design has to incorporate all the inputs to the system. [26] presents the design of a fuzzy feedback linearisation control of the non-linear MIMO system. The controller is designed to track and decouple the disturbance based on the fuzzy logic control. As this is a full vehicle system there are four system inputs, which makes designing for MIMO systems a challenge and a tedious exercise.

2.6.3 Stochastic variation within AVSS

The integrity of the AVSS relies on the accuracy of the measurement components within the system. Therefore conditions such as wear and tear lead to stochastic variations in the system components. [27] conducted a study on multi-objective stochastic optimisation of the road vehicle's suspension system. Measurement systems are based on bandwidth and time-based performance, hence due to wear and tear the readings will come with a greater standard deviation and enhanced stochastic element in the system performance.

2.6.4 Non-linearities within AVSS

Suspension system components such as springs and dampers have non-linear elements. Further integration of these systems to varying parameter components such as sensors and actuators introduces high non-linear model dynamics. Therefore in controller designs, the employed control techniques should handle non-linearities or a linearisation technique should be applied to ensure an accurate model of the linearised physical system.

2.7 Control Methods

Control methods are based on the fundamentals of control techniques such as optimal, classical, quantitative feedback and robust control aimed at improving system performance. As discussed, suspension system components such as springs and dampers have non-linear components and uncertainties, therefore the considered controllers should be capable of handling systems with non-linearities, parametric uncertainties and multi-varied. Applications and limitations of input output FBL, optimal control and robust control techniques such as backstepping with sliding mode and adaptive capabilities are the main controllers discussed in this section.

2.7.1 Feedback linearisation

The application of a Feedback linearisation technique is based on the Lie derivative or the differentiation method. Both methods are based on differentiating the output (y) until the input (u) appears. The principles of IOFBL techniques are based on cancelling the system's non-linearities so that the resulting closed loop dynamics are linear [28], [29]. This linearisation technique can be applied to both Single Input Single Output (SISO) and MIMO affine systems, therefore can be applied to quarter, half and full-car vehicle suspension systems. The application of IOFBL technique typically results in a transformed system with reduced number of states (r) when compared to the original system (n). This is due to the linearisation technique resulting in external and internal (hidden) states, $(n - r)$. The developed control law is designed to control the external states which resulted from the linearisation process. It is important for the control designer to ensure that the internal states are stable. Therefore in order to apply the linear controller to the linearised system, stability analysis should be performed on the hidden states to ensure that they are

bounded. If these hidden states are unstable, there are limitations on the application of IOFBL on non-minimum phase systems.

Stability verification of the transformed system is achieved through zero-dynamics analysis. The zero dynamics result from the internal states of the system when the input (u_0) is such that the output stays zero $y_{(u_0)} = 0$, [30]. Most literature sources compute zero dynamics using Lyapunov-based analysis. In addition to Lyapunov-based computations, recent work shows that zero dynamics can be computed through fibre bundle analysis of the state space manifold region [30]. With this approach, a link is established on the state space manifold, enabling the lifting of the linearised dynamics from the base to the total space. The zero dynamics are the computed by obtaining the difference between the original and the resulting lifted linear dynamics. These are modelled so that they represent the vertical motion of the system along the fibres whereas the linearised dynamics represent the motion of the system within fibres. Unstable internal dynamics imply a non-minimum phase system.

Once a non-linear system has been linearised, a linear controller can be applied to the linearised model by controllers such as negative state feedback. In [31], using IOFBL techniques for controlling a non-linear non-minimal phase system, is achieved through two methods; neglecting internal dynamics and stabilisation of the internal dynamics. The first approach on neglecting internal dynamics, is based on an approximate IOFBL method. The vanishing perturbation theory is used to address the neglected part which is modelled as perturbation. The results from this method are accurate for very small values of the perturbation, otherwise the internal dynamics cannot be destroyed therefore requiring stabilisation, which is achieved through predictive control. The developed solution results in global stability of the closed form and does not require any precondition on the stability of the open-loop system, [31]. [32], applies input state FBL to a non-linear Anti-lock Braking System while addressing stability challenges. Simulation results on the quarter-car demonstrate the validity of the approach and the solution highlights the disadvantages of feedback linearisation as it results in internal stability challenges where there are hidden states. Therefore, it circumvents these challenges with an output to state transformation that ensures no hidden states.

2.7.2 Negative state feedback

The use of a negative state feedback controller design is commonly utilised as it is easy to apply since it is based on state space modelling. The state feedback

controller can be designed incorporating proportional integral derivative controller characteristics where each value in the state gain matrix has K_p, K_d and K_i effects. For a proportional controller the values of K_d and K_i are zero. The pole placement method is used to obtain the gain matrix. Pole placement can be mathematically achieved by using the direct comparison method that compares the poles of the open loop system and the poles of the desired system to obtain the required gain matrix [33]. The controller assumes the availability of all the states. In practice it is challenging to obtain these states in a short period of time therefore the full state observer can be used to obtain the states [34]. In the event that some of the states are not available, a partial observer can be used to estimate these states.

2.7.3 Optimal control

Within active suspension system optimal controller design, a linear quadratic form is employed to analyse for the performance indicators such as driver ride comfort, design constraints and road-handling requirements [35],[36]. An optimal control system with a Linear Quadratic Regulator (LQR) for an active suspension system with a hydraulic actuator is proposed in [37], [38]. In [39], the LQR and Composite Nonlinear Feedback (CNF) are also used to design active suspension system controllers. The LQR controller is optimized for the weighting matrices in the performance index while the CNF comprises a linear control law that minimises the damping ratio. The CNF achieves a fast rise time and a feedback control with a high damping ratio that eliminates the system's overshoots. The LQR is based on the linear quadratic optimal control theory and the feedback control law [40].

Although these controllers are advanced and can achieve good performance characteristics for the suspension system, they also have shortfalls as their system models are developed based on optimal control theory that requires solving the Ricatti equation associated with the suspension system, which can be tedious to implement. The LQR also assumes linear systems, which is hardly the case in industries therefore during control design, robustness against parameter variations has to be considered [40]. In [20], energy efficiency analysis is achieved through the design of an AVSS which is optimised by the modification of a standard controller to allow for varying the motor-required energy. In the case of [41], the energy demands of a motor are analysed and then optimized for, using H_∞ control theory. Another optimal control technique is applied in [42], for known road travel and positive results are achieved for ride comfort and optimal energy usage.

[43] uses a penalty function approach for optimal control. It is used to reformulate the original constrained problem as an unconstrained minimisation problem. The solution uses open loop control input as a function of time such that an objective function is minimised and the constraints are met. It is applied to a container crane model, with an objective to minimise the swing of the container [43]. The solution uses dynamic minimisation method of Snyman that yields efficiency when solving penalty functions. [44] uses an optimal control to solve a chemical system with a small disturbance in the system states and in the control input constraints. It is solved through a cost penalty function approach due to the benefit of convergence of the local optimal solution without the need to obtain the global solution [44].

2.7.4 Backstepping controller

The backstepping controller design technique has the ability to be exploited in satisfying conflicting concepts of driver ride comfort and vehicle suspension travel [15]. This technique is based on the use of linear filters whose input is the displacement of the unsprung mass and the effective bandwidth. The relative displacement between the vehicle's sprung (x_s) and unsprung (x_{us}) mass on the closed loop dynamics is defined as the regulated variable. This control methodology ensures that the closed-loop system has the ability of focusing on different control objectives for different operating ranges [15]. The backstepping controller is formulated based on the Lyapunov control theory therefore stability is achieved as the motion of a stable physical system continuously decreases [45]. In [45], the backstepping control method is used on a non-linear AVSS to optimise between the force transmitted to the driver and the tire road contact for improved car handling. This methodology has no adaptive capabilities, therefore [46] introduces sliding mode and adaptive properties to enhance the robustness performance of the backstepping controller for varying loads and inputs.

2.7.5 Sliding mode controller

To improve robustness in the control of non-linear systems, a sliding mode control technique is applied. It is based on the fundamentals of applying a discontinuous control signal so that the model slides along the cross-section of the system's regular response which results in altered model dynamics. Although this control approach maintains stability and consistent performance [47], its limitations are realised when the knowledge of the bounds of the system uncertainties is required as chattering is

observed. In [48], through applying a disturbance observer, a sliding mode control method is used on an AVSS. It was evident from the results that it achieved ride comfort for different road disturbances. The limitations in this application is that the control technique did not address road-handling capability and the suspension deflection parameters [48]. This limitation can be addressed by introducing a controller with robust capabilities. Sliding mode control is also utilised in [18] for a quarter-car suspension system using simulation and experimental analysis. There is a non-ideal actuator, with a dead-zone and hysteresis, solved by a disturbance observer used together with a sliding mode controller. The results show the attenuated impact of the non-ideal actuator, which is compared to the adaptive tracking control and it demonstrated improved performance with much reduced complexity [18].

2.7.6 Adaptive backstepping controller

Adaptive controllers are useful in handling system parametric and non-parametric uncertainties. Unlike sliding mode controllers, this control method eliminates the need to know system parameter bounds. The principle of an adaptive controller is to achieve robustness while the control model updates during plant operation, based on the measured performance [47]. The integration of adaptive and sliding mode controllers can achieve robustness for varying system conditions. In [46], Adaptive Sliding Backstepping is used on a quad rotor to achieve a controller that does not require prior knowledge of the uncertainty upper bounds. This methodology is applied to strict feedback models, with matched uncertainties. Simulations in [46] show that this control method can produce global asymptotic tracking of the desired trajectory, therefore this methodology can be applied in suspension systems to test for robustness and adaptive properties for uneven road surfaces.

2.7.7 PID controller

The Proportional Integral Derivative controller (PID) is one of the most fundamentally applied control techniques. Its design aims to improve the settling time, rise time overshoots and eliminate the steady state error in control models [49]. Similar to the discussed controllers, PID also operates on the feedback mechanism and achieves the desired response by tuning the proportional gain K_p, integral gain K_i and derivative gain K_d. Tuning these gains results in a system with enhanced time domain characteristics.

In [50], a two-loop, suspension travel PID control system is applied to a four degrees-of-freedom, non-linear, half-car active vehicle suspension system. The two-loop system consists of an inner actuator force control loop based on a PID hydraulic model and an outer PID vehicle suspension travel control loop. The simulation results showed improvements for the active suspension system when compared to the passive system with the same model parameters [50]. The recommendation was to test the control methodology on a physical model so as to analyse its practical limitations.

2.8 Preview Control

The concept of preview control is based on using the knowledge of the displacement of the road surface in front of the vehicle to improve the actuation responsiveness latency [1]. This is achieved by minimising the time required for computations and sending communication signals between the controller and the physical system as shown below in Fig. 2.1. The pre-disturbance detection algorithm utilises sensors to obtain the information about the road ahead.

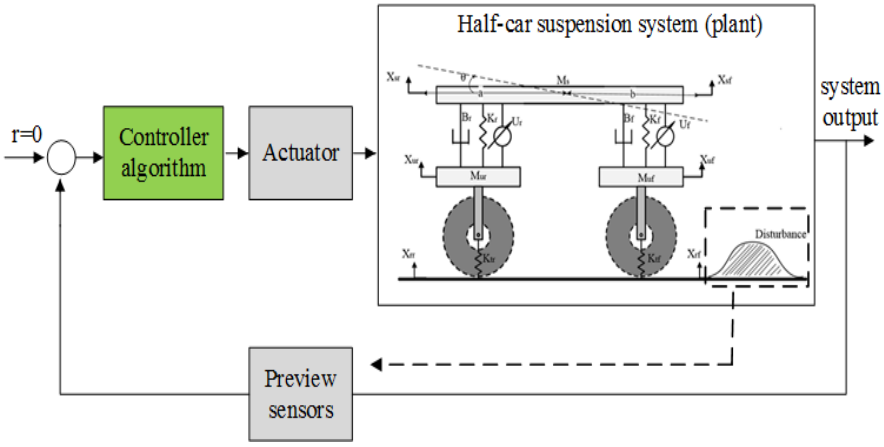

Figure 2.1: Active vehicle suspension system with preview control

In [51], the system comprises of a quarter car with a hydraulic actuator spool voltage as the control input. The preview information is obtained through sensors that measure the range to the ground. These sensors are rigidly attached to the vehicle's body at the same pitch, roll and heave and the vehicle's chassis is assumed to have negligible warp. For a straight path motion the utilisation of only range-finding

sensors is sufficient to obtain preview information, thereby simplifying the sensor requirements and algorithm [51].

In [52], to study ride comfort and road-handling capabilities, a half-car model with the hydro-pneumatic AVSS is designed. Two systems are implemented, of which one is a partial preview which only considers the information from the front suspension to decide the controller input for the rear wheel. The other system is a full preview where the disturbance is pre-detected for both the front and rear systems. In this study the results of the simulation show that although the full preview control method yielded improved system performance, the partial preview control technique was a more cost-effective solution [52].

[1] states that feedback control of mechanical vibrations has been extensively studied, the inclusion of preview control is a relatively new concept. The integration of a pre-disturbance detection algorithm to the AVSS will improve the level of disturbance mitigation and reduce response latency. Active preview control involves three main system components; the model's state variables that describe the dynamics of the system, the preview of the road disturbances used as a feed forward component of the control system and the control system that integrates the information from the preview system to the dynamics of the system ensuring that the performance aimed for is achieved [52], [53].

2.9 Summary of the background review

The literature review shows that significant research has been conducted on the control of suspension systems to achieve ride comfort. Since most research results are based on simulation results, this shows a fairly good indication of the behaviour of the active system but it takes away exploring the experimental and practical analysis of the limitations of the physical systems. Also, most test-rigs are modelled as quarter-cars for simplicity; this also gives an indication of the controller performance but does not address challenges in coupled MIMO systems. Therefore in this work, challenges related to non-linear, multi-varied systems with parametric uncertainties will be addressed.

Chapter 3

Research details

This section discusses the details of this research work: the problem statement, problem context and research gap of the pragmatic applications of active suspension systems. Furthermore it discusses the research contribution, research question and methodology.

3.1 Problem statement

3.1.1 Problem context

The demand for AVSS is increasing due to impact of damping vibrations on the driver's health and the lifespan of the vehicle [1]. While the vehicle encounters road irregularities such as humps and potholes, the driver experiences discomfort. This has influenced control system researchers to develop active suspension systems that aim at mitigating the impact of these road irregularities. As discussed, these systems are aimed at improving and optimising performance measures such as ride quality, road-handling capabilities and suspension deflection [15]. The suspension system separates the wheels (unsprung mass) from the vehicle's body (sprung mass). This ensures that displacements in the wheels due to the unevenness of the road surface do not fully impact the car causing discomforts for those in the vehicle. Unlike AVSS, passive suspension systems only comprise of springs and dampers, they do not have controller-embedded actuators. AVSS consist of an actuator which applies the computed force between the vehicle and the wheel ensuring that the tracked performance measures are optimised.

To improve the vehicle's performance, the use of preview control is introduced to ensure that the control unit computes the desired force to reach the pre-determined performance objectives prior to encountering the disturbance [1]. There are different types of disturbances that a vehicle can encounter, such as road roughness and sinusoidal humps. Hence, it becomes challenging to measure performance for different road types. The complexity of the system's environment leads to different model-based approaches in understanding all inputs influencing disturbances to the vehicle. Suspension systems consist of non-linear parameters such as high performance springs, dampers and actuators. The nature of a suspension system has many uncertainties as the components' dynamics vary [1]. The input to these systems cannot be approximated by single input as these systems have Multiple Input Multiple Output (MIMO) based on the vehicle wheels and can be even more complicated for trucks with increased modelling dynamics. Therefore active suspension system analysis must be compatible to multi-varied systems. The main focus for this research is to address challenges that come with the practical application of vehicle suspension systems, namely:

1. *Non-linearities:* A lot of suspension system models approximate the model to be linear [54], [55], this work will address the non-linearities within the half-car suspension system modelling such as springs and dampers modelled by the linear and non-linear component (nl), [18]:

$$\begin{aligned} Spring: \quad & F_s = kx + k_{nl}x^2 \\ Damper: \quad & F_d = b\dot{x} + b_{nl}\dot{x}^2 \end{aligned} \tag{3.1}$$

2. *Multi-varied coupled systems:* Limitations of strong coupled multi-varied systems when applying control techniques by considering system and control partitioning

3. *Robustness:* Addressing robustness challenges for systems with non-parametric uncertainties and road input variations

3.1.2 Research gap

A lot of research conducted on AVSS, assumes that the suspension system model is linear [54], [55], [56]. This assumption introduces a limitation in terms of modelling parameterisation of the system's components such as springs and dampers since they consist of non-linear components. Additionally, in a lot of literature AVSS are modelled as single input single output systems which has proven to be an

insufficient model as it does not consider other dynamics such as pitch dynamics [18], [57], [58]. Research on suspension system performance measurement focuses on road comfort, road handling and stability, however most developed techniques are not tested on different road surfaces to verify the performance of the controller. The challenge is measuring the size and frequency for the road disturbance such as white noise. Also the practical application of these control systems introduces components with inaccuracies such as sensors, motors and actuators that necessitate the study of robustness-oriented vehicle dynamics [1]. The performance of suspension systems is bounded by system constraints for both the states and the control input. This research work will focus on state constrained optimal control for the half-car suspension system. Different approaches to state constrained optimal control should be explored to analyse the trade-offs in terms of practical application, computational costs and system performance.

Linearisation will enable the non-linear system to have linear control which will result in less computational costs although it could potentially compromise the system performance [35]. In IOFBL, the use of output (y) can yield hidden state dynamics. The choice of these dynamics is complex and furthermore the proof for stability of these internal states is complex, therefore it is necessary to find a methodology that ensures that the result does not yield any hidden states. To ensure robustness that caters for the system's uncertainties an extension to backstepping has to be applied to investigate system performance for varying road disturbances. The application of these controllers is aimed at improving the AVSS performance measurement quantified through road comfort, handling and stability [28]. The research gaps addressed in this research work are to address the issues associated with implementing traditional control techniques such as: feedback linearisation, optimal control and backstepping, to a non-linear multi-varied suspension system with uncertainties. In particular to address typical driving conditions such as braking, road roughness, humps and potholes. The focus is on the analysis of challenges within the practical control for the constructed half-car suspension system, involving:

1. *State constrained optimal control:* Practical systems operate within the physical limitations of the system. Conducting energy analysis in half-car suspension systems through the use of state constrained optimal control will ensure that the suspension system constraints are incorporated in the Hamiltonian computation. Analysis is conducted on the displacement attenuation, performance index and control input signals. This involves the analysis of the complicated Hamiltonian for a half-car suspension system, initial conditions for costates and boundary value problem analysis.

2. *State constrained optimal control on complete linearised system:* Complete feedback linearisation will enable the application for state constrained optimal control without the need for considering hidden state constraints. Therefore the need to motivate for a solution that yields no hidden states by highlighting the complexities of hidden state computations, Jacobian invertibility analysis and hidden state analysis through zero dynamics analysis.

3. *Backstepping control:* To achieve robustness, the state constraint is modelled as the regulating variable in the application of a backstepping controller. It has the capability to update while the plant is in operation for a half-car suspension system for unknown boundaries and systems with high uncertainties and load variations.

3.2 Research Contributions

This research aims to develop a high performance controller for an active half-car suspension system that aims at improving driver comfort through road disturbance mitigation. To achieve this, an optimised-based performance measure for a non-linear multi-varied vehicle suspension with non-parametric uncertainties is modelled, designed and tested on the half-car suspension model. This work addresses the challenges and limitations discussed in the research gaps within the application of state constrained optimal control, state feedback control through feedback linearisation and backstepping control. Therefore the main contributions of this work are:

3.2.1 State constrained optimal control

In traditional optimal control formulation, the resulting Hamiltonian for MIMO systems is complicated and results in singular control. The initial conditions for co-states and the boundary value problem are not always helpful in optimal control and the Hamiltonian solution. Moreover, since suspension systems have stochastic elements, the above are more complicated. The model of the suspension rattle space for both the front and rear suspension system is considered by modelling as the system's constraints. Elements of this contribution have been presented and published in the Control Conference Africa [59].

CONTRIBUTION 1: To investigate state constrained optimal control on the half-car suspension system by addressing the limitations of penalty function-based methodology through the use of slack variable methodology to achieve energy efficiency, through:

1. Identification of the limitations in the simulation of the penalty function state constrained optimal control on the half-car suspension due to the application of the switching functions in modelling packages.
2. Modelling the inequality constraint through the definition of slack-based constraint model to ensure that the front and rear optimal control is operating within the half-car suspension travel limits.
3. Computing the Hamiltonian, co-states, boundary conditions and the optimal controller on the half-car suspension system. Then conducting an analysis of the controller performance on the front and rear suspension system focusing on the displacement, acceleration, control input, cost function for both $mass = m$ and $mass = 2m$ for energy efficiency analysis.

3.2.2 Optimal control of completely linearised systems

Research has proven that the application of IOFBL on suspension systems can result in the introduction of hidden states. In the case of a quarter suspension system, the four original states which are sprung mass displacement, sprung mass velocity, unsprung mass displacement and unsprung mass velocity can result in two transformed linear states and two hidden states. This will require a solution for the hidden states stability, which involves complex computations of a zero dynamics analysis. This leads to complexities when conducting state constrained analysis therefore this contribution aims at finding the conditions for complete linearisation. Elements of this contribution have been published and presented in the Mining, Mineral and Metal Processing (MMM2019) Conference [60].

CONTRIBUTION 2: *To extend the application of slack variable state constrained optimal control to the completely feedback linearised half-car suspension system at the point of IOFBL and ISFBL equivalency, to enable state transformation without hidden constraints, through:*

1. Demonstrating the complexities of applying IOFBL in MIMO systems as it can result in control and system partitioning, complex computation of hidden states and hidden state stability analysis, for the half-car suspension system

2. Applying-slack based state constrained optimal control on the complete feedback linearised half-car suspension system.

3.2.3 Backstepping

Robust multi-varied systems consider the sensitivity of un-modelled dynamics and parameter variation in a system. Therefore it necessitates a backstepping control technique. Elements of this contribution have been published and presented in the IFAC2017 conference [61].

CONTRIBUTION 3: Applying an Adaptive Sliding Backstepping technique to a half-car suspension so as to test for robustness and adaptive properties on the constructed test-rig, through:

1. Application of backstepping control-based candidate Lyapunov function for stabilisation of the constructed half-car suspension model.
2. Application of the Adaptive Sliding backstepping on the half-car suspension system to enhance robustness within the given boundaries.
3. Comparison of the performance of the backstepping, adaptive backstepping to a general PID controller.

3.3 Research objectives and questions

The aim of this research is to establish the best performing controller between three main controllers applied to the half-car suspension system. The research work focuses on the limitations of IOFBL and the application of slack-based optimal control aiming on energy efficiency and adaptive sliding backstepping aimed at robustness control on the constructed half-car suspension system. Therefore the objective of conducting this research is to answer the following questions within suspension systems:

How does the performance of the state constrained optimal control compare for the non-linear and completely linearised system when aimed at energy efficiency and how do these results compare to the adaptive sliding backstepping controller aimed at robustness? The research will answer the following sub-questions:

- Can a cost-effective and rigid half-car suspension test-rig be constructed for passive and active vehicle performance analysis for varying road disturbances?
- How much optimisation of the ride quality and energy efficiency can be achieved by the slack variable based optimal control for the half-car suspension considering the front and rear suspension travel constraints?
- Can conditions for complete linearisation be met to enable state constrained slack-based optimal control analysis on the transformed linear system?
- How does the performance of a backstepping controller compare to the adaptive sliding backstepping on a half-car suspension system with un-modelled dynamics and varying input signal?

3.4 Research approach

The development of a high performance AVSS requires the construction of a mechanical test rig and the implementation of advanced controllers that demonstrate reduced disturbance impact. The development of the preview control system for the AVSS involves non-linear suspension system identification and modelling. This will also include a feed forward control technique that tracks the road terrain and counteracts the forces due to the road disturbance. Also, a non-linear system control technique design for a feedback control system that aims at mitigating damping and the vibrations caused by road surface irregularities. The constructed mechanical test-rig will consist of actuation motors for disturbance mitigation. The constructed system utilises linear displacement sensors to detect the road disturbance. The research analyses three control techniques, namely: slack variable-based state constrained optimal control, complete linearisation state constrained optimal control and adaptive sliding backstepping on the half-car suspension model.

3.5 Research methodology

The research methodology is to conduct a literature review and to analyse the existing solutions to the practical application of active suspension systems and its limitations. Once these limitations have been established, the physical model will be constructed to meet the requirements of chassis rigidity and cost-effectiveness. Parameter identification for the physical model is implemented and the mathematical

model of the constructed model is derived. The proposed controllers will be applied to the developed half-car suspension model and their performance will be analysed to compare and quantify the performances variances and trade-offs for different road surfaces.

3.6 Research success criteria

The success criteria is based on the research results demonstrating the research objectives and answering the research questions posed. The development and construction of the half-car model is significant so as to enable the testing of the performance of the half-car mechanical test-rig. This work will be deemed a success by the researcher if the research work analyses the applied controllers on the half-car model to demonstrate the possibility of overall vehicle stability achieved by each controller considering the impact of non-linearities where significant stochastic elements exist. Furthermore, the research aimed to achieve the following:

1. A cost-effective and rigid half-car mechanical test rig has been designed and constructed.
2. Implementation and analysis of the three controllers on the multi-varied non-linear suspension model.
3. Integration of the developed controllers and the constructed suspension system for testing purposes and the comparison of the performance of these active suspension models.

3.7 Control system design overview

AVSS are used to eliminate disturbance actuation in mechanical bodies in conditions where vehicles experience road perturbations. The developed solution should be cost-effective and achieve improved driver comfort for different road disturbances. The designed controllers should be capable of handling a highly non-linear suspension system, varying system conditions and uncertainties. The solution comprises a cost-effective and rigid half-car mechanical suspension system and three main controllers to be applied to the half-car suspension model to test for their performance and compare their trade-offs. This section provides a detailed overview on how the control techniques are applied to the half-car suspension system to achieve overall

stability that aims to address challenges that come with practical application of control methodologies such as energy efficiency, non-linearities and robustness.

3.7.1 Solution overview

This research addresses these practical control challenges by developing a control system for the state constrained half-car suspension system that focuses on addressing energy efficiency techniques for the non-linear and the completely feedback linearised system. The application of these control techniques is then extended to adaptive sliding back-stepping which models the state constraint as a regulating variable, and its computations are based on the Lyapunov theorem. Therefore these control techniques target different practical performance areas of the suspension system such as energy optimisation, non-linearities and system uncertainties. The controllers are designed to work together on the half-car system and contribute their unique performance such as optimal energy control, robustness and stability to achieve overall ride comfort.

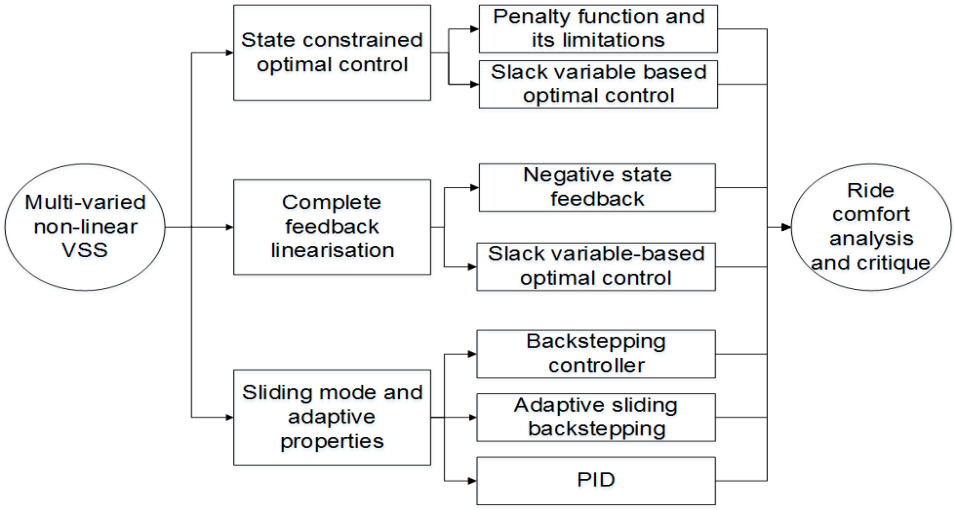

Figure 3.1: Overview of control techniques applied to achieve overall stability

Part 1: State constrained optimal control on the half-car

State constrained optimal control is applied to the half-car suspension model to analyse its energy efficiency performance. This technique is applied so that the front and rear suspension system constraints are modelled as system states. This control application involves the computation of the Hamiltonian, co-states and the optimality condition for the half-car model. Analysis is conducted on the performance of the front and rear suspension systems, focusing on testing the results for the displacement, acceleration, control input, cost function and the performance index for both $mass = m$ and $mass = 2m$. The limitations of the penalty function methodology are addressed by the use of slack variable methodology.

This analysis will address the **first contribution:** *CONTRIBUTION 1: To investigate state constrained optimal control on the half-car suspension system by addressing the limitations of penalty function-based methodology through the use of slack variable methodology to achieve energy efficiency.*

Part 2: Slack-based optimal control on the linearised system

The constructed half-car mechanical model has been represented by a non-linear system. This system will be linearised through Input Output Feedback Linearisation (IOFBL). The linearisation will explore hidden states analysis through zero dynamics computations. The main focus is to address the complexities within applying IOFBL as it results in hidden states dynamics to enable the handling of state constrained optimal control. Then establishing the conditions for the output to ensure that there are no hidden states. These conditions are obtained through adopting ISFBL to IOFBL by proving the case of equivalence between IOFBL and ISFBL through Lie-based proofs for feedback linearisation methodologies on the half-car suspension system. The linearised system is passed into a negative state feedback and the linear slack-based optimal controllers.

This analysis will address the **second contribution:** *To extend the application of slack variable state constrained optimal control to the completely feedback linearised half-car suspension system at the point of IOFBL and ISFBL equivalency, to enable state constraints transformation without hidden constraints.*

Part 3: Adaptive sliding backstepping on the half-car

To address robustness and adaptive properties in the half-car suspension system the backstepping and adaptive sliding backstepping is applied to the plant to analyse the robustness performance. The focus is to test for robustness in an environment with uncertainties. The backstepping controller analysis is based on Lyapunov control. To enhance the performance of the backstepping controller, sliding mode and adaptive control is introduced for a more robust solution. Therefore the adaptive sliding backstepping is applied to the constructed half-car suspension model, tested and compared to the other controllers such as a PID controller.

This analysis will address the **third contribution:** *Applying an Adaptive Sliding Backstepping technique to a half-car suspension so as to test for robustness and adaptive properties on the constructed test-rig.*

3.8 Conclusion

The research approach is to develop three controllers and apply them to the constructed suspension system model. Chapters 5, 6 and 7 show the formulation, application and proposed contributions for each of the focus control areas for the active suspension system. The developed controllers are then applied onto simulation and test-rig suspension system models through the use of Simulink and Dspace programming environments. The results from each system are analysed through comparisons with the passive systems and other implemented controllers. The analysis also compares performance for different disturbances to ensure consistence in the designed controller performance. Conglomerating the proposed control techniques would achieve a robust, energy efficient non-linear multi-varied solution as shown in Fig. 3.1. This section discussed the controller techniques whose limitations will be explored in this research work, also highlighting the contributions of the research to extend traditional optimal control, input output feedback linearisation and backstepping. A collaboration of these solutions on the constructed test-rig will result in a multi-varied optimised suspension system.

Chapter 4

System characterisation

4.1 Introduction

In order to construct a test-rig that is robust and cost-effective, system identification, modelling and parameter identification are significant parts of the design. Therefore this section focuses on system dynamics of a half-car model. The dynamics are represented by a mathematical model showing the forces acting on the suspension system. The model also details the discussion of parameterisation and functionalities of the constructed test-rig.

4.2 System description

The physical system of an AVSS consists of force generating components such as actuators, springs and dampers as shown in Fig. 4.1 for the quarter car and Fig. 4.2 for the half-car. The aforementioned springs and dampers consist of non-linear components that generate forces acting on the vehicle's body and wheels producing displacement variations. Force distribution on the quarter and the half car is crucial to the succession modelling of these systems. Hence, a unique distinction modelling between the two systems should be understood. The mathematical modelling of a quarter car assumes that the driver is seating directly on top of the wheel whereas the half-car model assumes that the vehicle driver is seating at the centre of the two wheels. A generic quarter car representative model, its dynamics and the resulting forces are shown in Fig. 4.1(a) and Fig. 4.1(b), where the signs indicate the direction of the force from the spring, damper and actuation on the mass.

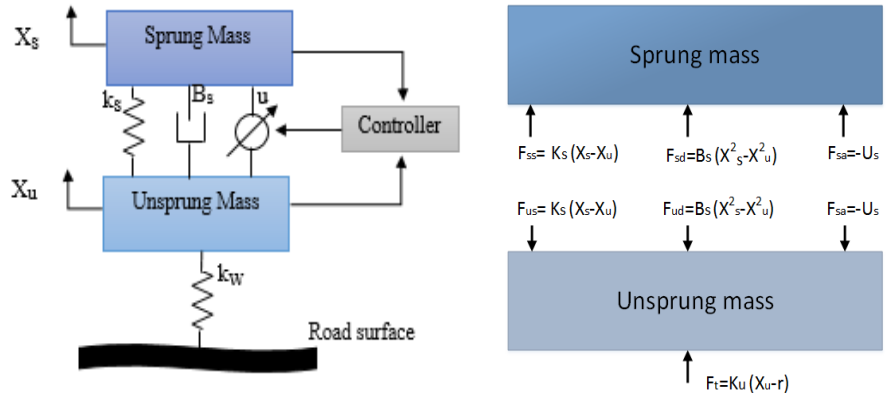

(a) Quarter-car suspension model. (b) Forces acting on the quarter-car.

Figure 4.1: A generic quarter car model

4.3 Physical system modelling

This section focuses on the mathematical model of the constructed half-car test-rig. The link between the front and rear system leads to pitch dynamics, which are not considered for quarter-car suspension systems. Fig. 4.2 shows the dynamics of a half-car.

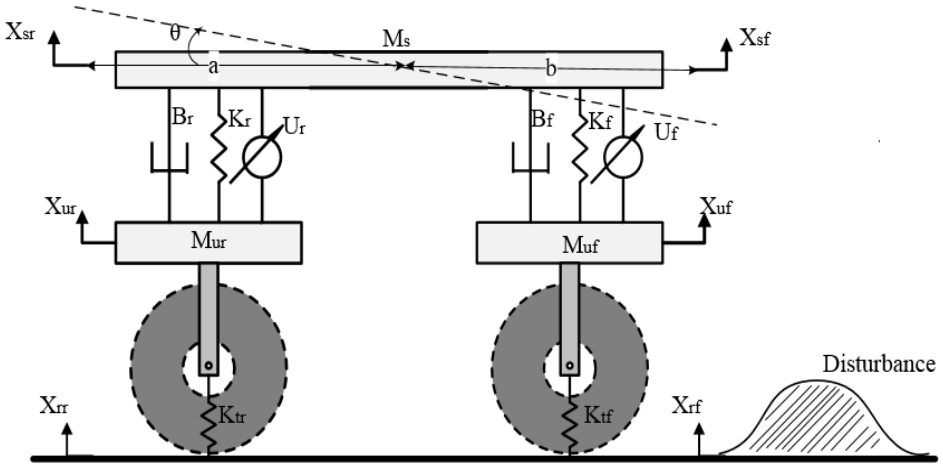

Figure 4.2: Half-car suspension model

4.3.1 Mathematical representation of the system dynamics

The equations of motion results from applying Newton's second law: $F = ma$ on the vehicle's body and wheels. The resulting force equations applied on the front sprung mass, rear sprung mass, front unsprung mass and rear unsprung mass are shown in eq. 4.1 to eq. 4.5 respectively. The system equations consider the non-linearities in the spring and damper components.

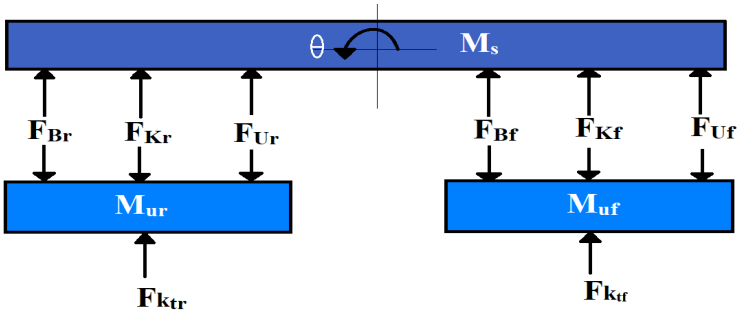

Figure 4.3: Half-car free body diagram

Front sprung mass

$$\ddot{x}_{sf} = 1/m_s[-K_f(x_{sf}-x_{uf})-K_{f_{nl}}(x_{sf}-x_{uf})^2-B_f(\dot{x}_{sf}-\dot{x}_{uf})-B_{f_{nl}}(\dot{x}_{sf}-\dot{x}_{uf})^2$$
$$-K_r(x_{sr}-x_{ur})-K_{rnl}(x_{sr}-x_{ur})^2-B_r(\dot{x}_{sr}-\dot{x}_{ur})-B_{rnl}(\dot{x}_{sr}-\dot{x}_{ur})^2+u_f+u_r+am_s\ddot{\theta}]$$
$$= \quad M_s f_2 + M_s u_f \quad (4.1)$$

Front unsprung mass

$$\ddot{x}_{uf} = 1/m_u[-K_f(x_{sf}-x_{uf})-K_{f_{nl}}(x_{sf}-x_{uf})^2-B_f(\dot{x}_{sf}-\dot{x}_{uf})$$
$$-B_{f_{nl}}(\dot{x}_{sf}-\dot{x}_{uf})^2-K_{tf}(x_{uf}-x_{rf})-u_f] = \quad M_u f_4 - M_u u_f \quad (4.2)$$

Rear sprung mass

$$\ddot{x}_{sr} = 1/m_s[-K_f(x_{sf}-x_{uf})-K_{f_{nl}}(x_{sf}-x_{uf})^2-B_f(\dot{x}_{sf}-\dot{x}_{uf})-B_{f_{nl}}(\dot{x}_{sf}$$
$$-\dot{x}_{uf})^2-K_r(x_{sr}-x_{ur})-K_{rnl}(x_{sr}-x_{ur})^2-B_r(\dot{x}_{sr}-\dot{x}_{ur})-B_{rnl}(\dot{x}_{sr}-\dot{x}_{ur})^2$$
$$+u_f+u_r+bm_s\ddot{\theta}] = \quad M_s f_6 + M_s u_f \quad (4.3)$$

Rear unsprung mass

$$\ddot{x}_{ur} = 1/m_u[-K_f(x_{sr}-x_{ur})-K_{f_{nl}}(x_{sr}-x_{ur})^2-B_f(\dot{x}_{sr}-\dot{x}_{ur})-B_{f_{nl}}(\dot{x}_{sr}$$
$$-\dot{x}_{ur})^2-K_{tr}(x_{ur}-x_{rr})-u_r]-M_r g = \quad M_u f_8 - M_u u_f \quad (4.4)$$

Pitch motion dynamics

$$\ddot{\theta} = 1/I[aK_f(x_{sf} - x_{uf}) - bK_r(x_{sr} - x_{ur}) - aB_f(\dot{x}_{sf} - \dot{x}_{uf}) - B_r(\dot{x}_{sr} - \dot{x}_{ur}) - au_r + bu_f] \quad (4.5)$$

4.3.2 System dynamics state space representation

The state variables assignment arising from the mathematical model of the system dynamics is shown in eq. 4.6 and eq. 4.7. There are eight resulting states for the half-car model, assuming the front and rear of the car are acting as independent systems; pitch dynamic states are to be introduced for a more accurate representation of a strongly coupled system.

$$(x_1, x_2, x_3, x_4, x_5, x_6, x_7, x_8) \quad = \quad (x_{sf}, \dot{x}_{sf}, x_{uf}, \dot{x}_{uf}, x_{sr}, \dot{x}_{sr}, x_{ur}, \dot{x}_{ur}) \quad (4.6)$$

The state assignment is such that the states relationship is described by:

$$\dot{x}_1 = x_2,\ \dot{x}_3 = x_4,\ \dot{x}_5 = x_6,\ \dot{x}_7 = x_8 \quad (4.7)$$

The full state space linear model of the half-car suspension system considering the pitch dynamics is:

$$FrontCar:$$

$$\dot{x}_1 = x_2 \quad (4.8)$$

$$\dot{x}_2 = \alpha[-K_f x_1 - B_f x_2 + k_f x_3 + B_f x_4 + U_f] + \beta[-k_r x_5 - B_r x_6 + k_r x_7 + B_r x_8 + U_r] \quad (4.9)$$

$$\dot{x}_3 = x_4 \quad (4.10)$$

$$\dot{x}_4 = \frac{1}{m_{uf}}[K_f x_1 + B_f x_2 - (K_f + K_{tf})x_3 - B_f x_4 + K_{tf} x_{rf} - U_f] \quad (4.11)$$

$$RearCar:$$

$$\dot{x}_5 = x_6 \quad (4.12)$$

$$\dot{x}_6 = \beta[-K_f x_1 - B_f x_2 + K_f x_3 + B_f x_4 + U_f] + \gamma[-K_r x_5 - B_r x_6 + K_r x_7 + B_r x_8 + U_r] \quad (4.13)$$

$$\dot{x}_7 = x_8 \quad (4.14)$$

$$\dot{x}_8 = \frac{1}{m_{ur}}[K_r x_5 + B_r x_6 - (K_r + K_{tr})x_7 - B_r x_8 + K_{tr} x_{rr} - U_r] \quad (4.15)$$

Where $\alpha = \frac{1}{m_s} + \frac{a^2}{J_y}$, $\beta = \frac{1}{m_s} - \frac{ab}{J_y}$ and $\gamma = \frac{1}{m_s} + \frac{b^2}{J_y}$

This state assignment, allows for the system dynamics representation to be as shown in eq. 4.8 to eq. 4.15. For a generic non-linear state space equation, the overall system full state model can thus be represented in the form shown by eq. 4.16.

$$\dot{\mathbf{x}} = \mathbf{f}(\mathbf{x}) + \mathbf{g}\mathbf{u} \tag{4.16}$$

where:

$$\mathbf{f(x)} = \begin{bmatrix} 1 & 0 & 0 & 0 & 0 & 0 & 0 & 0 \\ -\alpha K_f & \alpha B_f & \alpha K_f & \alpha B_f & -\beta K_r & -\beta B_r & \beta K_r & \beta B_r \\ 0 & 1 & 0 & 0 & 0 & 0 & 0 & 0 \\ \frac{K_f}{m_{uf}} & \frac{B_f}{m_{uf}} & -\frac{(K_f+K_{tf})}{m_{uf}} & \frac{-B_f}{m_{uf}} & 0 & 0 & 0 & 0 \\ 0 & 0 & 0 & 0 & 1 & 0 & 0 & 0 \\ -\beta K_f & \beta B_f & \beta K_f & \beta a B_f & -\gamma K_r & -\gamma B_r & \gamma K_r & \gamma B_r \\ 0 & 0 & 0 & 0 & 0 & 0 & 1 & 0 \\ 0 & 0 & 0 & 0 & \frac{K_r}{m_{ur}} & \frac{B_r}{m_{ur}} & -\frac{(K_r+K_{tr})}{m_{ur}} & \frac{-B_r}{m_{ur}} \end{bmatrix} \begin{bmatrix} x_1 \\ x_2 \\ x_3 \\ x_4 \\ x_5 \\ x_6 \\ x_7 \\ x_8 \end{bmatrix} \tag{4.17}$$

f consists of the system's state variables and **g** is the input to the system modelling the road profile. The road perturbation is external to the suspension plant therefore it is not modelled as part of the system dynamics. The resulting non-linear state vector equation is shown in eq. 4.18 for the partitioned **f** and **g**. The non-linear system matrices f_f and f_r are computed from the front and rear sub-system equations respectively. The g_1 and g_2 matrices are shown in eq. 4.19.

$$\dot{\mathbf{x}} = \begin{bmatrix} f_f \\ f_r \end{bmatrix} (\mathbf{x}) + \begin{bmatrix} g_1 & 0 \\ 0 & g_2 \end{bmatrix} (\mathbf{x})u \tag{4.18}$$

$$g_1 = \begin{bmatrix} 0 \\ \frac{1}{M_{sf}} \\ 0 \\ -\frac{1}{M_{uf}} \end{bmatrix}, \; g_2 = \begin{bmatrix} 0 \\ \frac{1}{M_{sr}} \\ 0 \\ -\frac{1}{M_{ur}} \end{bmatrix} \tag{4.19}$$

4.4 Half-car constructed test-rig

The constructed mechanical test-rig consists of the plant, four linear displacement sensors and two actuation motors as demonstrated by Fig. 4.4 and Fig. 4.5.

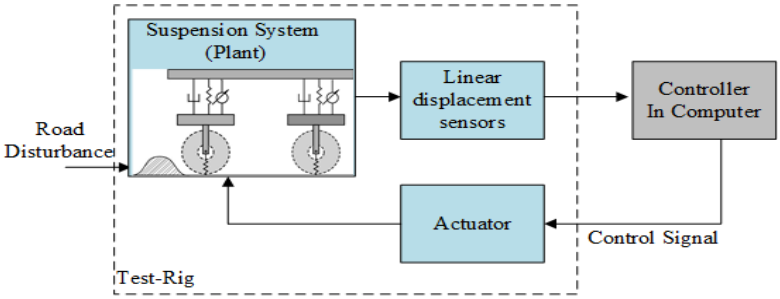

Figure 4.4: Half-car system overview without preview

The displacement sensors measure the linear variation in the displacement of the front and rear sprung (car's body) and unsprung mass (wheel). The displacement signal from these sensors is sent to the controller using Dspace integration software. The control algorithm then computes the required actuation force required to achieve the desired sprung mass trajectory. Once this actuation force has been computed by the controllers, a signal is sent to the servo motors which produce rotational motion, that is converted to linear displacement through the use of a rack and pinion.

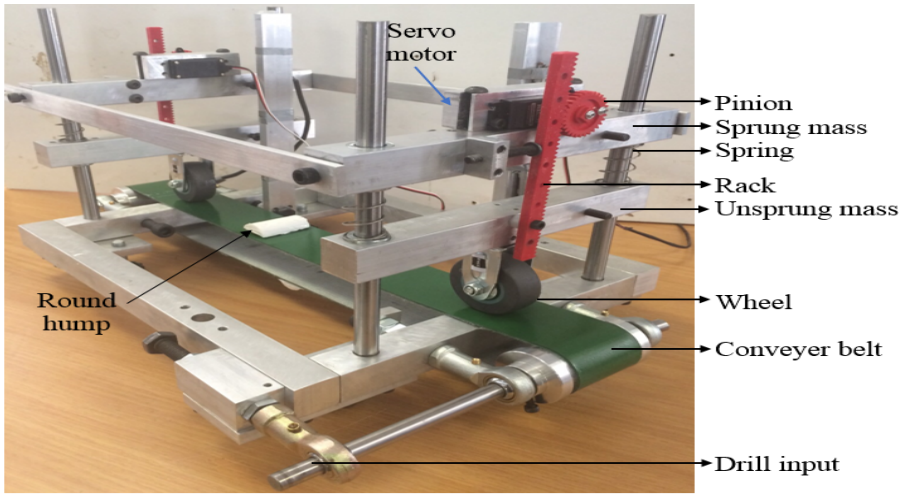

Figure 4.5: Constructed half-car mechanical test-rig

This design ensures that when the vehicle encounters a road perturbation, the signals from the sensors will enable the computer system to compute the change in displacement in that particular actuator and result in a response that compensates for the change in vertical displacement. The physical system parameters used to construct the half-car model demonstrated in Fig. 4.5 are described in Table 4.1. These parameters were carefully chosen to ensure the test-rig is cost-effective and it can be used for testing the designed controllers. The parameter identification for the springs and dampers was obtained through experimental setup using stiffness force against displacement and damping force against velocity respectively as adopted from [62].

Table 4.1: Half-car physical parameters

Parameter	**V**alue	**U**nits
Sprung mass (M_s)	1.2	kg
Front unsprung mass (M_uf)	0.45	kg
Rear unsprung mass (M_ur)	0.45	kg
Front spring coefficient (K_f)	901	N/m
Front suspension damper (B_f)	12	Ns/m
Front tyre stiffness (K_tf)	1527	N/m
Rear spring coefficient (K_r)	901	N/m
Rear damper coefficient (B_r)	12	Ns/m
Rear tyre stiffness (K_tr)	1527	N/m

The components utilised for constructing the physical system are the 14MB159 servo motors that produce the actuation force for mitigation of the impact of the road disturbance. Linear sliding potentiometers are used as displacement sensors to dictate and monitor the variations on the suspension masses. The components for constructing the model are four displacement sensors, 2 servo motors, rack and pinion for vertical motion, drill for speed control, conveyor with road disturbance objects such as round and square humps, springs and linear bearings for damping effect. The cost analysis of the construction of the test-bed is shown in Chapter 10. Fig. 4.6 to Fig. 4.7 show the side and angle view of the constructed test-rig respectively. The road disturbance signals used for testing the designed controllers is in Fig. 4.8.

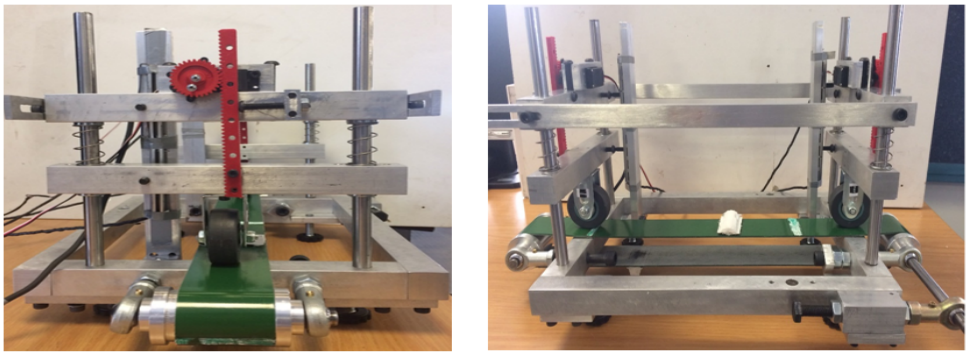

Figure 4.6: Rear view and side view

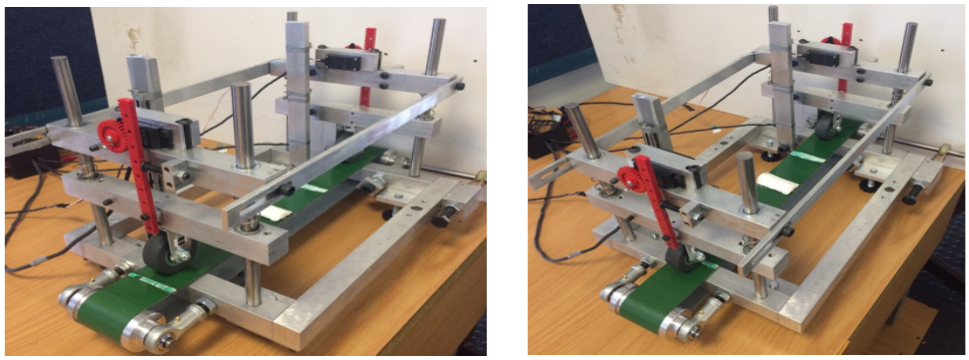

Figure 4.7: Angle view

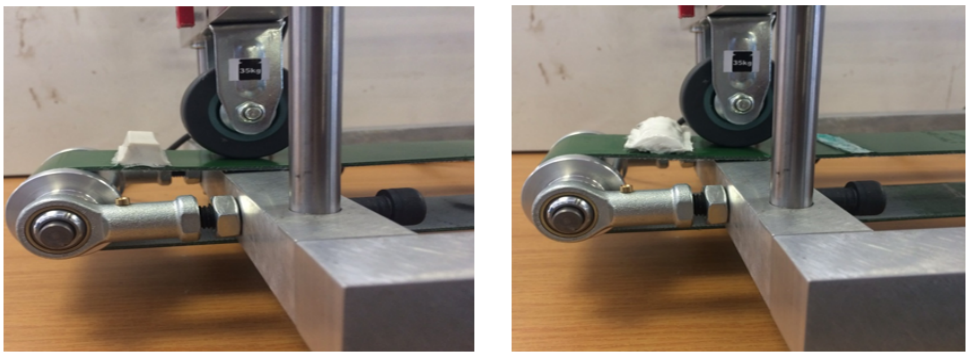

Figure 4.8: Square and round hump input

4.5 Constructed test-rig with preview functionality

The preview system enables the controller to observe the incoming disturbance before the suspension encounters the disturbance. The mechanical test-rig consists of the plant, preview radar sensor and two actuation motors. The preview sensor detects the road disturbance before it is experienced by the vehicle.

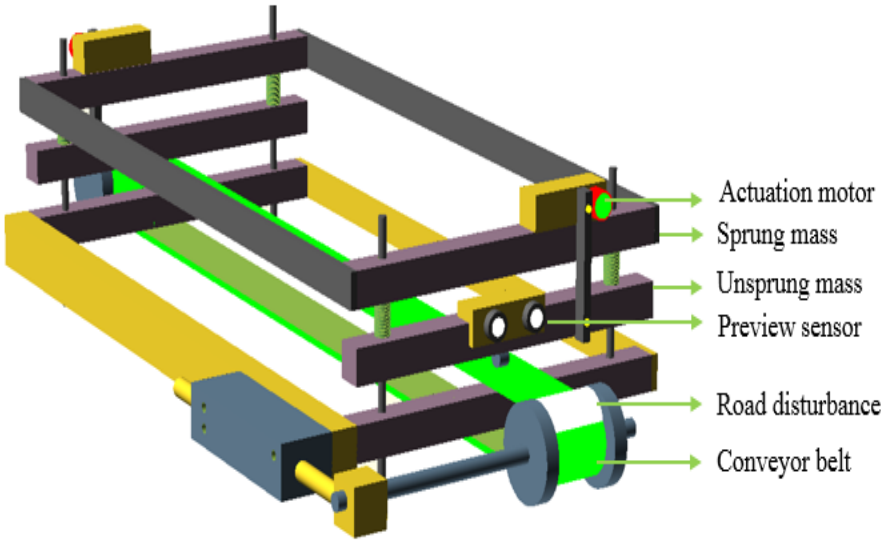

Figure 4.9: Schematic of half-car mechanical test bed with preview functionality

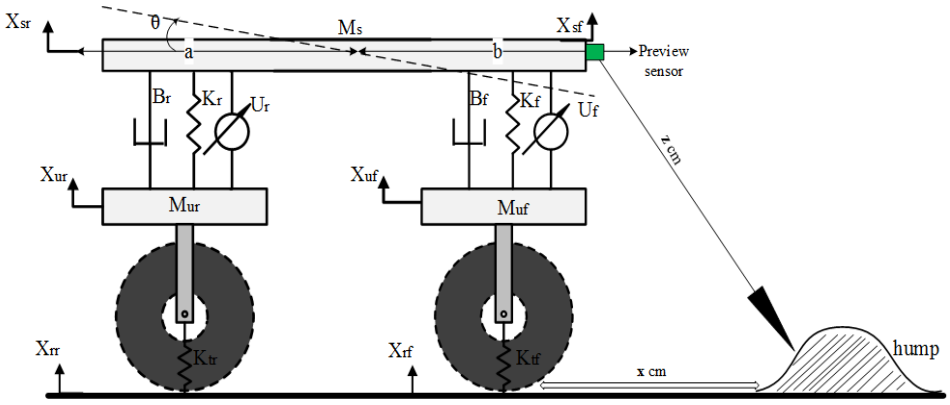

Figure 4.10: Schematic of preview correction computation

Fig. 4.9 shows the design of the preview control for the half-car model. The preview sensor is positioned so that it can compute an incoming disturbance as shown in Fig. 4.10. The preview functionality introduces a time delta in the system response, since the controller knows of the road disturbance prior to it being encountered. Sensor measurement systems have to be very accurate to be able to predict the dynamics (shape and size) of the road disturbance. The higher the sensor accuracy, the better the disturbance mitigation results from the controller. The developed test-rig is used with the designed controllers to ensure active vehicle suspension performance is at its maximum.

4.6 Summary on suspension system modelling

The system dynamics are modelled through mathematical equations for force representation of the vehicle suspension system. The developed half-car is cost-effective so as to meet the project requirements on scope, time and budget. Due to the imposed cost constraints, the choice of components minimised the cost of constructing the half-car mechanical test-rig. Matlab, Simulink and Dspace are utilised as programming environments to implement the controllers and enable communication for transmitting signals to the mechanical system. The performance of the suspension system can be tested to obtain the passive behaviour but to ensure an active suspension with improved ride quality performance, control techniques are applied to the test-rig. Therefore the slack-based optimal control, state constrained linear control and the adaptive sliding backstepping controllers are designed and applied to the half-car suspension model.

Chapter 5

State Constrained Suspension System Optimal Control

5.1 Introduction

Optimal control is used in suspension systems allowing the performance index to optimise for the actuation energy and ride comfort. In the engineering field, state constrained optimal control analysis is of high priority due to most physical systems having system state constraints. Various methodologies attempt to model for these inequality state constraints, so that they are incorporated into the optimal control solution as equality constraints. In the constructed half-car suspension system, the physical constraints are experienced in the suspension deflection between the sprung and unsprung mass. Therefore, the optimal control application is modelled and addressed through the penalty function model, which ensures that the further away the system operates from the feasible region, the higher the penalty. The computational simulations of this approach encounter limitations due to challenges resulting from the implementation of the switching functions within the software development space.

To address the penalty function limitations, the slack variable methodology is implemented on the half-car suspension system, and the control problem is formulated as a bounded state optimal control problem. A number of techniques exist in solving bounded state optimization problems as illustrated in [63], [64]. A method of transforming the inequality constraint to an equality constraint is presented in [65]. The optimal control formulation computes the system's performance index, state and costate initial conditions, Hamiltonian, costates and the resulting optimal control

input which tend to be more complex for MIMO systems. Moreover, since suspension systems have stochastic elements, the above are more complicated. Elements of this section have been published in the Control Conference Africa as presented in [59].

CONTRIBUTION 1: To investigate state constrained optimal control on the half-car suspension system by addressing the limitations of penalty function-based methodology through the use of slack variable methodology to achieve energy efficiency through:

1. Identification of the limitations in the simulation of the penalty function state constrained optimal control on the half-car suspension due to the application of the switching functions in modelling packages.
2. Modelling the inequality constraint through the definition of slack-based constraint model to ensure that the front and rear optimal control is operating within the half-car suspension travel limits.
3. Computing the Hamiltonian, co-states, boundary conditions and the optimal controller on the half-car suspension system. Then conducting analysis of the controller performance on the front and rear suspension system focusing on the displacement, acceleration, control input, cost function for both $mass = m$ and $mass = 2m$ for energy efficiency analysis.

5.2 General optimal control for state constrained systems

The optimal control performance index aims at minimising the control and displacement energy while ensuring ride comfort. Optimal control application requires an understanding on the conditions for optimal control, the choice of the performance index and the constraints model.

5.2.1 Conditions for general optimal control

The formulation of general optimal control is shown as adapted from [66]. A Hamiltonian function is obtained by adjoining the performance index with the constraints as shown by eq. 5.1.

$$\mathcal{H} = L(x, u, t) + \lambda^T \mathbf{f}(\mathbf{x}, u, t) \tag{5.1}$$

Where the adjoint or co-state equation is given by eq. 5.2.

$$\dot{\lambda} = \frac{\partial \mathcal{H}}{\partial \mathbf{x}} \tag{5.2}$$

The optimality condition to be satisfied is:

$$\frac{\partial \mathcal{H}}{\partial \mathbf{u}} = \mathbf{0} \tag{5.3}$$

and boundary conditions are obtained from eq. 5.4 by considering the solution as either a free or fixed initial time and free or fixed final state problem.

$$(\frac{\partial \psi}{\partial \mathbf{x}} - \lambda)^T|_{t_f} d\mathbf{x}(t_f) + (\frac{\partial \psi}{\partial \mathbf{x}} - H)^T|_{t_f} d(t_f) = 0 \tag{5.4}$$

5.2.2 Performance index and inequality constraints

For the half-car suspension model, focus is on ride comfort and energy efficiency therefore the performance index will optimise for these objectives. The optimal control problem is to find the input $u(t)$ on the time interval $[0, t_f]$ which will drive the plant so that the cost function is minimized. For a general system of the form:

$$\dot{\mathbf{x}}(t) = \mathbf{f}(\mathbf{x}, \mathbf{u}, t) \tag{5.5}$$

The system's optimal control is described by the optimal performance index eq. 5.6 and constraints in eq. 5.7 [35].

$$J_{opt} = \psi(x(t_f), t_f) + \int_0^{t_f} L(x(t), u(t), t) dt \tag{5.6}$$

$$\mathbf{g}(\mathbf{x}, t) \leq 0 \tag{5.7}$$

In this work, the optimal control objective is to generate a minimum control input for the front and rear systems that will reduce sprung body displacement and energy, within the suspension deflection inequality constraint.

5.3 Application of optimal control on the half-car

The penalty function will be applied to the half-car suspension based on the formulated equations from Chapter 4. The state assignment was as shown in 5.8

$$(x_1 = x_{sf}, x_2 = \dot{x}_{sf}, x_3 = x_{uf}, x_4 = \dot{x}_{uf}, x_5 = x_{sr}, x_6 = \dot{x}_{sr}, x_7 = x_{ur}, x_8 = \dot{x}_{ur}) \tag{5.8}$$

resulting in:

$$\dot{x}_1 = x_2,\ \dot{x}_3 = x_4,\ \dot{x}_5 = x_6,\ \dot{x}_7 = x_8 \tag{5.9}$$

The half-car suspension cost function consists of sum of squares which represent the energy of the front and rear displacements as well as the energy in the control signals: u_f and u_r. The weighting coefficients q_1 and q_2 allow the designer to define the performance of the suspension system. The optimal performance index that minimizes the control signal and the sprung body energy for front and rear is thus defined as:

$$J_{opt} = \int_0^{t_f} q_1 x_1^2 + q_2 x_5^2 + \frac{1}{2}u_f^2 + \frac{1}{2}u_r^2 dt \tag{5.10}$$

The variables x_1 and u_f are associated to the front system, whereas x_5 and u_r are for the rear system, therefore the performance index optimises for the sprung displacement of the half-car and its controllers. The half-car is subject to the front and rear inequality constraints:

$$\begin{aligned} x_3 - x_1 &\leq 0.1 \\ x_7 - x_5 &\leq 0.1 \end{aligned} \tag{5.11}$$

This inequality constraint models the suspension travel within its limits and it will be converted to an equality constraint through the penalty function methodology.

5.4 Inequality state constraints for optimal control

State constraints in optimal control formulation can be modelled using various methodologies that attempt to convert the state inequality constraint to an equality constraint as discussed in [67] and [68]. This section focuses on the application and limitations of two methodologies that are applied to suspension systems to solve for the state constrained optimal control: penalty function and slack variable methodology.

5.4.1 Penalty function state constrained conversion optimal control

The penalty function method is based on modelling the inequality constraint in eq. 5.7 as an equality constraint and modelling it as an additional state as shown in eq. 5.12, as illustrated in [65] and [69].

$$\dot{x}_{n+1} = [g(x,t)]^2 \hat{\mathbf{H}}(-g(x,t)) \tag{5.12}$$

where:

$$\begin{aligned} \hat{\mathbf{H}}(-g(x,t)) &: 0, if - g(x,t) \geq 0, \\ &: 1, if - g(x,t) < 0 \end{aligned} \tag{5.13}$$

The optimal control solution for the half-car will introduce new states for the front and rear suspension based on the inequality constraint due to the suspension deflection x_{sd}. Although this method is less complex to implement as it does not change the system input, the cost function or the performance index, we observe its limitations when it comes to its' implementation due to the complications introduced by the switching functions, as computed and demonstrated in section 6.3.

5.4.2 Slack variable state constrained conversion optimal control

The slack variable methodology converts the inequality state constraint in eq. 5.7 to an equality through the function described in eq. 5.14.

$$g(x,t) - \frac{1}{2}{\alpha_0}^2 = 0 \tag{5.14}$$

The slack function allows for the inequality to be converted to an equality constraint by introducing the variable α_0 as demonstrated in [70] and [71]. This methodology is based on differentiating eq. 5.14 until the input u explicitly appears. Once the input appears on the p^{th} derivative, the computation will result in eq. 5.15.

$$g_p(X,U,t) + \alpha_0, \alpha_1, ..., \alpha_p = 0 \tag{5.15}$$

The slack variable state constrained optimal control inequality constraint in eq. 5.7 is converted into an equality constraint and the resulting $\alpha_0, \alpha_1, .., \alpha_{p-1}$ become additional states of the transformed system in [66]. α_p is the unconstrained input for the transformed system. The resulting transformed system results in (p) additional states therefore there are $(n+p)$ states and $(n+p)$ co-states. The transformed system dynamics due to the slack conversion optimal control will be modelled by:

$$\dot{X} = f[X, g(X, g(\alpha, \alpha_1, .., \alpha_p, t)t)] \tag{5.16}$$

And the control problem will be modelled by the cost function:

$$J = \Psi(X_f, t_f) + \int_{t_0}^{t_f} L(X, g(X, \alpha, \alpha_1, .., \alpha_p, t)t)dt \tag{5.17}$$

The slack variable results feasible solutions since the solver does not have implementation limitations, as computed and demonstrated in section 6.4.

5.5 Penalty function-based optimal control formulation for the half-car AVSS

The application of the penalty function based on the half-car AVSS modelling will formulate the costates including the constraints as the additional states, conduct boundary condition analysis, Hamilton and co-states analysis and demonstrate the resulting simulation results.

5.5.1 Penalty function-based state constraint modelling

The inequality constraint is converted into an equality constraint and included as additional states as shown by eq. 5.18, where $\hat{\mathbf{H}}(.)$ is the Heaviside function.

$$\begin{aligned} \dot{x}_9 &= [0.1 - x_3 + x_1]^2 \hat{\mathbf{H}}(x_3 - x_1 - 0.1) \\ \dot{x}_{10} &= [0.1 - x_7 + x_5]^2 \hat{\mathbf{H}}(x_7 - x_7 - 0.1) \end{aligned} \tag{5.18}$$

The additional states result in the half-car model having two additional states modelled by:

$$\begin{aligned} \dot{x}_{n+1} &= \frac{\partial \mathcal{H}}{\partial \lambda_{n+1}} \\ \dot{x}_{n+2} &= \frac{\partial \mathcal{H}}{\partial \lambda_{n+2}} \end{aligned} \tag{5.19}$$

The Hamiltonian function is not an explicit function of x_{n+1} or x_{n+2}, therefore the costates due to the additional states are:

$$\begin{aligned} \dot{\lambda}_{n+1} &= -\frac{\partial \mathcal{H}}{\partial x_{n+1}} = 0 \\ \dot{\lambda}_{n+2} &= -\frac{\partial \mathcal{H}}{\partial x_{n+2}} = 0 \end{aligned} \tag{5.20}$$

Therefore, in addition to the 8 costates relating to the half-car's system states, an additional 2 costates are introduced:

$$\dot{\lambda}_9 = -\frac{\partial \mathcal{H}}{\partial x_9} = 0 \tag{5.21}$$

$$\dot{\lambda}_{10} = -\frac{\partial \mathcal{H}}{\partial x_{10}} = 0 \tag{5.22}$$

5.5.2 Boundary condition analysis

The boundary conditions on the final time (t_f) for the front and rear suspension states are set to:

$$\begin{aligned} x_1(t_f) = x_2(t_f) = x_3(t_f) = x_4(t_f) = 0, \\ x_5(t_f) = x_6(t_f) = x_7(t_f) = x_8(t_f) = 0 \end{aligned} \tag{5.23}$$

and the boundary conditions for the additional states are:

$$\begin{aligned} x_{n+1}(t_0) = x_{n+1}(t_f) = 0, \\ x_{n+2}(t_0) = x_{n+2}(t_f) = 0 \end{aligned} \tag{5.24}$$

5.5.3 Hamiltonian and co-states for the half-car model

Now to compute the Hamiltonian function $\mathcal{H}$ is:

$$\begin{aligned}\mathcal{H} = k_f x_1^2 + k_r x_5^2 + \frac{k_f}{2}u_f^2 + \frac{k_r}{2}u_r^2 + \lambda_1 x_2 + \lambda_2\alpha[-k_f x_1 \\ - B_f x_2 + k_f x_3 + B_f x_4 + U_f] + \lambda_2\beta[-k_r x_5 - B_r x_6 \\ + k_r x_7 + B_r x_8 + U_r] + \lambda_3 x_4 + \frac{\lambda_4}{m_{uf}}[k_f x_1 + B_f x_2 - \\ (k_f + K_{tf})x_3 - B_f x_4 + K_{tf}x_{rf} - U_f] + \lambda_5 x_6 + \lambda_6\beta \\ [-k_f x_1 - B_f x_2 + k_f x_3 + b_f x_3 - B_f x_4 + U_f] + \lambda_6\gamma \\ [-k_r x_5 - B_r x_6 + k_r x_7 + B_r x_8 + U_r] + \lambda_7 x_8 + \frac{\lambda_8}{m_{ur}} \\ [k_r x_5 + B_r x_6 - (k_r + K_{tr})x_7 - B_r x_8 + K_{tr}x_{rr} - U_r] \\ + \lambda_9(0.1 - x_3 + x_1)^2\hat{\mathbf{H}}(x_3 - x_1 - 0.1) + \\ \lambda_{10}(0.1 - x_7 + x_5)^2\hat{\mathbf{H}}(x_7 - x_5 - 0.1)\end{aligned} \tag{5.25}$$

And the co-state computation for the half-car is:

$$\begin{aligned}\dot{\lambda}_1 &= -\frac{\partial\mathcal{H}}{\partial x_1} = -[2k_f x_1 - \alpha\lambda_2 k_f + \frac{\lambda_4}{m_{uf}}k_f - \lambda_6\beta k_f - \\ &\quad 2\lambda_9(0.1 - x_3 + x_1)\hat{\mathbf{H}}(x_3 - x_1 - 0.1)] \\ \dot{\lambda}_2 &= -\frac{\partial\mathcal{H}}{\partial x_2} = -[\lambda_1 - \alpha\lambda_2 B_f + \frac{\lambda_4}{m_{uf}}B_f - \lambda_6\beta B_f] \\ \dot{\lambda}_3 &= -\frac{\partial\mathcal{H}}{\partial x_3} = -[\alpha\lambda_2 k_f - \frac{\lambda_4}{m_{uf}}(k_f + K_{tf}) + \lambda_6\beta k_f + \\ &\quad 2\lambda_9(0.1 - x_3 + x_1)\hat{\mathbf{H}}(x_3 - x_1 - 0.1)] \\ \dot{\lambda}_4 &= -\frac{\partial\mathcal{H}}{\partial x_4} = -[\lambda_3 + \alpha\lambda_2 B_f - \frac{\lambda_4}{m_{uf}}B_f + \lambda_6\beta B_f] \\ \dot{\lambda}_5 &= -\frac{\partial\mathcal{H}}{\partial x_5} = -[2k_r x_5 - \beta\lambda_2 k_r + \frac{\lambda_8}{m_{ur}}k_r - \lambda_6\gamma k_r + \\ &\quad 2\lambda_{10}(0.1 - x_7 + x_5)\hat{\mathbf{H}}(x_7 - x_5 - 0.1)] \\ \dot{\lambda}_6 &= -\frac{\partial\mathcal{H}}{\partial x_6} = -[\lambda_5 - \beta\lambda_2 B_r + \frac{\lambda_8}{m_{ur}}B_r - \lambda_6\gamma B_r] \\ \dot{\lambda}_7 &= -\frac{\partial\mathcal{H}}{\partial x_7} = -[\beta\lambda_2 k_r - \frac{\lambda_8}{m_{ur}}(k_r + K_{tr}) + \lambda_6\gamma k_r - \\ &\quad 2\lambda_{10}(0.1 - x_7 + x_5)\hat{\mathbf{H}}(x_7 - x_5 - 0.1)] \\ \dot{\lambda}_8 &= -\frac{\partial\mathcal{H}}{\partial x_8} = -[\lambda_7 + \beta\lambda_2 B_r - \frac{\lambda_8}{m_{ur}}B_r + \lambda_6\beta B_r] \\ \dot{\lambda}_9 &= -\frac{\partial\mathcal{H}}{\partial x_9} = 0 \\ \dot{\lambda}_{10} &= -\frac{\partial\mathcal{H}}{\partial x_{10}} = 0\end{aligned} \tag{5.26}$$

5.5.4 Half-car optimal control inputs

The resulting Hamiltonian and costate equations are complex due to the co-dependency between the front and rear suspension systems. The resulting front and rear control law is determined from the optimality condition:

$$\frac{\partial \mathcal{H}}{\partial \mathbf{u}} = 0 \tag{5.27}$$

Therefore computing $\frac{\partial \mathcal{H}}{\partial \mathbf{u}}$, for the front and rear suspensions results in:

$$\begin{aligned} \frac{\partial \mathcal{H}}{\partial u_f} &= k_f u_f + \lambda_2 \alpha - \frac{\lambda_4}{m_{uf}} + \lambda_6 \beta \\ \frac{\partial \mathcal{H}}{\partial u_r} &= k_r u_r + \lambda_2 \beta - \frac{\lambda_8}{m_{ur}} + \lambda_6 \gamma \end{aligned} \tag{5.28}$$

Applying eq. 5.27 to eq. 5.28, the front and rear controls laws are:

$$\begin{aligned} u_f &= \frac{\lambda_4}{m_{uf}} - \frac{\lambda_6 \beta}{k_f} - \frac{\lambda_2 \alpha}{k_f} \\ u_r &= \frac{\lambda_8}{m_{ur}} - \frac{\lambda_6 \gamma}{k_r} - \frac{\lambda_2 \beta}{k_r} \end{aligned} \tag{5.29}$$

The final states of the unsprung masses are allowed to be non-zero as long as this ensures zero final states for the sprung body. Thus the final time and the final state are free. Therefore:

$$\lambda(tf) = 0 \tag{5.30}$$

$$\mathcal{H} = 0 \tag{5.31}$$

To determine $\lambda_2, \lambda_4, \lambda_6$ and λ_8, the Hamiltonian system is solved as a boundary value problem using Matlab.

5.5.5 Simulation testing results

In the Matlab environment, simulation computations were performed using the *bvp4c* solver. Some information about the initial and final values of the states $\mathbf{x}$ and co-states λ is required in order to solve for the optimal control in eq. 5.29. The only information that is known is $\lambda(0)$ from eq. 5.30 and the initial states $x(t_0)$ are assumed to be zero and this is sufficient to solve the problem. The disturbance profile of a road hump was created using a parabolic function modified via a piecewise function so that it only switches on for a specific time interval. This is depicted by Fig. 5.1. The weighting coefficients q_1 and q_2 determine the active suspension performance. These were thus adjusted in order to give the best performance for the system. This performance was defined to be a displacement reduction of 95% from passive to active for the front and the rear part. Upon this adjustment, the optimal control signal that will guarantee an outcome of the defined performance is then computed. Ride comfort is measured by monitoring the half-car's displacement and acceleration for both the front and the rear sub-systems.

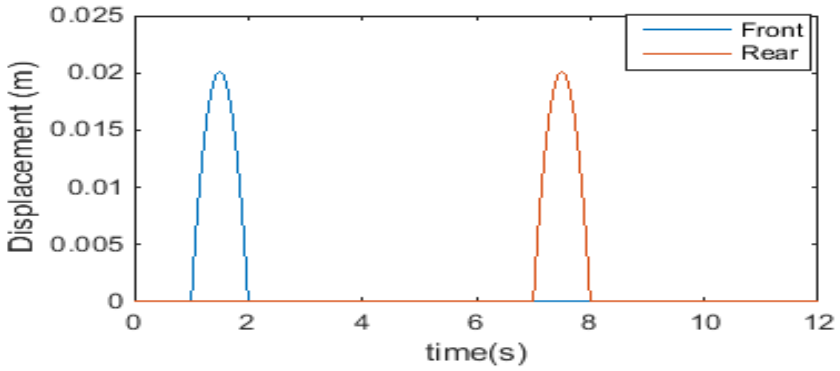

Figure 5.1: Road disturbance profile for front and rear part

Fig. 5.2 to 5.5 show the optimal trajectories for the front and rear displacement and acceleration. Fig. 5.2 illustrates the passive and active response comparisons for two different weight conditions. First, we note the effect of the pitch motion occurring around the 8^{th} second. This illustrates that the disturbance experienced by the rear sub-system impacts the dynamics of the front sub-system due to the pitch linkage between the two sub-systems. The active response is reduced as intended for both the weight conditions. The same result is evident for the rear part in Fig. 5.3.

5.5.6 Displacement plots

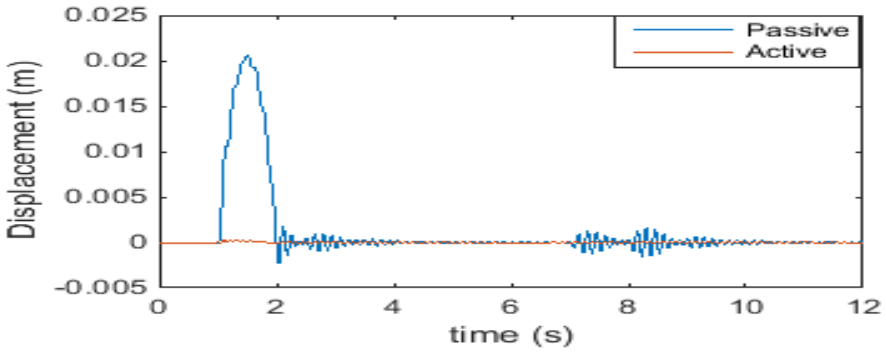

(a) Mass=m

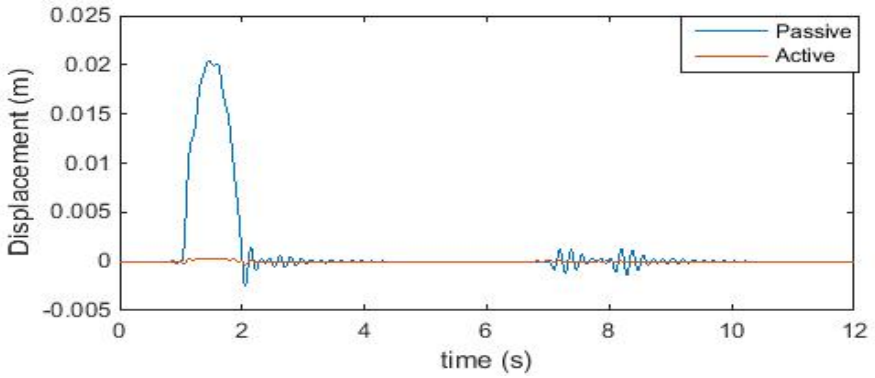

(b) Mass=$2m$

Figure 5.2: Front active vs passive displacement

The displacement optimal trajectories can be observed and the impact of the pitch motion is observed at 8 seconds. This illustrates the disturbance to the rear part affecting the front part due to the pitch dynamics. The active response is reduced as intended for both the weight conditions. The peaks on the passive system are an indication that the passive system tracks the trajectory of the road disturbance whereas the active systems attenuates this disturbance.

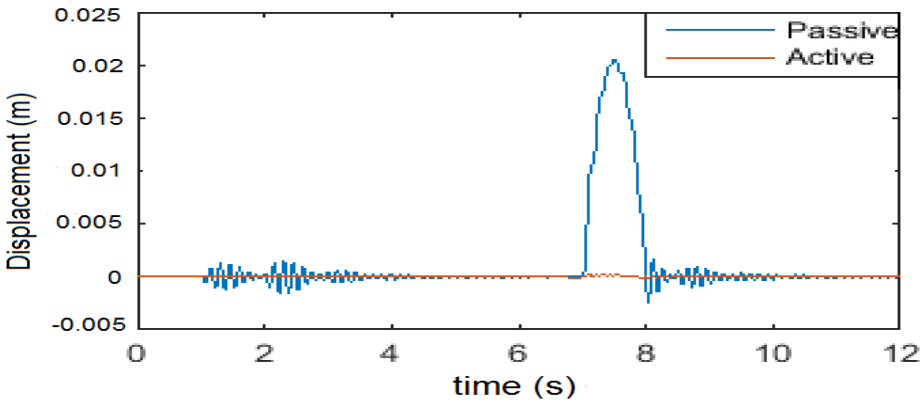

(a) Mass=m

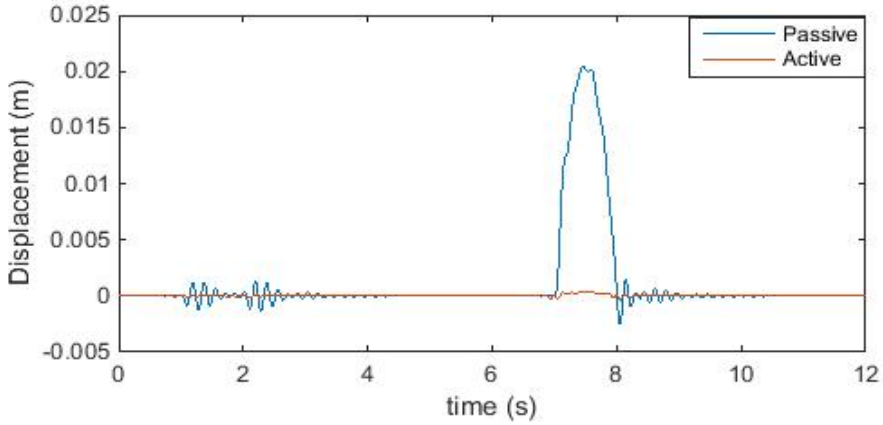

(b) Mass=$2m$

Figure 5.3: Rear active vs passive displacement

5.5.7 Acceleration plots

The acceleration is also significantly attenuated in Fig. 5.4 and 5.5. The acceleration plots show a significant attenuation between the passive and active suspension systems for both $mass = m$ and $mass = 2m$. In both the front and rear systems, the acceleration attenuation is highly reduced for $mass = m$ as compared to $mass = 2m$.

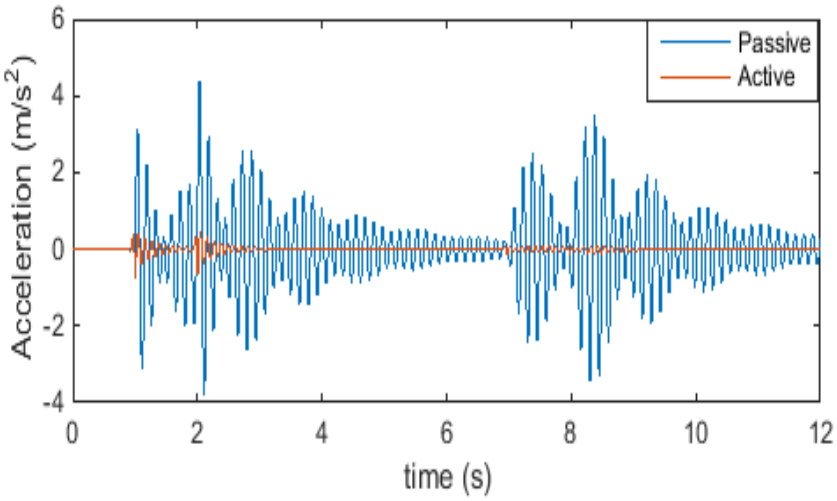

(a) Mass=m

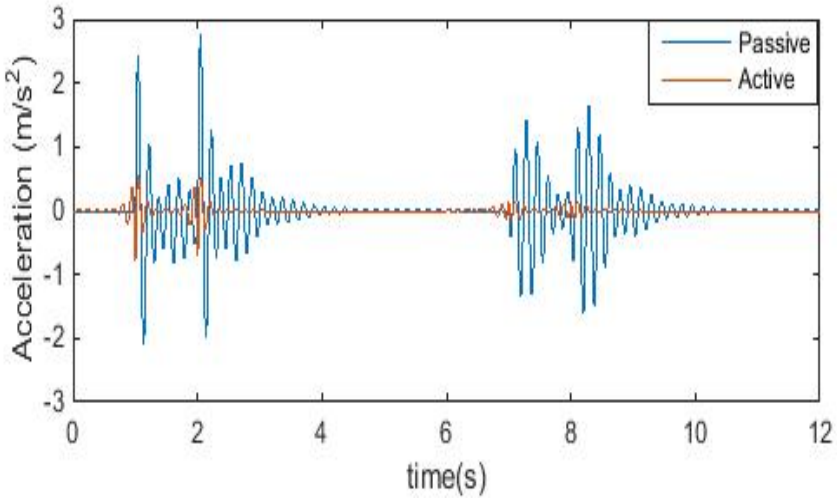

(b) Mass=$2m$

Figure 5.4: Front active vs passive acceleration

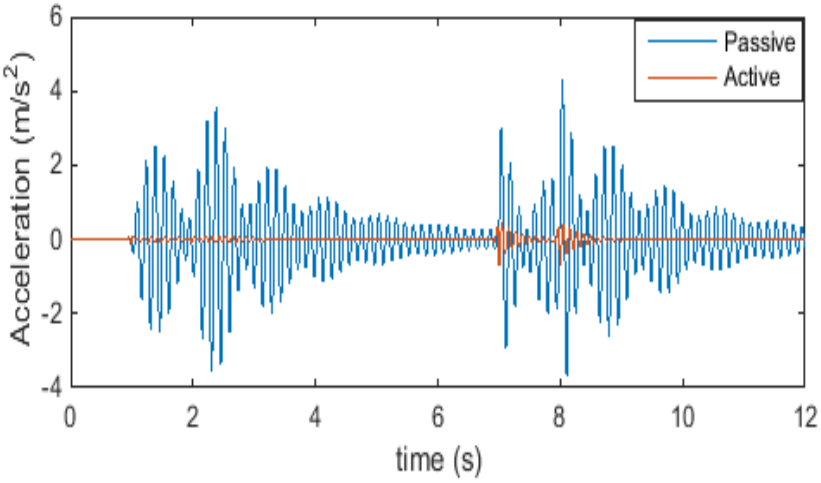

(a) Mass=m

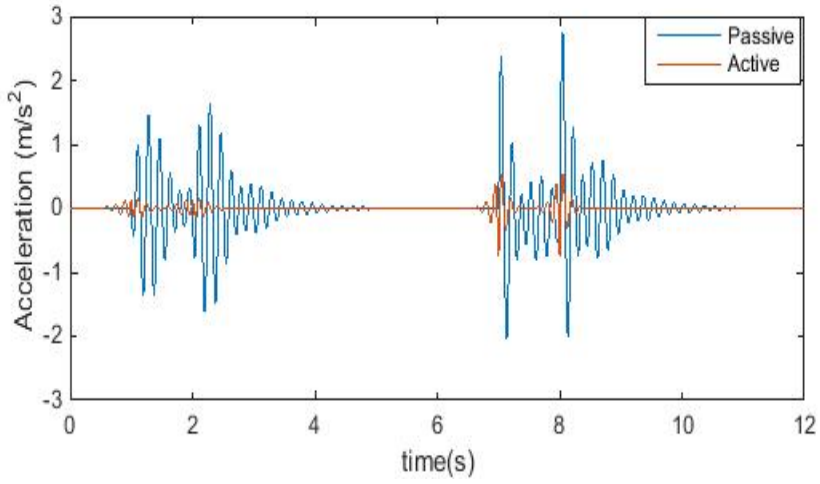

(b) Mass=$2m$

Figure 5.5: Rear active vs passive acceleration

5.5.8 Control signal plots

The major effect of increasing the mass to $2m$ occurs on the optimal control inputs force (N) in Fig. 5.6. For $2m$ in Fig. 5.6(b), the optimal control signal doubles

in order to guarantee effective controller performance. The performance index is significantly reduced in the active case for both mass conditions, with the cost for $2m$ being higher than for m.

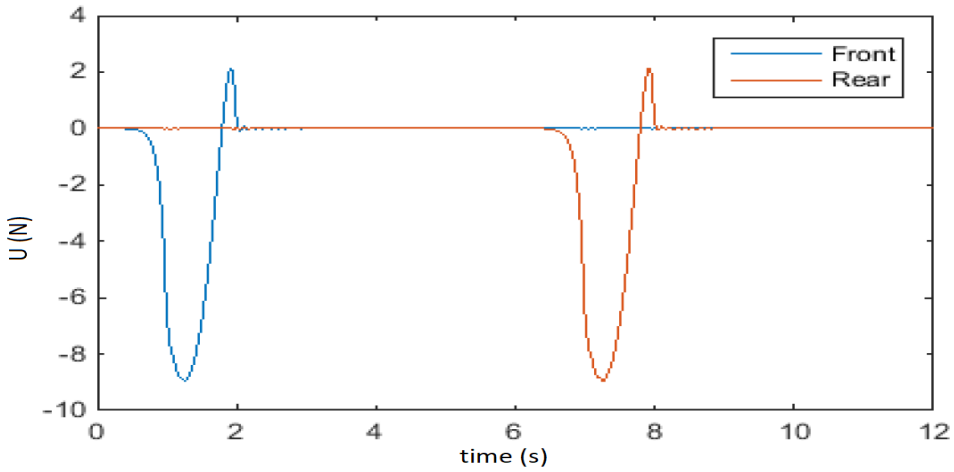

(a) Mass=m

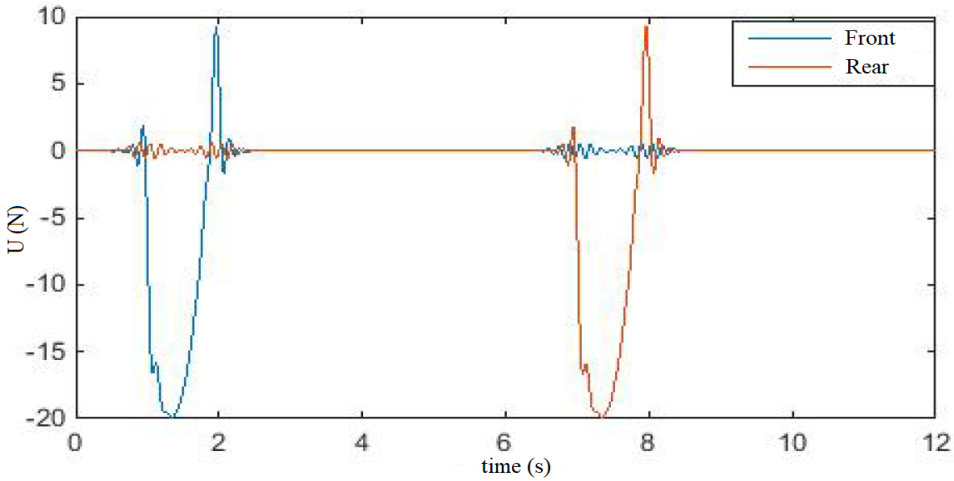

(b) Mass=$2m$

Figure 5.6: Optimal control signal for the front and rear parts

5.5.9 Cost function and performance index plots

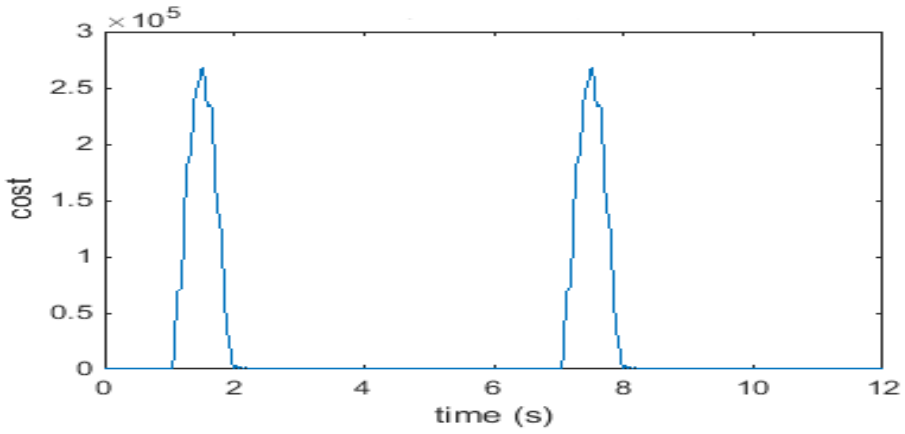

(a) Mass=m

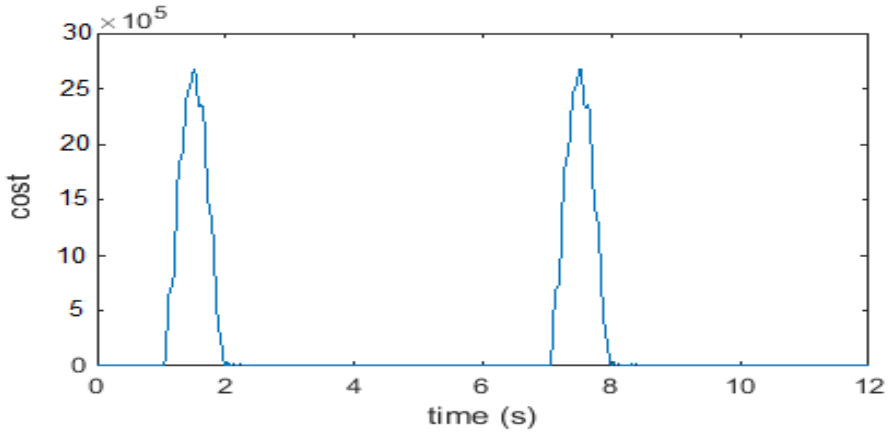

(b) Mass=$2m$

Figure 5.7: Performance index/cost function for passive case

Fig. 5.7 and 5.8 compare the performance index for the passive and active responses. It is clear that the performance index is significantly reduced in the active case for both mass conditions, with the cost for $2m$ being higher than for m. The cost function for the passive case is high due to the disturbance that the passive system is exposed to, the active system shows a reasonable cost due to the system having a reduced.

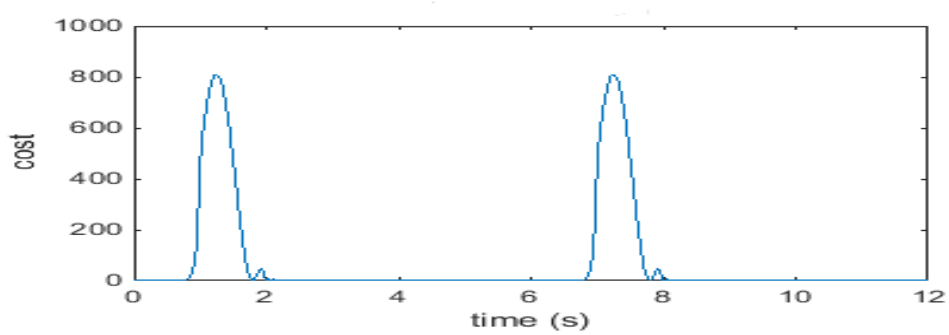

(a) Mass=m

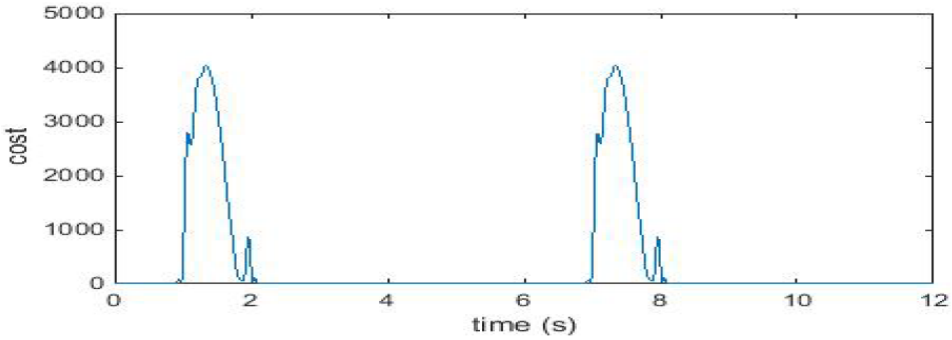

(b) Mass=$2m$

Figure 5.8: Performance index/cost function for active case

5.5.10 Discussion of the limitations of the penalty function

The penalty function application on the state constrained half-car suspension system employs a model where the performance index is a combination of ride comfort and actuation energy for both the front and rear sub-systems. The limitation with the practical application of this methodology is that the simulation framework such as Matlab approximate the switching point to 0.5 as shown in eq. 5.32. This leads to discontinuity therefore resulting in challenges within the practical application of this methodology.

$$\begin{aligned} x < 0, \quad & \hat{\mathbf{H}}(x) = 0 \\ x > 0, \quad & \hat{\mathbf{H}}(x) = 1 \\ x = 0, \quad & \hat{\mathbf{H}}(x) = \frac{1}{2} \end{aligned} \tag{5.32}$$

The Matlab approximation of the Heaviside function is not continuous, therefore this results in complications in the differentiation of such systems. Similar challenges can be observed with different switching functions such as ramps and the Dirac delta therefore an alternative approach to penalty function state constrained methodology on the half-car suspension is explored. The slack variable methodology converts the inequality to an equality constraint based on slack equation. The focus will be on the formulation of the slack variable to the application of the half-car system, to show how the computational challenges brought by the penalty function will be addressed by the slack variable.

5.6 Half-car slack-based constrained optimal control

To address the limitations within the penalty function, the slack variable methodology is applied to the half-car suspension system model. This constraint conversion methodology transforms the inequality constraints for the front and rear suspension parts into equality constraints. The transformation results in the introduction of additional state variables from the differentiation of Valentine's slack definition shown in eq. 5.14 [66].

5.6.1 Half-car suspension system slack variable application

With the front suspension system inequality constraints as:

$$x_{sd} \leq 0.1 \tag{5.33}$$

$$(x_3 - x_1) \leq 0.1 \tag{5.34}$$

The inequality modeling the suspension deflection $x_{sd} = x_3 - x_1$. Based on the slack definition: $g(X,t) + \frac{1}{2}\alpha^2 = 0$ used to transform the front suspension inequality constraint in eq. 5.33, to an equality constraint. The result is:

$$x_{sd} + \frac{1}{2}\alpha_f^2 = 0.1 \tag{5.35}$$

The slack conversion methodology is based on differentiating the slack definition until input (u) explicitly appears therefore the computation of the first derivative yields:

$$g_1(X,t) + \alpha_f \alpha_1 = 0 \tag{5.36}$$

where $g_1(X,t)$ is $\dot{g}(X,t)$ and $\alpha_1 = \dot{\alpha}$ resulting in:

$$\dot{x}_{sd} + \alpha_f \alpha_1 = 0 \tag{5.37}$$

$$(\dot{x}_3 - \dot{x}_1) + \alpha_f \alpha_1 = 0 \tag{5.38}$$

based on the suspension system state assignment, eq. 5.38 becomes eq. 5.39.

$$(x_4 - x_2) + \alpha_f \alpha_1 = 0 \tag{5.39}$$

At this point, the input has not explicitly appeared, therefore computing the second derivative will yield:

$$g_2(X,t) + \alpha_1^2 + \alpha_f \alpha_2 = 0 \tag{5.40}$$

$$\ddot{x}_{sd} + \alpha_1^2 + \alpha_f \alpha_2 = 0 \tag{5.41}$$

which is:

$$(\dot{x}_4 - \dot{x}_2) + \alpha_1^2 + \alpha_f \alpha_2 = 0 \tag{5.42}$$

For the front part of the suspension system:

$$\begin{aligned} \dot{x}_2 = \alpha[-K_f x_1 - B_f x_2 + k_f x_3 + B_f x_4 + u_f] \\ +\beta[-k_r x_5 - B_r x_6 + k_r x_7 + B_r x_8 + U_r] \\ \dot{x}_2 = \alpha[f_{2a} + u_f] + \beta[f_{2b} + u_r] \end{aligned} \tag{5.43}$$

and:

$$\begin{aligned} \dot{x}_4 =& \frac{1}{m_{uf}}[K_f x_1 + B_f x_2 - (K_f + K_{tf}) x_3 - B_f x_4 \\ &+ K_{tf} x_{rf} - u_f] \\ \dot{x}_4 =& \frac{1}{m_{uf}}[f_4 - u_f] \end{aligned} \tag{5.44}$$

Where: $\alpha = \frac{1}{m_s} + \frac{a^2}{J_y}$,$\beta = \frac{1}{m_s} - \frac{ab}{J_y}$ and $\gamma = \frac{1}{m_s} + \frac{b^2}{J_y}$ The resulting expression showing the relationship between the control input u_f and the new p states is:

$$\alpha(f_{2a} + u_f) + \beta(f_{2b} + u_r) - \frac{1}{m_{uf}}(f_4 - u_f) + \alpha_1^2 + \alpha_f \alpha_2 = 0 \tag{5.45}$$

Therefore the resulting input (u_f) and (u_r) are modelled by:

$$u_f = \frac{-1}{\alpha - \frac{1}{m_{u_f}}}[\alpha_1^2 + \alpha_f\alpha_2 - \frac{1}{m_{uf}}f_4 + \alpha f_{2a} + \beta(f_{2b} + u_r)] \tag{5.46}$$

$$u_r = \frac{-1}{\beta - \frac{1}{m_{u_r}}}[\alpha_3^2 + \alpha_r\alpha_4 - \frac{1}{m_{ur}}f_8 + \beta f_{6a} + \gamma(f_{6b} + u_f)] \tag{5.47}$$

And the new inputs (α_2) and (α_4) for the transformed half-car suspension system are:

$$\alpha_2 = \frac{-1}{\alpha_f}[\alpha(f_{2a} + u_f) + \beta(f_{2b} + u_r) - \frac{1}{m_{uf}}(f_4 - u_f) + \alpha_1^2] \tag{5.48}$$

$$\alpha_4 = \frac{-1}{\alpha_r}[\beta(f_{6a} + u_r) + \gamma(f_{6b} + u_r) - \frac{1}{m_{ur}}(f_8 - u_f) + \alpha_3^2] \tag{5.49}$$

Since the constraint equation was differentiated twice to result in an explicit function of the input (u), therefore $p = 2$ and the transformed control input is α_2 that is unconstrained. The resulting front car transformed state equation is modelled by $(n + p)$ dimension state vector:

$$Z \equiv [X, \alpha_f, \alpha_1, .., \alpha_{p-1}]^T \tag{5.50}$$

which results in:

$$\begin{aligned}
z_1 =& \dot{x}_1 = x_2 \\
z_2 =& \dot{x}_2 = \alpha[-K_f x_1 - B_f x_2 + k_f x_3 + B_f x_4 + U_f] \\
&+ \beta[-k_r x_5 - B_r x_6 + k_r x_7 + B_r x_8 + U_r] \\
z_3 =& \dot{x}_3 = x_4 \\
z_4 =& \dot{x}_4 = \frac{1}{m_{uf}}[K_f x_1 + B_f x_2 - (K_f + K_{tf})x_3 - B_f x_4 + K_{tf} x_{rf} - U_f] \\
z_5 =& \dot{x}_5 = x_6 \\
z_6 =& \dot{x}_6 = \beta[-K_f x_1 - B_f x_2 + K_f x_3 + B_f x_4 + U_f] \\
&+ \gamma[-K_r x_5 - B_r x_6 + K_r x_7 + B_r x_8 + U_r] \\
z_7 =& \dot{x}_7 = x_8 \\
z_8 =& \dot{x}_8 = \frac{1}{m_{ur}}[K_r x_5 + B_r x_6 - (K_r + K_{tr})x_7 - B_r x_8 + K_{tr} x_{rr} - U_r] \\
z_9 =& \alpha_f \\
z_{10} =& \dot{\alpha}_f = \alpha_1 \\
z_{11} =& \alpha_r \\
z_{12} =& \dot{\alpha}_r = \alpha_3
\end{aligned} \tag{5.51}$$

The rear suspension system is computed to obtain α_r and α_3 and the new input α_4.

5.6.2 State initial conditions

Now to solve for the initial conditions t_0 for the additional states: $\alpha_f, \quad \alpha_1 \quad and \quad \alpha_2$:

$$\alpha_f = (-2(x_{sd}))^{\frac{1}{2}} = -2(x_3 - x_1)^{\frac{1}{2}} \tag{5.52}$$

And:

$$\alpha_1(t_0) = \frac{g(x_0, t0)}{x_o} \tag{5.53}$$

$$\alpha_1(t_0) = \frac{\dot{x}_3 - \dot{x}_1}{-2(x_3 - x_1)^{\frac{1}{2}}} \tag{5.54}$$

And:

$$\alpha_2(t_0) = \frac{1}{\alpha_0}[g_2(x_0)(t_0) + \alpha_1^2(t_0)] \tag{5.55}$$

$$\alpha_2(t_0) = \frac{1}{(-2(x_3 - x_1)^{\frac{1}{2}})}[(\ddot{x}_3 - \ddot{x}_1)(t_0) + \alpha_1^2(t_0)] \tag{5.56}$$

$$\alpha_2(t_0) = \frac{1}{\alpha_0}[(\ddot{x}_3 - \ddot{x}_1)(t_0) + (\frac{\dot{x}_3 - \dot{x}_1}{-2(x_3 - x_1)^{\frac{1}{2}}})^2] \tag{5.57}$$

5.6.3 Slack methodology transformed performance index

The performance index of the transformed system on the suspension system is modelled through:

$$\begin{aligned} V(z, \alpha_p, t) =& q_f x_1^2 + q_r x_5^2 + \frac{1}{2}[\frac{-1}{\alpha - \frac{1}{m_{uf}}}[\alpha_1^2 + \alpha_f \alpha_2 - \frac{1}{m_{uf}} f_4 + \alpha f_{2a} + \beta(f_{2b} + u_r)]]^2 \\ &+ \frac{1}{2}[\frac{-1}{\beta - \frac{1}{m_{ur}}}[\alpha_3^2 + \alpha_r \alpha_4 - \frac{1}{m_{ur}} f_8 + \beta f_{6a} + \gamma(f_{6b} + u_f)]]^2 \end{aligned} \tag{5.58}$$

Therefore the performance index for the transformed half-car system is:

$$J = \int_{t_0}^{t_f} V(z, \alpha_p, t)dt \tag{5.59}$$

$$\begin{aligned} J = \int_{t_0}^{t_f} & q_f x_1^2 + q_r x_5^2 + \frac{1}{2}[\frac{-1}{\alpha - \frac{1}{m_{u_f}}}[\alpha_1^2 + \alpha_f \alpha_2 - \frac{1}{m_{uf}} f_4 + \alpha f_{2a} + \beta(f_{2b} + u_r)]]^2 \\ & + \frac{1}{2}[\frac{-1}{\beta - \frac{1}{m_{u_r}}}[\alpha_3^2 + \alpha_r \alpha_4 - \frac{1}{m_{ur}} f_8 + \beta f_{6a} + \gamma(f_{6b} + u_f)]]^2 dt \end{aligned} \tag{5.60}$$

5.6.4 Slack-based Hamiltonian and co-states

Based on the state transformation due to the slack methodology:

$$\dot{z} = F(Z, \alpha_p, t), \quad Z(t_0) = Z_0 \tag{5.61}$$

The optimal control Hamiltonian formulation is: $\mathcal{H} = V + \lambda_{(n+p)}^T F(z)$, where λ is $(n+p)$ dimensional lagrange multiplier. The Hamiltonian is then defined by:

$$\begin{aligned} \mathcal{H} = & q_f x_1^2 + q_r x_5^2 + \frac{1}{2}[\frac{-1}{\alpha - \frac{1}{m_{u_f}}}[\alpha_1^2 + \alpha_f \alpha_2 - \frac{1}{m_{uf}} f_4 + \alpha f_{2a} + \beta(f_{2b} + u_r)]]^2 \\ & + \frac{1}{2}[\frac{-1}{\beta - \frac{1}{m_{u_r}}}[\alpha_3^2 + \alpha_r \alpha_4 - \frac{1}{m_{ur}} f_8 + \beta f_{6a} + \gamma(f_{6b} + u_f)]]^2 \\ & + \lambda_{(n+p)}^T [\dot{x}_1, \dot{x}_2, .., \alpha_{0f}, \alpha_1, \alpha_{0r}, \alpha_3] \end{aligned} \tag{5.62}$$

At this point, the suspension system co-dependence resulting from the pitch dynamics between the front and rear sub-systems leads to limitations in the slack variable methodology as it cannot solve for two control inputs (α_f) and (α_r). To address the limitation to the application of slack to the MIMO system the optimal control solution will assume weak coupling between the two sub-systems therefore solve for the front and rear system as decoupled systems. The Hamiltonian is then modelled by:

$$\begin{aligned}\mathcal{H} =& q_f x_1^2 + q_r x_5^2 + (\frac{1}{2}[(\frac{M_{uf}M_{sf}}{M_{sf}+M_{uf}})^2(\alpha_1^4 + 2\alpha_1^2\alpha_f\alpha_2 + 2\alpha_1^2 f_2 + 3\alpha_1^2 f_4 \\ &+ \alpha_f^2\alpha_2^2 + f_2^2 + f_4^2 + \alpha_1^2 f_2 + 2f_2\alpha_f\alpha_2 + 2f_4\alpha_f\alpha_2)] + \frac{1}{2}[(\frac{M_{ur}M_{sf}}{M_{sf}+M_{ur}})^2(\alpha_3^4 \\ &+ 2\alpha_3^2\alpha_r\alpha_4 + 2\alpha_3^2 f_6 + 3\alpha_3^2 f_8 + \alpha_r^2\alpha_4^2 + f_6^2 + f_8^2 + \alpha_3^2 f_6 + 2f_6\alpha_r\alpha_4 + 2f_8\alpha_r\alpha_4)] \\ &+ \lambda_{(n+p)}^T[\dot{x}_1, \dot{x}_2, .., \alpha_{0f}, \alpha_1, \alpha_{0r}, \alpha_3] \end{aligned} \tag{5.63}$$

Expanding the Hamiltonian results in function $\mathcal{H}$ as:

$$\begin{aligned}\mathcal{H} =& q_f x_1^2 + q_r x_5^2 + (\frac{1}{2}[(\frac{M_{uf}M_{sf}}{M_{sf}+M_{uf}})^2(\alpha_1^4 + 2\alpha_1^2\alpha_f\alpha_2 + 2\alpha_1^2 f_2 + 3\alpha_1^2 f_4 \\ &+ \alpha_f^2\alpha_2^2 + f_2^2 + f_4^2 + \alpha_1^2 f_2 + 2f_2\alpha_f\alpha_2 + 2f_4\alpha_f\alpha_2)] + \frac{1}{2}[(\frac{M_{ur}M_{sf}}{M_{sf}+M_{ur}})^2 \\ &(\alpha_3^4 + 2\alpha_3^2\alpha_r\alpha_4 + 2\alpha_3^2 f_6 + 3\alpha_3^2 f_8 + \alpha_r^2\alpha_4^2 + f_6^2 + f_8^2 + \alpha_3^2 f_6 + 2f_6\alpha_r\alpha_4 \\ &+ 2f_8\alpha_r\alpha_4)] + \lambda_1 x_2 + \lambda_2\alpha[-k_f x_1 - B_f x_2 + k_f x_3 + B_f x_4 + \frac{1}{2}[\frac{M_{uf}M_{sf}}{M_{sf}+M_{uf}} \\ &(\alpha_1^2 + \alpha_f\alpha_2 + f_2 + f_4)] + \lambda_2\beta[-k_r x_5 - B_r x_6 + k_r x_7 + B_r x_8 \\ &+ \frac{1}{2}[\frac{M_{uf}M_{sf}}{M_{sf}+M_{uf}}(\alpha_1^2 + \alpha_f\alpha_2 + f_2 + f_4)] + \lambda_3 x_4 + \frac{\lambda_4}{m_{uf}}[k_f x_1 + B_f x_2 \\ &- (k_f + K_{tf})x_3 - B_f x_4 + K_{tf} x_{rf} - \frac{1}{2}[\frac{M_{ur}M_{sr}}{M_{sr}+M_{ur}}(\alpha_3^2 + \alpha_r\alpha_4 + f_2 + f_4)] \\ &+ \lambda_5 x_6 + \lambda_6\beta[-k_f x_1 - B_f x_2 + k_f x_3 + b_f x_3 - B_f x_4 + U_f] + \lambda_6\gamma[-k_r x_5 \\ &- B_r x_6 + k_r x_7 + B_r x_8 + U_r] + \lambda_7 x_8 + \frac{\lambda_8}{m_{ur}}[k_r x_5 + B_r x_6 - (k_r + K_{tr})x_7 - B_r x_8 \\ &+ K_{tr} x_{rr} - \frac{1}{2}[\frac{M_{uf}M_{sf}}{M_s + M_{ur}}(\alpha_3^2 + \alpha_r\alpha_4 + f_2 + f_4)] + \lambda_9\alpha_f + \lambda_{10}\alpha_1 + \lambda_{11}\alpha_r + \lambda_{12}\alpha_3] \end{aligned} \tag{5.64}$$

where: $M = \frac{M_{uf}M_{sf}}{M_{sf}+M_{uf}}$. The slack-based optimal control co-state equation is:

$$\dot{\lambda} = -(\frac{\partial H}{\partial z}) \tag{5.65}$$

The co-state computation for the half-car is:

$$\begin{aligned}
\dot{\lambda}_1 &= -\frac{\partial \mathcal{H}}{\partial x_1} = -[2k_f x_1 - \alpha\lambda_2 k_f + \frac{\lambda_4}{m_{uf}}k_f - \lambda_6\beta k_f - 3\frac{k_s}{m_s} + 3\frac{k_s}{m_u f}] \\
\dot{\lambda}_2 &= -\frac{\partial \mathcal{H}}{\partial x_2} = -[\lambda_1 - \alpha\lambda_2 B_f + \frac{\lambda_4}{m_{uf}}B_f - \lambda_6\beta B_f - \frac{3B_f}{m_s} + \frac{3B_f}{m_{uf}}] \\
\dot{\lambda}_3 &= -\frac{\partial \mathcal{H}}{\partial x_3} = -[\alpha\lambda_2 k_f - \frac{\lambda_4}{m_{uf}}(k_f + K_{tf}) + \lambda_6\beta k_f + 3\frac{k_f}{m_s} - 3\frac{(k_s + k_u)}{m_{uf}}] \\
\dot{\lambda}_4 &= -\frac{\partial \mathcal{H}}{\partial x_4} = -[\lambda_3 + \alpha\lambda_2 B_f - \frac{\lambda_4}{m_{uf}}B_f + \lambda_6\beta B_f + \frac{3B_f}{m_s} - \frac{3B_f}{m_{uf}}] \\
\dot{\lambda}_5 &= -\frac{\partial \mathcal{H}}{\partial x_5} = -[2k_r x_5 - \beta\lambda_2 k_r + \frac{\lambda_8}{m_{ur}}k_r - \lambda_6\gamma k_r - 3\frac{k_r}{m_s} + 3\frac{k_r}{m_u r}] \\
\dot{\lambda}_6 &= -\frac{\partial \mathcal{H}}{\partial x_6} = -[\lambda_5 - \beta\lambda_2 B_r + \frac{\lambda_8}{m_{ur}}B_r - \lambda_6\gamma B_r - 3\frac{B_r}{m_s} + 3\frac{B_r}{m_{ur}}] \\
\dot{\lambda}_7 &= -\frac{\partial \mathcal{H}}{\partial x_7} = -[\beta\lambda_2 k_r - \frac{\lambda_8}{m_{ur}}(k_r + K_{tr}) + \lambda_6\gamma k_r + 3\frac{k_r}{m_s} - 3\frac{(k_r + k_u)}{m_{ur}}] \\
\dot{\lambda}_8 &= -\frac{\partial \mathcal{H}}{\partial x_8} = -[\lambda_7 + \beta\lambda_2 B_r - \frac{\lambda_8}{m_{ur}}B_r + \lambda_6\beta B_r + \frac{3B_r}{m_s} - \frac{3B_r}{m_{ur}}] \\
\dot{\lambda}_9 &= -\frac{\partial \mathcal{H}}{\partial \alpha_f} = \frac{1}{2}M^2(2\alpha_1^2\alpha_2 + 2\alpha_2^2 + 2f_2\alpha_2 + 2f_4\alpha_2) + \lambda_9 + M\alpha_2 \\
\dot{\lambda}_{10} &= -\frac{\partial \mathcal{H}}{\partial \alpha_1} = \frac{1}{2}M^2(4\alpha_1^3 + 4\alpha_1\alpha_f\alpha_2 + 4\alpha_1 f_2 + 10\alpha_1 f_4) + \lambda_{10} + M^2\alpha_1 \\
\dot{\lambda}_{11} &= -\frac{\partial \mathcal{H}}{\partial \alpha_r} = \frac{1}{2}M^2(2\alpha_3^2\alpha_4 + 2\alpha_4^2 + 2f_6\alpha_4 + 2f_8\alpha_4) + \lambda_1 1 + M\alpha_4 \\
\dot{\lambda}_{12} &= -\frac{\partial \mathcal{H}}{\partial \alpha 3} = \frac{1}{2}M^2(4\alpha_3^3 + 4\alpha_3\alpha_r\alpha_4 + 4\alpha_3 f_6 + 10\alpha_3 f_8) + \lambda_{12} + M^2\alpha_3
\end{aligned} \tag{5.66}$$

5.6.5 Slack-based optimal control input

The resulting control law is determined from the optimality condition:

$$\frac{\partial \mathcal{H}}{\partial \alpha_p} = 0 \tag{5.67}$$

For the front and the rear parts:

$$\begin{aligned}
\frac{\partial \mathcal{H}}{\partial \alpha_2} &= 2\alpha_1^2\alpha_f + 2\alpha_f^2 f_2^2\alpha_2 + 2f_2\alpha_f + 2f_4\alpha_f + \frac{1}{M}\alpha_f \\
\frac{\partial \mathcal{H}}{\partial \alpha_4} &= 2\alpha_3^2\alpha_r + 2\alpha_r^2 f_6^2\alpha_4 + 2f_6\alpha_r + 2f_8\alpha_r + \frac{1}{M}\alpha_r
\end{aligned} \tag{5.68}$$

Applying eq. 5.67 to eq. 5.68, the front and rear controls laws are:

$$\begin{aligned}
u_{fnew} = \alpha_2 &= \frac{-1}{M^2\alpha_f^2 f_2^2}[2\alpha_1^2\alpha_f + 2f_2\alpha_f + 2f_4\alpha_f + \frac{\alpha_f}{M}] \\
u_{rnew} = \alpha_4 &= \frac{-1}{M^2\alpha_r^2 f_6^2}[2\alpha_3^2\alpha_r + 2f_6\alpha_r + 2f_8\alpha_r + \frac{\alpha_r}{M}]
\end{aligned} \tag{5.69}$$

5.6.6 Simulation testing results

The formulated slack-based controller is simulated as a boundary value problem in Matlab and solved through the use of *bvp4c* solver. The displacement of the front and rear sprung mass indicates an increased reduction in the sprung mass attenuation but the signal has more white noise. The signals for the active front and rear displacement for m and $2m$ show that the active response is reduced for both weight conditions.

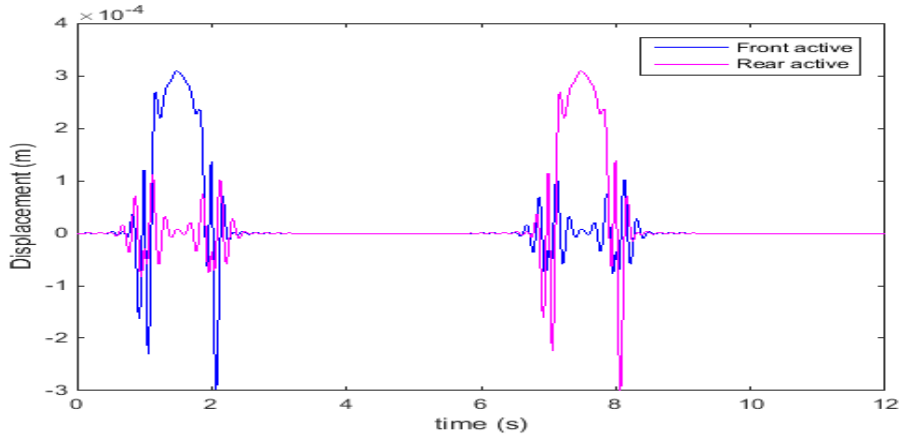

(a) Mass=m

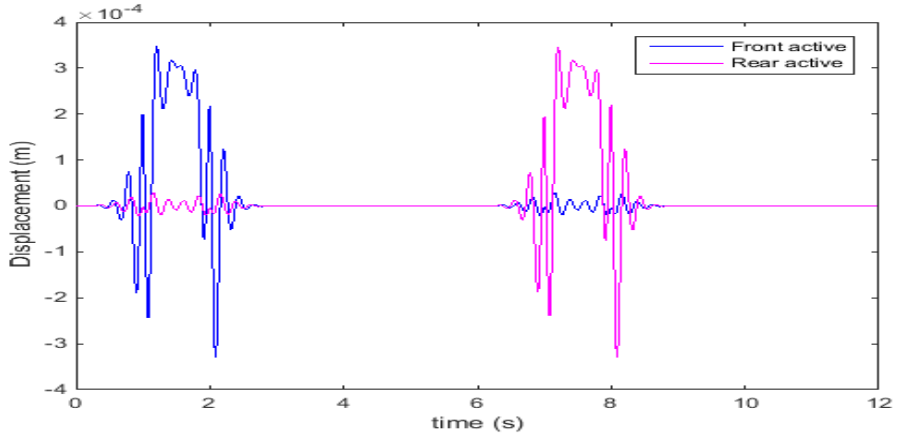

(b) Mass=$2m$

Figure 5.9: Front and rear active displacement

The displacement plots show that there is a reduction in attenuation, similarly to the penalty function. Therefore, this trend is expected with the acceleration, cost function and the performance index.

5.6.7 Discussion on slack variable method

The slack variable methodology is applied to the half-car state constrained optimal control, to address the limitations in the practical simulation of the penalty function. Although this methodology results in feasible computational solutions, it has limitations due to changes in the original u, since the bounds of u, cannot be violated by the resulting control input α_p. As seen in the application of the half-car suspension system, strong coupling of the front and rear suspension system results in complications due to the slack variable method limited in handling more than one control variable affecting a state constraint.

5.7 Summary of state constrained based optimal control

This section motivated a need for optimizing the amount of energy consumed by active suspension systems. An optimal control method was proposed which minimizes the suspension energy composed of the control signal and the car body displacement. The controller was evaluated for a half-car suspension model. The optimal controller demonstrated energy reduction as it can be seen in Fig. 5.2, Fig. 5.3 and Fig. 5.9(b), through the defined performance index. The formulation successfully caters for the suspension rattle space physical limitations and ensures an optimised control input.

A penalty function methodology models for the pitch dynamics within the half-car suspension system which are usually overlooked. This allowed for the demonstration of the front and rear controllers as they counteract the disturbances propagated by the pitch motion. The solution also assumes that the road profile is deterministic, whereas practically, road disturbances are a pseudo random phenomenon which can be best modelled as a stochastic input. However, the results show that the energy composed in the control signal and the sprung body displacements can be significantly minimized. The focus of the analysis is to measure the road disturbance attenuation for different masses and for the control technique to be able to perform at different masses. This is more evident when comparing the passive and the active performance indices as this eliminates the need of compensating for lost energy since only a necessary amount is used. To further extend the formulation of state

constrained optimal control, singular value decomposition-based Kalman filter is recommended as it allow for the updating and prediction of the system's states in order to have a good estimation of the system's dynamic behaviour.

The trade-offs between the penalty function and the slack-variable methodology can be observed through the analysis of the practical limitations of each methodology. Further recommendations of this work would be analysing how to create a hybrid system based on both methodologies to address the discussed limitations. Since the application of the optimal control procedure on the non-linearised half-car suspension system was solved using the Hamiltonian optimal condition, this led to a mathematical model with a relatively complex system of ordinary differential equations (ODE) with a set of boundary conditions. Solving complex ODEs typically requires a lot of computational power. Thus, such a system will have challenges when being run online due to the computational limitations such as lag or latency, which is subject to the computing hardware. To address this challenge the next chapter will analyse applying the state constrained optimal control on the linearised half-car suspension system.

Chapter 6

Optimal control on the feedback linearised suspension system

6.1 Introduction

The active vehicle suspension system consists of highly non-linear components such as springs and dampers. The non-linear elements make it challenging to apply linear control techniques. Linear controllers are preffered as they result in reduced computational challenges since they do not involve the computation of complex non-linear models. To enable the use of linear controllers on highly non-linear constructed systems, the non-linear system has to be transformed to its equivalent linear system. In the control field, one of the commonly applied linearisation techniques is Input Output Feedback Linearisation (IOFBL) [32]. In this chapter, the challenges that come with the practical application of IOFBL are explored to enable the application of state constrained optimal control and negative state feedback on the linearised system. The focus is on highlighting the complexities of IOFBL due to stability analysis of hidden states resulting from the state transformation and handling the state constraints during this transformation. This work demonstrates the adaptation of the conditions for ISFBL to IOFBL so that the transformation results in no hidden states on the half-car suspension system.

CONTRIBUTION 2: *To extend the application of slack variable state constrained optimal control to the completely feedback linearised half-car suspension system at the point of IOFBL and ISFBL equivalency, to enable state constraints transformation without hidden constraints, through:*

1. Demonstrating the complexities of applying IOFBL in MIMO systems as it can result in control and system partitioning, complex computation of hidden states and hidden state stability analysis, for the half-car suspension system
2. Applying-slack based state constrained optimal control on the complete feedback linearised half-car suspension system.

The application of Lie based IOFBL is based on differentiating the mechanical system output (y) until the input (u) appears, the output (y) is assigned to $h(x)$. A typical quarter-car suspension system model results in a Single Input Single Output (SISO) model whereas for the half-car and full-car suspension systems these would require MIMO system analysis. This is due to the wheel of each vehicle resulting in a separate input (road disturbance impact) and output (sprung mass displacement).

6.2 Single input single output system linearisation

Linearisation of SISO systems is relatively direct as there is one output (y) to track. Applying IOFBL to this system implies differentiating the output with respect to time. If the input does not appear after the first differentiation, continue differentiating until the input appears. As modelled in [72], the particular derivative of y is explicitly related to the input as shown in eq. 6.6.

6.2.1 General conditions for SISO IOFBL

Conducting Lie-based IOFBL, for (r) differentiations before the input appears, the governing equations are:

$$\mathbf{y}^{(r)} = L_f^r h(x) + L_g L_f^{r-1} h(x) u \tag{6.1}$$

until:

$$L_g L_f^{(r-1)} h(x) \neq 0 \tag{6.2}$$

The system's relative degree (r) of the transformation represents the number of differentiations prior to the input appearing as shown by eq. 6.2. Strong observability is a necessary condition for state transformation as it ensures that the transformation $T(x)$ is a diffeomorphism. A function $T : \mathbb{R}^n \to \mathbb{R}^n$, defined in a space Ψ, is named a diffeomorphism if it is smooth and if it's inverse T^{-1} exists [31], [72].

Therefore the resulting IOFBL state transformation $T(x)$ is represented by:

$$T(x) = \begin{bmatrix} T_1(x) \\ T_2(x) \\ . \\ T_n(x) \end{bmatrix} = \begin{bmatrix} h(x) \\ L_f h(x) \\ . \\ L_f^{n-i} h(x) \end{bmatrix} = \begin{bmatrix} y \\ \dot{y} \\ . \\ \dot{y}^{(n-i)} \end{bmatrix} \tag{6.3}$$

The new linear input (v) is formulated once the derivative of y is explicitly related to u. The relationship between the original input (u) and the new input (v) from the transformed system, is shown by eq. 6.4 as derived from [72], thereby modelling the feedback control law formulation for a single input.

$$u = \frac{1}{L_g L_f^{n-1} h(x)} - L_f^n h(x) + v \tag{6.4}$$

To illustrate the application and complication that results from this linearisation approach, a quarter suspension system consisting of four original states namely both the displacement of the sprung mass and unsprung mass (x_s, x_u) and their velocities ($\dot{x}_s, \dot{x}_u$). On the quarter-car suspension analysis, the road disturbance experienced by the wheel is modelled as the system's input (u) and the output y is the displacement of the sprung mass (x_s).

6.2.2 Application of SISO IOFBL on a quarter-car

As discussed, the modelling of the quarter-car results in four original states ($x_s, \dot{x}_s, x_u$ and $\dot{x}_u$). The output to be monitored is the displacement of the car's body (x_s).

$$y = h(x) = x_s \tag{6.5}$$

Using Lie-based IOFBL formulation, the first differentiation computation is:

$$\dot{\mathbf{y}} = \frac{\partial h}{\partial \mathbf{x}} \dot{\mathbf{x}} = \frac{\partial h}{\partial \mathbf{x}} f(x) + \frac{\partial h}{\partial \mathbf{x}} g(x) u = L_f h(x) + L_g L_f h(x) u \tag{6.6}$$

Differentiating the suspension system's output once yields:

$$\dot{\mathbf{y}} = \frac{\partial h}{\partial \mathbf{x}} \dot{\mathbf{x}} = \dot{x}_s \tag{6.7}$$

At this stage the input does not appear in the $\dot{x_s}$. Two differentiations are required before the output appears, therefore the relative degree (r) is less than the original number of system states (n) prior to the transformation as shown in eq. 6.8.

$$\ddot{\mathbf{y}} = \ddot{x}_s = \frac{1}{M_s}[k_s(x_s - x_u) + k_{snl}(x_s - x_u)^2 + b_s(\dot{x}_s - \dot{x}_u) + b_{snl}(\dot{x}_s - \dot{x}_u)^2 - M_s g + U] \quad (6.8)$$

Although the non-linear system has four original states ($n = 4$), the transformed system resulted in two controllable states ($r = 2$) which leads to complexities within the IOFBL technique.

6.2.3 Complexity with SISO IOFBL

For a quarter car model the relative degree (r) is two as the output is differentiated twice prior to the input appearing. This implies that they are two external states and two internal states, since there were four original states. To ensure that the developed control law for this linearised system is well-behaved, the internal hidden states have to be tested for stability [73], [74]. Therefore stability analysis is later explored using zero dynamics analysis, to ensure the internal hidden states are bounded and stable.

6.3 Linearisation of MIMO systems

The complexity of linearisation increases as one deals with multi-varied non-linear systems. For the integration of the analysis of the different sub-systems that conglomerately produce the main system, one has to consider different dynamics for each of the different sub-systems. The state variables resulting from MIMO system modelling and their interdependence introduces the next level of challenges within feedback linearisation. Similarly to the SISO system, the conditions for MIMO systems have to be met to achieve a valid state transformation.

6.3.1 General linearisation formulation for MIMO systems

The Lie derivative-based feedback linearisation for MIMO states that each of the outputs should be derivative until its corresponding input appears.

For a system with i independent outputs and j corresponding inputs the feedback linearisation output-input relationship is modelled by:

$$\dot{\mathbf{y}} = \begin{bmatrix} y_1^{(r_i)} \\ ... \\ y_m^{(r_m)} \end{bmatrix} = \begin{bmatrix} {L_f}^r h_1(x) \\ ... \\ {L_f}^{r_m} h_m(x) \end{bmatrix} + E(x)u \tag{6.9}$$

In-terms of the input, it can be written as:

$$u = E^{-1} \begin{bmatrix} v_t - L_f^{r_i} h_i(x) \\ ... \\ v_m - L_f^{r_m} h_m(x) \end{bmatrix} \tag{6.10}$$

resulting in m equations of the form $y_i^{(r_i)} = v_i$ as modelled in [72]. Since the input v_i only impacts y_i, this results in the decoupling matrix. If $(r < n)$ then the linearisation transforms n original states to w states that compose of the n external states and $n - r$ hidden states. Therefore the transformed system can be represented by σ_{n-r}.

The transformed system can be represented by: $w = [w_r \quad \sigma_{n-r}]^T$. To enable the Lie derivative to capture the interdependence within the sub-system dynamics and their control dynamics, the challenge of partitioning rises, if the problem is not treated as if each sub-system is operating independently. The limitation of treating the MIMO as one system is that complex manifold analysis would be required to analyse the resulting computations as demonstrated by attempts on system and control partitioning.

6.3.2 System and control partitioning

Two partitioning methodologies are explored to highlight the limitations of Lie derivative analysis when applied to MIMO systems with strong coupling of the rear and front sub-system. The first methodology explores partitioning the non-linear system matrix $\mathbf{f}$ whereas the second methodology is on partitioning of the control matrix $\mathbf{g}$ advanced manifold analysis to evaluate the Lie algebra across a different basis as described in [75] and [76].

Partitioning the non-linear system matrix for the half-car suspension system results in $\mathbf{f} = [f_f \ f_r]^T$ where f_f and f_r are the non-linear system equations for the front and rear sub-system respectively. The half-car's control matrix $\mathbf{g}$ is also partitioned

to result in g_1 and g_2. Similarly, the output equation y comprises of the front sub-system's output (y_1) and the rear sub-systems output (y_2) as shown in eq. 6.11.

$$\mathbf{y} = \begin{bmatrix} y_1 \\ y_2 \end{bmatrix} = \begin{bmatrix} h_1(x) \\ h_2(x) \end{bmatrix} \tag{6.11}$$

Method 1: Partitioning of the system matrix

The MIMO system Lie notation-based FBL requires the differentiation of the output until the original system input appears. Therefore the first derivative of the output (y) is shown in eq. 6.13, for the partitioned system matrix $\mathbf{f}$ and output $\mathbf{y}$. Since:

$$\dot{\mathbf{y}} = L_{\mathbf{f}}h(x) + L_{\mathbf{g}}h(x)u \tag{6.12}$$

Therefore, partitioning the system matrix:

$$\dot{\mathbf{y}} = \begin{bmatrix} \dot{y}_1 \\ \dot{y}_2 \end{bmatrix} = \begin{bmatrix} L_{f_1}h_1 + L_g h_1 u_1 \\ L_{f_2}h_2 + L_g h_2 u_2 \end{bmatrix} = \begin{bmatrix} L_{f_1}h_1 \\ L_{f_2}h_2 \end{bmatrix} \tag{6.13}$$

For the half-car suspension system, the inputs u_f and u_r do not appear in 6.13, therefore the relative degree (r_i) is not equal to one. Now computing the second derivative of the output with matrices [f] partitioned results in eq. 6.14. For a state vector partitioned into two spaces $\dot{\mathbf{x}_1}$ and $\dot{\mathbf{x}}_2$ we obtain a $\ddot{y}$ equation eq. 6.14, which expands to 6.15.

$$\ddot{\mathbf{y}} = \begin{bmatrix} \frac{\partial L_{f_1}h_1}{\partial \mathbf{x_1}}\dot{\mathbf{x}_1} + \frac{\partial L_{f_1}h_1}{\partial \mathbf{x_2}}\dot{\mathbf{x}}_2 \\ \frac{\partial L_{f_2}h_2}{\partial \mathbf{x}_1}\dot{\mathbf{x}}_1 + \frac{\partial L_{f_2}h_2}{\partial \mathbf{x}_2}\dot{\mathbf{x}_2} \end{bmatrix} \tag{6.14}$$

$$\ddot{\mathbf{y}} = \begin{bmatrix} L_{f_1}h_1 + L_g L_{f_1}h_1 u1 & L_{f_2}L_{f_1}h_1 + L_g L_{f_1}h_1 u_2 \\ L_{f_1}L_{f_2}h_2 + L_g L_{f_2}h_2 u_1 & L_{f_2}h_2 + L_g L_{f_2}h_2 u_2 \end{bmatrix} \tag{6.15}$$

The computation of $\ddot{y}$ when the $\mathbf{f}$ matrix is partitioned results in necessity of computing the $L_{f_1}L_{f_2}h_2$ and $L_{f_2}L_{f_1}h_1$ which are in different vector bases. This computation would require advanced manifold analysis,[75], therefore an alternative method is sought.

Particularly for MIMO IOFBL for partitioned system matrix with a relative degree $(r_i) > 1$ requires an alternative method. Therefore the partitioning of the control matrix g to $[g_1\ g_2]^T$ is computed to check if it would result in less complex analysis for linearisation of MIMO systems with inter-dependent sub-systems.

Method 2: Partitioning the control matrix

Partitioning only the control matrix ($\mathbf{g}$) and leaving the non-linear system matrix un-partitioned will result in eq. 6.17. Computing the 1^{st} derivative of the output equation (y) yields eq. 6.16. Since the system input does not appear in eq. 6.17, therefore the second derivative $\ddot{y}$ is eq. 6.18.

$$\dot{\mathbf{y}} = \begin{bmatrix} \dot{y_1} \\ \dot{y_2} \end{bmatrix} \begin{bmatrix} \frac{\partial h_1}{\partial \mathbf{x}} \dot{\mathbf{x}} \\ \frac{\partial h_2}{\partial \mathbf{x}} \dot{\mathbf{x}} \end{bmatrix} \tag{6.16}$$

$$\dot{\mathbf{y}} = \begin{bmatrix} \frac{\partial h_1}{\partial \mathbf{x}} \mathbf{f} + \frac{\partial h_1}{\partial \mathbf{x}} g_1 u_1 + \frac{\partial h_1}{\partial \mathbf{x}} g_2 u_2 \\ \frac{\partial h_2}{\partial \mathbf{x}} \mathbf{f} + \frac{\partial h_2}{\partial \mathbf{x}} g_1 u_1 + \frac{\partial h_2}{\partial \mathbf{x}} g_2 u_2 \end{bmatrix} = \begin{bmatrix} L_{\mathbf{f}} h_1 \\ L_{\mathbf{f}} h_2 \end{bmatrix} \tag{6.17}$$

$$\ddot{\mathbf{y}} = \begin{bmatrix} \dot{L_{\mathbf{f}} h_1} \\ \dot{L_{\mathbf{f}} h_2} \end{bmatrix} = \begin{bmatrix} {L_{\mathbf{f}}}^2 h_1 + L_{g_1} L_{\mathbf{f}} h_1 u_1 + L_{g_2} L_{\mathbf{f}} h_1 u_2 \\ {L_{\mathbf{f}}}^2 h_2 + L_{g_1} L_{\mathbf{f}} h_2 u_1 + L_{g_2} L_{\mathbf{f}} h_2 u_2 \end{bmatrix} \tag{6.18}$$

Partitioning both the system and control matrix led to the necessity of computing mathematical equations in different bases. While manifold analysis allows for such analysis through pull back functions across tangent spaces, this mathematical analysis is complex [77], [78]. Thus for systems with a relative degree (r_i) that is greater than one, linearising for a partitioned system matrix gets extremely cumbersome.

This sub-section demonstrated the complexities introduced by MIMO systems for linearisation of the decoupling matrix invertibility through control matrix re-partitioning. The approach to the linearisation of MIMO systems would involve the complexities of partitioning the MIMO system which is not necessary for SISO systems due to its dynamics. Therefore to simplify the MIMO system analysis, this work will utilise the fact that the constructed system is weakly coupled between the front and rear sub-systems, therefore each sub-system can be linearised as a separate system and the integration will only occur based on the results from the linearisation of each sub system. Applying this to the constructed half-car model, the front sub-system

($y = x_{sf}$ and $u = u_f$) car linearisation analysis will be independently computed to the rear sub-system ($y = x_{sr}$ and $u = u_r$).

6.3.3 Front sub-system IOFBL analysis

Computing the Lie analysis for the front sub-system of the half-car model, the output (y_1) is assigned to the front spring mass displacement x_{sf} as shown by eq. 6.19.

$$y_1 = x_{sf} = h_1(x) \tag{6.19}$$

Applying the Lie notation principles where the outputs are differentiated until the input appears, in the first derivative of the outputs the input does not appear as shown in eq. 6.20.

$$\dot{y}_1 = L_{\mathbf{f}} h_1 = \dot{x}_{sf} \tag{6.20}$$

Differentiating the output y_1 twice yields eq. 6.20. The front input u_f appears after the second differentiation of the output therefore the relative degree is two.

$$\ddot{y_1} = L_{\mathbf{f}}^2 h_1 = L_{\mathbf{f}}(\nabla x_1 \mathbf{f}) = L_{\mathbf{f}} x_2 = \nabla x_2 \mathbf{f} = f_2 \tag{6.21}$$

$$\begin{aligned}\ddot{y}_1 = \ddot{x}_{sf} = 1/m_s[&-K_f(x_{sf} - x_{uf}) - K_{f_{nl}}(x_{sf} - x_{uf})^2 - B_f(\dot{x}_{sf} - \dot{x}_{uf}) \\ &- B_{f_{nl}}(\dot{x}_{sf} - \dot{x}_{uf})^2 - K_r(x_{sr} - x_{ur}) - K_{rnl}(x_{sr} - x_{ur})^2 - B_r(\dot{x}_{sr} - \dot{x}_{ur}) \\ &- B_{rnl}(\dot{x}_{sr} - \dot{x}_{ur})^2 + u_f + u_r] - M_s g - a M_s \ddot{\theta}\end{aligned} \tag{6.22}$$

and the $L_{gj} L_{fi}^{r-1} h_i(x)$ terms are:

$$L_{g_1} L_{\mathbf{f}} h_1 = L_{g_1} h_1 \mathbf{f} = L_{g_1} \nabla x_1 \mathbf{f} = L_{g_1} x_2 = \nabla x_2 g_1 = \frac{1}{M_{sf}} \tag{6.23}$$

$$L_{g_2} L_{\mathbf{f}} h_1 = L_{g_2} \nabla x_2 g_2 = L_{g_2} x_2 = \nabla x_2 g_2 = 0 \tag{6.24}$$

Therefore the resulting linearised system is:

$$u_1 = M_{sf}(v_1 - f_2) \tag{6.25}$$

Therefore the control equations are shown by 6.26:

$$v_1 = \frac{u_1}{M_{sf}} + f_2 \tag{6.26}$$

The state transformation for the front sub-system resulted in a linear system with relative degree two. Therefore there are two hidden states, whose stability should be verified through zero dynamic analysis. To complete the analysis of the half car model similar analysis has to be conducted for the rear sub-system.

6.3.4 Rear sub-system IOFBL analysis

Similarly, computing the Lie analysis for the rear sub-system of the half car model, the output y_2 is assigned to the rear spring mass displacement x_{sr} shown in eq. 6.27.

$$y_2 = h_2(x) = x_{sr} \tag{6.27}$$

$$\dot{y}_2 = L_{\mathbf{f}} h_2 = \dot{x}_{sr} \tag{6.28}$$

The input appears in $\ddot{x}_{sr}$ as shown by eq. 6.27, therefore the output differentiation is computed twice and the relative degree (r_i) is two. Eq. 6.28 shows the results from differentiating the output twice.

$$\ddot{y}_2 = L_{\mathbf{f}}^2 h_2 = L_{\mathbf{f}}(\nabla x_5 \mathbf{f}) = L_{\mathbf{f}}(x_6) = \nabla x_6 \mathbf{f} = f_6 \tag{6.29}$$

and the $L_{gj} L_{fi}^{r-1} h_i(x)$ terms are:

$$L_{g_2} L_{\mathbf{f}} h_2 = L_{g_2} \nabla h_2 \mathbf{f} = L_{g_2} \nabla x_{sr} = L_{g_2} x_6 = \frac{1}{M_{sr}} \tag{6.30}$$

$$L_{g_1} L_{\mathbf{f}} h_2 = L_{g_1} \nabla h_2 g_2 = L_{g_1} \nabla x_{sr} g_2 = L_{g_1} x_6 = 0 \tag{6.31}$$

The system has a total relative degree of 4 since both the front and rear Lie derivatives result in a r_i of 2. Therefore the control equations are shown by eq. 6.34.

$$\ddot{\mathbf{y}} = \begin{bmatrix} \ddot{y}_1 \\ \ddot{y}_2 \end{bmatrix} = \begin{bmatrix} f_2 \\ f_6 \end{bmatrix} + \begin{bmatrix} \frac{1}{M_{sf}} & 0 \\ 0 & \frac{1}{M_{sr}} \end{bmatrix} \begin{bmatrix} u_1 \\ u_2 \end{bmatrix} = \begin{bmatrix} v_1 \\ v_2 \end{bmatrix} \tag{6.32}$$

$$u_2 = M_{sr}(v_2 - f_6) \tag{6.33}$$

$$v_2 = \frac{u_2}{M_{sr}} + f_6 \tag{6.34}$$

Both the front and rear sub-systems resulted in a combined relative degree (r) of four, as opposed to the eight states from the non-linear system. The behaviour of the four new states that resulted from the linearisation system can be observed and controlled for tracking control. However, the challenge rises with the $(n-r)$ internal hidden states whose behaviour is unknown. If these hidden states prove to be stable the system will be minimum phase and the state transformation is valid, whereas if hidden states are unstable, the system would be non-minimum phase.

6.4 Stability analysis on hidden states

As discussed, stability analysis is paramount to verify the behaviour of the hidden states. In a case where the hidden states are stable *(minimum phase system)*,the linearised system can be fully controlled. Just assuming that the hidden states are stable, without adequate analysis, might result in partly or no tracking control. The state transformation can be represented by eq. 6.35, where ψ represents the known new states and ϕ represents the hidden states resulting from a system with $n = 8$ and $r = 4$.

$$T = [\psi_{1f} \quad \psi_{2f} \quad \phi_{1f} \quad \phi_{2f} \quad \psi_{1r} \quad \psi_{2r} \quad \phi_{1r} \quad \phi_{2r}] \tag{6.35}$$

6.4.1 Hidden states analysis

Since the new transformed states with a total relative degree (r_t) are less than the original system states (n), the difference $(n - r_t)$ is the system's internal dynamics. Since these dynamics cannot be controlled by the designed linear controller, it is important to ensure that these hidden states are bounded and not causing the system instabilities as discussed in [79], [80] and [81]. To obtain the hidden states ϕ_{1f}, ϕ_{2f}, ϕ_{1r} and ϕ_{2r}, compute the states that will meet the definition for state transformation:

$$\nabla\phi_1 \begin{bmatrix} 0 & \frac{1}{M_{sf}} & 0 & \frac{-1}{M_{uf}} & 0 & \frac{1}{M_{sr}} & 0 & \frac{-1}{M_{ur}} \end{bmatrix}^T = 0 \tag{6.36}$$

The candidate hidden states (ϕ_{1f}) and (ϕ_{2f}) are:

$$\phi_{1f} = x_{uf} + \frac{m_{uf}}{m_{sf}}\dot{x}_{uf} \tag{6.37}$$

$$\phi_{2f} = \dot{x}_{uf} + \frac{m_uf}{m_sf}\ddot{x}_{uf} \tag{6.38}$$

Similarly for the rear sub-system: The candidate hidden states (ϕ_{1r}) and (ϕ_{2r}) are:

$$\phi_{1f} = x_{ur} + \frac{m_{ur}}{m_{sr}}\dot{x}_{ur} \tag{6.39}$$

$$\phi_{2r} = \dot{x}_{ur} + \frac{m_{ur}}{m_s r}\ddot{x}_{ur} \tag{6.40}$$

For the transformation to be valid, the Jacobian matrix $\frac{\partial w}{\partial x}$ must not be singular therefore the inverse must exist. To obtain the Jacobian:

$$J = \frac{\partial w_i}{\partial x_i} = \begin{bmatrix} 0 & 0 & k_{wf} & 0 & 0 & 0 & k_{wr} & 0 \\ 0 & 0 & 0 & k_{wf} & 0 & 0 & 0 & k_{wr} \\ 0 & 1 & 0 & \frac{m_{uf}}{m_{sf}} & 0 & 1 & 0 & \frac{m_{ur}}{m_{sr}} \\ a & 1 & b & \frac{m_{uf}}{m_{sf}} & c & 1 & d & \frac{m_{ur}}{m_{sr}} \end{bmatrix} \tag{6.41}$$

If the Jacobian shown by eq. 6.41 is non singular there should be no zero rows and columns. Therefore the choice of candidate hidden states is computed so that there are no zero columns. Choosing the candidate solution so that the $\frac{\partial \phi_i}{\partial x_j}$ is a constant non-zero real number enables for a global Jacobian to exist.

6.4.2 Zero dynamics analysis

Zero dynamics analysis is conducted on the hidden states to ensure the stability of the hidden state dynamics. This analysis ensures that the internal states $(n - r)$ remain bounded. Zero dynamics analysis is the process of analysing the system's hidden state dynamics for a particular control input that would result in the output being maintained at zero [79]. The imposed constraint on the output implies that the output's time derivatives will result in zero. The zero dynamics describe motion confined to the $(n - r)$ manifold M_o defined by $M = 0$. For the state x to remain on the manifold surface, the first state of the system $x_{(0)}$ has to exist on the surface. The system's input u must be such that $y^{(r)}(t) = 0$, therefore the initial input is represented by:

$$u_o(x) = -\frac{L_f^r h(x)}{L_g L_f^{r-1} h(x)} \tag{6.42}$$

The dynamics (ϕ_{1f}, ϕ_{2f}, ϕ_{1r} and ϕ_{2r}) are not observable as they are hidden states resulting from the linearisation technique. FBL analysis uses the concept of zero dynamics to establish the behaviour of the internal dynamics of ϕ. A singularity test on $\frac{\partial z}{\partial x}$ is to be conducted to conclude on the global validity of the new linearised

system [32]. For an input of $U_f = 0$ and $U_r = 0$, the output $(x_3 - x_1)$ is zero. When the zeros are stable (left half-plane) the system is termed minimum phase, implying a stable system otherwise it is a non-minimum phase (zeros at the right half plane). The diffeomorphism T: $\mathbb{R}^8 \rightarrow \mathbb{R}^8$ is of the form.

$$\phi x = \begin{bmatrix} T_1 \\ T_2 \\ T_3 \\ T_4 \\ T_5 \\ T_6 \\ T_7 \\ T_8 \end{bmatrix} = \begin{bmatrix} h(x)_f \\ L_f h(x)_f \\ \psi_{1f} \\ \psi_{2f} \\ h(x)_r \\ L_f h(x)_r \\ \psi_{1r} \\ \psi_{2r} \end{bmatrix} = \begin{bmatrix} x_1 \\ x_2 \\ x_3 + \frac{m_{uf}}{m_{sf}} \dot{x}_4 \\ \dot{x_3} + \frac{m_{uf}}{m_{sf}} \ddot{x}_4 \\ x_5 \\ x_6 \\ x_7 + \frac{m_{ur}}{m_{sr}} \dot{x}_8 \\ \dot{x_7} + \frac{m_{ur}}{m_{sr}} \ddot{x}_8 \end{bmatrix} \tag{6.43}$$

Although Lyapunov-based analysis and fibre bundle-based analysis can be applied to prove the stability of the hidden state dynamics, it is often very complex to conduct this analysis for multi-varied systems. Therefore it is necessary to explore feedback linearisation methodologies that would result in a system with no hidden states meaning that the number of states of the linear transformed system would be equal to the number of states of the original non-linear system, $n = r$. To overcome the so far discussed complexities of IOFBL with hidden state analysis and stability analysis, the study will now demonstrate the adoptability of the conditions of feedback linearisation technique termed: Input State Feedback Linearisation, $ISFBL$. The analysis is carried out through analysing the application of this methodology on the half-car suspension system.

6.5 ISFBL conditions applied to IOFBL

The IOFBL analysis computed on the quarter car and the half-car suspension results in hidden states since the number of states for the transformed system is less than the original states. As demonstrated, the computation of these hidden states and the analysis of their stability proves to be tedious. The hidden states can also prove to be unstable, thereby hindering the application of linear controllers to the transformer since there are uncertainties in the behaviour of the internal states. Therefore the limitations of IOFBL become evident as multi-varied coupled systems are incorporated [82], [83]. To address the complexities and limitations of IOFBL, analysis is conducted on adopting the conditions of Input State linearisation so as to guarantee state transformation that will result in no hidden states.

Alternatively to Input Output FBL, Input State FBL can be applied to linearise affine systems [84]. For ISFBL to be applied, the system has to meet two main conditions of controllability and involutivity. When the conditions of ISFBL are applied to IOFBL, it will eliminate the iterative process for choosing the output y that would result in a state transformation with no hidden states. Therefore to establish a relationship between the two feedback linearisation methods, proof of equivalence between the two linearisation methods, and how the conditions for IS can be adopted to solve for IO linearisation, is necessary.

As in [72], applying the proof for equivalence for both methodologies we demonstrate the equivalence between the states and output transformations and also the equivalence in the resulting inputs v for a special condition. The proof also highlights that if a system meets the condition for IS linearisation, the resulting first state z_1 will yield no hidden states if utilised as the output y in IOFBL. Both linearisation methodologies are based on the Frobenius theorem, which states that two vector fields in a distribution are completely integrable if and only if they are involutive [72].

6.5.1 Conditions for input state feedback linearisation

For a system to be input-state linearisable, two conditions have to be satisfied. The first condition is based on the controllability of the system whereas the second condition depends on the involutivity of the non-linear system. A system satisfying these two conditions can be completely feedback linearisable. A non-linear suspension model is in input-state linearisable if there exists a region Ψ so that the vector fields $[\mathbf{g}, ad_f\mathbf{g}, .., ad_f^{(n-1)}]$ are linearly independent in Ψ and also if the set $[g(x), ad_f^g(x), ..., ad_f^{(n-2)}g(x)]$ is involutive [72].

By Frobenius theorem, vector fields are involutive if the Lie bracket of every pair in the particular set is part of the area spanned by all members of the set. The result requires a group of partial differential equations that include derivatives up to order $n-1$, which depends on Frobenius theorem. The required condition for existence of this function results from a rank condition of the vector fields $f(x)$, $g(x)$ and the Lie Brackets [72]. Therefore to perform complete feedback linearisation, conditions for ISFBL must be met.

6.5.2 Overlaps between IOFBL and ISFBL

The relationship between ISFBL and IOFBL is demonstrated in application of the half-car suspension model based on testing for the conditions for involutivity and the Jacobian invertibility. The equivalency transformation summarised and utilised in this section is adopted from [72]. [72] provides the proof for equivalency for ISFBL and IOFBL. In this work, it is then applied and demonstrated on the half-car suspension system. The linearised system is then used for the slack variable optimal control as applied in the previous chapter to the non-linear system.

Involutivity and Jacobian

As discussed, a system can only be input state linearisable if both conditions of controllability and involutivity are met, also a system is input output linearisable if the Jacobian matrix is invertible. Therefore to establish the case of equivalence between the two methodologies, this section elaborates the case of equivalence, as an extension to [72], by showing that an input state linearisable system would result in a non-singular square matrix Jacobian for $h(x) = z_1$. This is conducted through: proving that the involutivity test implies a non-singular, square matrix Jacobian and that the non-singular, square matrix Jacobian will result in an $n = r$ IOFBL.

The involutivity test on the set of vector fields implies that $[\mathbf{f}, \mathbf{g}] = \alpha_1\mathbf{f} + \alpha_2\mathbf{g}$. To prove that z_1 obtained through ISFBL, guarantees IOFBL with no hidden states, the IS linearisable system should meet the condition of controllability and involutivity. Therefore an IS linearisable system has vector fields that are linearly independent and there exists scalar function z_1 satisfying $n-1$ partial differential equations as supported by Frobenius. Therefore when the involutivity condition is met, the first $n-1$ states verify $\dot{z} = z_{k+1}$ for $k = 1..n-1$ as detailed in [72]. The transformation results in an invertible Jacobian. Since by Frobenius theorem an involutive $\mathbf{g}$ ensures that there exists n-1 linearly independent gradient functions ∇T_i which satisfies $\nabla T_i \mathbf{g} = 0$, therefore such a system would have an invertible Jacobian. If the Jacobian is non-singular then $n = r$ for IOFBL. Since $J = \frac{\partial z_i}{\partial x_i}$, therefore a non-singular jacobian matrix implies that there will be no zero columns or rows, therefore no requirement to obtain candidate solution hidden states.

For an affine system that passes the involutivity test: $[g, ad_f g] = \frac{\partial (ad_f g)}{\partial x} g$, the Jacobian is a square matrix and non-singular. To adopt the conditions for ISFBL, it is necessary to demonstrate and prove for equivalence between the $n-1$ resulting

state equation with the output derivatives and also the the n^{th} state being the input equation. The equivalence of the two feedback linearisation methodologies can also be demonstrated through their application formulation. If the Jacobian matrix has $m = n$, then it is a square matrix and its determinant carries significant detail on the local behaviour of the local neighbourhood of a point x, an inverse function that is differentiable if and only if the Jacobian determinant is zero at x.

Demonstration of equivalence on the application of ISFBL and IOFBL

To show the equivalence described by the above proof, this section highlights the similarities within the application of the two methodologies. As discussed, to apply the conditions for ISFBL within IOFBL analysis, the relationship between the two FBL methodologies should be demonstrated. Both feedback linearisation methodologies are based on the Frobenius theorem, which ensures linearly independent gradient functions for the involutive vector field $\mathbf{g}$ satisfying $\nabla h_i \mathbf{g} = 0$ [72].

$$\nabla h_j \mathbf{g} = 0 \quad 1 \leq j \leq n \tag{6.44}$$

Forcing $z_1 = y$, prove that ISFBL transformation holds if $n = r$, through demonstrating that with the transformation $\dot{z} = Az + bv$ meaning:

$$\frac{d}{dt}\begin{bmatrix} y_1 \\ .. \\ y_{n-1} \\ y_n \end{bmatrix} \equiv \begin{bmatrix} z_2 \\ .. \\ z_n \\ f(z) + b(z)v \end{bmatrix} \tag{6.45}$$

where the states $z_2, ..., z_n$ are linearly independent of the input u which is equivalent to:

$$\nabla h(x) a d_f^{n-1} g = (-1)^{n-1} L_g z_n; \quad \nabla h(x) a d_f^{n-1} g \neq 0 \tag{6.46}$$

which meets the transformation criterion $\dot{z}_k = z_{k+1} \quad for \quad k = 1, ...n-1$.

1. *Verify that the ISFBL n-1 state equation is equivalent to IOFBL n-1 output differentiations.*

To demonstrate equivalence, force that the first state z_1 obtained from step 3 of ISFBL is equivalent to the output assigned to $h(x)$ for IOFBL as shown in 6.47.

$$z_1 \quad \equiv \quad h(x) \tag{6.47}$$

The consecutive ISFBL states are computed through the differentiation of the previous state as shown in:

$$\begin{aligned} \dot{z}_1 &= z_2 \\ &.. \\ until : \dot{z}_{n-1} &= z_n \end{aligned} \tag{6.48}$$

Through eq. 6.47 and the derivation of consecutive states in ISFBL, eq. 6.49 can be referred:

$$\begin{aligned} \dot{h}(x) \equiv \dot{z}_1 = z_2 \quad : \quad by \quad IOFBL &= L_f h(x) + L_g L_f h(x) u \\ \ddot{h}(x) \equiv \dot{z}_2 = z_3 \quad : \quad by \quad IOFBL \quad &= L_f^2 h(x) + L_g L_f h(x) u \\ & until : \\ \dot{h}^{n-2}(x) \equiv \dot{z}_{n-2} = z_{n-1} \quad : \quad by \quad IOFBL \quad &= \dot{h}^{n-1}(x) = {L_f}^{n-1} h(x) + L_g L_f^{n-2} h(x) u \end{aligned} \tag{6.49}$$

The $L_g L_f h(x) u$ terms will fall off since by assuming that $n = r$, the input is 0. Therefore: Assigning $z_1 = h(x)$ then:

$$\begin{aligned} L_f z_1 &= L_f h(x) + L_g L_f h(x) u \quad where \quad L_g L_f h(x) u \to 0 \\ L_f^2 z_1 &= L_f^2 h(x) + L_g^2 L_f h(x) u \quad where \quad L_g^2 L_f h(x) u \to 0 \\ Until : L_f^{(n-1)} z_1 &= L_f^{(n-1)} h(x) \quad where \quad L_g L_f^{(n-1)} h(x) u \to 0 \end{aligned} \tag{6.50}$$

2. *Verify that for ISFBL n-1 state equation equivalent to IOFBL n-1 output differentiations.*

Extending this proof to the n_{th} state, this condition can only hold if $n = r$ and the resulting input equation results in:

$$\dot{z}_n = \frac{\partial z_n}{\partial x}(f + gu) = v \tag{6.51}$$

where:

$$\dot{h}^{n-1}(x) \equiv \dot{z}_{n-1} = z_n \tag{6.52}$$

$$u = \frac{-L_f^n h(x)}{L_g L_f^{n-1} h(x)} + \frac{1}{L_g L_f^{n-1} h(x)} v \equiv \alpha(x) + \beta(x) v \tag{6.53}$$

The resulting input clearly shows equivalence between input u from ISFBL and IOFBL. If the system is controllable and involutive, a z_1 that satisfies:

$\nabla T_1 ad_f^i g = 0; \quad i = 1, 2, .., n-2, \quad \nabla T_1 ad_f^{n-1} g \neq 0$ is obtained.

Assume this z_1 to be equivalent to the output for IOFBL $h(x)$ results in a completely feedback linearisation that yields $n = r$ transformation, with the new input $v = z_n$. Therefore if the ISFBL conditions are met it can be implied that there are $n = r$ states for IOFBL. Resulting in the equivalence of the state transformation:

$$z(x) = [z_1, \quad L_f z_1, ..., L_f^{(n-1)} z_1] \equiv [h(x), L_f h(x), ..., L_f^{(n-1)} h(x)] \tag{6.54}$$

As demonstrated there is equivalence between IOFBL and ISFBL for the special case where $y = z_1$, therefore the conditions for ISFBL can be used to address the limitations and complexities of IOFBL. Therefore for a suspension system feedback linearisation will be conducted through ISFBL.

6.5.3 Steps for performing ISFBL

There are four main steps to performing ISFBL, these are characterise by computing $n-1$ vector fields, checking for satisfaction of controllability and involutive conditions, obtaining the first state and finally computing the transformation.

1. Construct the system's vector fields [$\mathbf{g}$, $ad_f\mathbf{g}$,..., $ad_f^{(n-1)}\mathbf{g}$]
2. Verify that the conditions for Input State (IS) are met
3. Obtain the initial state z_1: equivalent to y resulting in $n = r$ for IOFBL
4. Obtain the state and input transformation.

6.5.4 Application of ISFBL on suspension system

To simplify the computation the ISFBL linearisation is demonstrated through the use of a quarter car system with model shown in eq. 6.55. For a weak coupled half-car

suspension test rig, the half-car can be treated as a front and rear quarter-cars, this is done so as to simplify the ISFBL.

$$\begin{bmatrix} \dot{x}_1 \\ \dot{x}_2 \\ \dot{x}_3 \\ \dot{x}_4 \end{bmatrix} = \begin{bmatrix} 0 & 1 & 0 & 0 \\ -\frac{k_s}{m_s} & -\frac{b_s}{m_s} & \frac{k_s}{m_s} & \frac{b_s}{m_s} \\ 0 & 0 & 0 & 1 \\ \frac{k_s}{m_u} & \frac{b_s}{m_u} & \frac{-(k_s+k_u)}{m_u} & -\frac{b_s}{m_u} \end{bmatrix} \begin{bmatrix} x_1 \\ x_2 \\ x_3 \\ x_4 \end{bmatrix} + \begin{bmatrix} 0 \\ \frac{1}{m_s} \\ 0 \\ \frac{-1}{m_u} \end{bmatrix} U_s + \begin{bmatrix} 0 \\ 0 \\ 0 \\ \frac{k_u}{m_u} \end{bmatrix} r \tag{6.55}$$

where: x_1, x_2 are the car's sprung mass displacement and velocity and x_3, x_4 is the unsprung mass displacement and velocity. Note that for the quarter car suspension system $n = 4$. Therefore by IS, there should four new states if the IS conditions are met.

Constructing the vector fields for a quarter car

The construction of the vector fields $\mathbf{g}, ad_f\mathbf{g}$,..., $ad_f^{(n-1)}\mathbf{g}$ is:

The *first vector field* $\mathbf{g}$:

$$\mathbf{g} = \begin{bmatrix} 0 & \frac{1}{M_{sf}} & 0 & \frac{-1}{M_{uf}} \end{bmatrix}^T \tag{6.56}$$

The *second vector field* $ad_f\mathbf{g}$:

$$ad_f\mathbf{g} = [f, g] = L_f g - L_g f = \frac{\partial g}{\partial x} f - \frac{\partial f}{\partial x} g \tag{6.57}$$

but $\frac{\partial g}{\partial x} = 0$ therefore $ad_f g = -L_g f$

$$ad_f\mathbf{g} = -\begin{bmatrix} \frac{1}{M_{sf}} \\ \frac{-B_f}{{M_{sf}}^2} + \frac{B_f}{M_{sf}} \\ \frac{1}{M_{sf}} \\ \frac{B_f}{Ms_f M_{uf}} - \frac{B_f}{{M_{uf}}^2} \end{bmatrix} \tag{6.58}$$

The *third vector field* $ad_f^2\mathbf{g}$:

$$ad_f^2 g = [f, ad_f g] = \frac{\partial (ad_f g)}{\partial x} f - \frac{\partial f}{\partial x}(ad_f g) \tag{6.59}$$

since $\frac{\partial ad_f g}{\partial x} = 0$ therefore $ad_f^2 g = -L_g f^2$

$$ad_f^2\mathbf{g} = \begin{bmatrix} 0 & 1 & 0 & 0 \\ -\frac{k_f}{M_s f} & -\frac{B_f}{M_s} & \frac{k_f}{M_s} & \frac{B_f}{M_s} \\ 0 & 0 & 0 & 1 \\ \frac{k_f}{M_u f} & \frac{B_f}{M_{uf}} & -\frac{k_f+k_t}{M_{uf}} & -\frac{B_f}{M_{uf}} \end{bmatrix} * - \begin{bmatrix} \frac{1}{M_{sf}} \\ \frac{-B_f}{M_{sf}^2} + \frac{B_f}{M_{sf}} \\ \frac{1}{M_{sf}} \\ \frac{B_f}{M s_f M_{uf}} - \frac{B_f}{{M_{uf}}^2} \end{bmatrix} \tag{6.60}$$

$$ad_f^2\mathbf{g} = - \begin{bmatrix} \frac{-B_f}{{M_{sf}}^2} + \frac{B_f}{M_{sf}} \\ \frac{{B_f}^2}{{M_{sf}}^3} - \frac{{B_f}^2}{{M_{sf}}^2} + \frac{B_f}{{M_{sf}}^2 M_{uf}} - \frac{{B_f}^2}{M_{sf} {M_{uf}}^2} \\ \frac{B_f}{M s_f M_{uf}} - \frac{B_f}{{M_{uf}}^2} \\ -\frac{{B_f}^2}{M_{uf} {M_{sf}}^2} + \frac{{B_f}^2}{M_{uf} M_{sf}} - \frac{k_t}{M_{uf} M_{sf}} - \frac{{B_f}^2}{{M_{uf}}^2 M_{sf}} + \frac{{B_f}^2}{M_{uf}} \end{bmatrix} \tag{6.61}$$

To simplify the computations: $M_{sf} = M_{uf} = M$

$$ad_f^2\mathbf{g} = - \begin{bmatrix} \frac{-B_f}{M^2} + \frac{B_f}{M} \\ -\frac{{B_f}^2}{M^2} + \frac{B_f}{M^3} \\ 0 \\ -2\frac{{B_f}^2}{M^3} + \frac{{B_f}^2 - k_t}{M^2} + \frac{{B_f}^2}{M} \end{bmatrix} \tag{6.62}$$

The *fourth vector field* $ad_f^3\mathbf{g}$:

$$ad_f^3\mathbf{g} = [f, ad_f^2 g] \tag{6.63}$$

$$= - \begin{bmatrix} 0 & 1 & 0 & 0 \\ -\frac{k_f}{M_s f} & -\frac{B_f}{M_s} & \frac{k_f}{M_s} & \frac{B_f}{M_s} \\ 0 & 0 & 0 & 1 \\ \frac{k_f}{M_u f} & \frac{B_f}{M_{uf}} & -\frac{k_f+k_t}{M_{uf}} & -\frac{B_f}{M_{uf}} \end{bmatrix} * \begin{bmatrix} \frac{-B_f}{{M_{sf}}^2} + \frac{B_f}{M_{sf}} \\ \frac{{B_f}^2}{{M_{sf}}^3} - \frac{{B_f}^2}{{M_{sf}}^2} + \frac{B_f}{{M_{sf}}^2 M_{uf}} - \frac{{B_f}^2}{M_{sf} {M_{uf}}^2} \\ \frac{B_f}{M s_f M_{uf}} - \frac{B_f}{{M_{uf}}^2} \\ -\frac{{B_f}^2}{M_{uf} {M_{sf}}^2} + \frac{{B_f}^2 - k_t}{M_{uf} M_{sf}} - \frac{{B_f}^2}{{M_{uf}}^2 M_{sf}} + \frac{{B_f}^2}{M_{uf}} \end{bmatrix} \tag{6.64}$$

$$ad_f^3\mathbf{g} = - \begin{bmatrix} \frac{{B_f}^2}{{M_{sf}}^3} - \frac{{B_f}^2}{{M_{sf}}^2} + \frac{B_f}{{M_{sf}}^2 M_{uf}} - \frac{{B_f}^2}{M_{sf} {M_{uf}}^2} \\ l_1 \\ -\frac{{B_f}^2}{M_{uf} {M_{sf}}^2} + \frac{{B_f}^2}{M_{uf} M_{sf}} - \frac{k_t}{M_{uf} M_{sf}} - \frac{{B_f}^2}{{M_{uf}}^2 M_{sf}} + \frac{{B_f}^2}{M_{uf}} \\ l_2 \end{bmatrix} \tag{6.65}$$

where l_1 and l_2 are:

$$l_1 = (-\frac{{B_f}^2}{{M_{sf}}^2} + \frac{B_f}{M_{sf}})(\frac{-k_f}{M_{sf}}) + (\frac{{B_f}^2}{{M_{sf}}^3} - \frac{{B_f}^2}{{M_{sf}}^2} + \frac{B_f}{{M_{sf}}^2 M_{uf}} - \frac{{B_f}^2}{M_{sf}{M_{uf}}^2})(\frac{-B_f}{M_{sf}})$$
$$+(\frac{B_f}{Ms_f M_{uf}} - \frac{B_f}{{M_{uf}}^2})(\frac{k_f}{M_s})+(-\frac{{B_f}^2}{M_{uf}{M_{sf}}^2} + \frac{{B_f}^2 - k_t}{M_{uf}M_{sf}} - \frac{{B_f}^2}{{M_{uf}}^2 M_{sf}} + \frac{{B_f}^2}{M_{uf}})(\frac{B_f}{M_s}) \tag{6.66}$$

$$l_2 = (\frac{-B_f}{{M_{sf}}^2} + \frac{B_f}{M_{sf}})(\frac{k_f}{M_{sf}}) + (\frac{{B_f}^2}{{M_{sf}}^3} - \frac{{B_f}^2}{{M_{sf}}^2} + \frac{B_f}{{M_{sf}}^2 M_{uf}} - \frac{{B_f}^2}{M_{sf}{M_{uf}}^2})(\frac{B_f}{M_{uf}})$$
$$+ (\frac{B_f}{M_{sf}M_{uf}} - \frac{B_f}{{M_{uf}}^2})(\frac{-k_f + k_t}{M_{uf}}) + (\frac{-{B_f}^2}{M_{uf}{M_{sf}}^2} + \frac{{B_f}^2 - k_t}{M_{uf}M_{sf}} - \frac{{B_f}^2}{{M_{uf}}^2 M_{sf}}$$
$$+ \frac{{B_f}^2}{M_{uf}})(-\frac{B_f}{M_{uf}}) \tag{6.67}$$

Again for simplification, we design for a special condition $M_sf = M_uf = M$:

$$ad_f^3\mathbf{g} = -\begin{bmatrix} \frac{B_f}{M^2}(\frac{1}{M} - B_f) \\ \frac{{B_f}^2}{M^2}[k_f(\frac{1}{M} - 1) + B_f(\frac{1}{M^2} - \frac{1}{M} + 1) - \frac{1}{M^2}] \\ \frac{1}{M^2}(B_f - k_t) + \frac{{B_f}^2}{M}(1 - \frac{2}{M^2}) \\ \frac{B_f}{M^2}[{B_f}^2(\frac{2}{M^2} - \frac{2}{M} - 1) + k_f(1 - \frac{1}{M}) + \frac{k_t}{M} + \frac{B_f}{M^2}] \end{bmatrix} \tag{6.68}$$

Using the constructed vector fields $\mathbf{g}, ad_f\mathbf{g}$,..., $ad_f^{(n-1)}\mathbf{g}$, the investigation of the IS conditions of controllability and involutivity are conducted.

Investigating the controllability and involutivity of the system

Firstly, formulate an M, comprising of the vector fields so that:

$$M = (\mathbf{g}, ad_f\mathbf{g}, ad_f^2\mathbf{g} \quad and \quad ad_f^3\mathbf{g}) \tag{6.69}$$

therefore M is:

$$= -\begin{bmatrix} 0 & \frac{1}{M} & \frac{-B_f}{M^2} + \frac{B_f}{M} & \frac{B_f}{M^2}(\frac{1}{M} - B_f) \\ \frac{1}{M} & \frac{-B_f}{M^2} + \frac{B_f}{M} & -\frac{{B_f}^2}{M^2} + \frac{B_f}{M^3} & \frac{{B_f}^2}{M^2}[k_f(\frac{1}{M} - 1) + B_f(\frac{1}{M^2} - \frac{1}{M} + 1) - \frac{1}{M^2}] \\ 0 & \frac{1}{M} & 0 & \frac{1}{M^2}(B_f - k_t) + \frac{{B_f}^2}{M}(1 - \frac{2}{M^2}) \\ \frac{-1}{M} & \frac{B_f}{M^2} - \frac{B_f}{M^2} & \frac{{B_f}^2}{M}(1 - \frac{2}{M}) + \frac{{B_f}^2 k_f}{M^2} & \frac{B_f}{M^2}[{B_f}^2(\frac{2}{M^2} - \frac{2}{M} - 1) + k_f(1 - \frac{1}{M}) + \frac{k_t}{M} + \frac{B_f}{M^2}] \end{bmatrix} \tag{6.70}$$

The rank of the matrix is that $h(M)$ is equal to order of modelled suspension system and the resulting $det([\mathbf{g}, ad_f\mathbf{g}, ad_f^2\mathbf{g}, ad_f^3\mathbf{g}]) \neq 0$, implying that the computed vector

fields that are in the set $\mathbf{g}, ad_f\mathbf{g}, ad_f^2\mathbf{g}, ad_f^3\mathbf{g}$ are linearly independent, therefore each vector field is linearly independent and the modelled system is controllable. Similarly, due to the consistent rank of the $h(M) = h(P)$, the system is involutivity.

$$P = \mathbf{g}, ad_f\mathbf{g}, ..., ad_f^2\mathbf{g}ad_f^3\mathbf{g}, ad_f\mathbf{g}[ad_f^3\mathbf{g}]. \tag{6.71}$$

As the suspension system model meets the conditions for ISFBL, therefore the first state of the transformed system can be computed.

Obtaining the first state

Once the conditions for IS are met, to compute the first state z_1, use eq. 6.72:

$$\nabla T_1 ad_f^i g = 0; \quad i = 1, 2, .., n-2, \quad \nabla T_1 ad_f^{n-1} g \neq 0 \tag{6.72}$$

Therefore to solve for eq. 6.72, obtaining the first linear state:

$$0\frac{\partial T_1}{\partial x_1} + \frac{1}{M}\frac{\partial T_1}{\partial x_2} + (\frac{-B_f}{M^2} + \frac{B_f}{M})\frac{\partial T_1}{\partial x_3} + \frac{B_f}{M^2}(\frac{1}{M} - B_f)\frac{\partial T_1}{\partial x_4} = 0 \tag{6.73}$$

$$(\frac{1}{M})\frac{\partial T_1}{\partial x_1} + (\frac{-B_f}{M^2} + \frac{B_f}{M})\frac{\partial T_1}{\partial x_2} + (-\frac{{B_f}^2}{M^2} + \frac{B_f}{M^3})\frac{\partial T_1}{\partial x_3} + (\frac{{B_f}^2}{M^2}[k_f(\frac{1}{M} - 1) + B_f(\frac{1}{M^2} - \frac{1}{M} + 1) - \frac{1}{M^2})\frac{\partial T_1}{\partial x_4} = 0 \tag{6.74}$$

$$0\frac{\partial T_1}{\partial x_1} + (\frac{1}{M})\frac{\partial T_1}{\partial x_2} + 0\frac{\partial T_1}{\partial x_3} + (\frac{1}{M^2}(B_f - k_t) + \frac{{B_f}^2}{M}(1 - \frac{2}{M^2})\frac{\partial T_1}{\partial x_4} = 0 \tag{6.75}$$

$$(\frac{-1}{M})\frac{\partial T_1}{\partial x_1} + (\frac{B_f}{M^2} - \frac{B_f}{M^2})\frac{\partial T_1}{\partial x_2} + (\frac{{B_f}^2}{M}(1 - \frac{2}{M}) + \frac{{B_f}^2 k_f}{M^2})\frac{\partial T_1}{\partial x_3} + (\frac{B_f}{M^2}[{B_f}^2(\frac{2}{M^2} - \frac{2}{M} - 1) + k_f(1 - \frac{1}{M}) + \frac{k_t}{M} + \frac{B_f}{M^2})\frac{\partial T_1}{\partial x_4} \neq 0 \tag{6.76}$$

Solving the above equations yields:

$$\begin{aligned} \frac{\partial T_1}{\partial x_3} &= k_1 \frac{\partial T_1}{x_4} \\ \frac{\partial T_1}{\partial x_2} &= k_2 \frac{\partial T_1}{\partial x_4} \end{aligned} \tag{6.77}$$

At $k_1 = k_2 = 1$:

$$\frac{\partial T_1}{\partial x_2} = \frac{\partial T_1}{x_3} = \frac{\partial T_1}{\partial x_4} \quad and \quad \frac{\partial T_1}{\partial x_1} \neq 0 \tag{6.78}$$

Computing the state transformation

$$z = T(x) = \begin{bmatrix} T_1 & L_f T_1 & .. & L_f^{n-1} T_1 \end{bmatrix}^T \tag{6.79}$$

$$\begin{aligned} z_1 &= T_1 = x_1 \\ z_2 &= L_f z_1 = \dot{x}_1 = x_2 \\ z_3 = L_f z_2 = \dot{x}_2 &= \frac{1}{M_s}[K_{sf}(x_1 - x_3) - B_{sf}(x_2 - x_4) + U_s] \\ z_4 = L_f z_3 = \ddot{x}_2 &= \frac{1}{M_s}[K_{sf}(\dot{x}_1 - \dot{x}_3) - B_{sf}(\dot{x}_2 - \dot{x}_4)] \end{aligned} \tag{6.80}$$

And the input transformation is:

$$v = \dot{z}_n = \dot{z}_4 \tag{6.81}$$

The state transformation leads to $n = r$ for the front suspension system as there are no hidden states.

6.5.5 Discussion on adapting ISFBL conditions to IOFBL

The section explored viability to adopt ISFBL to IOFBL to ensure the linearisation state transformation does not result in any hidden states. A main feature is demonstration since the two linearisation methodologies are equivalent guaranteeing that if the first state from ISFBL is used as the IOFBL output, then there will no internal dynamics. For cases where $y \neq z_1$, an artificial output $y* = z_1$ that ensures $n = r$ can be defined then transformation between the artificial output $y*$ and original output y can be computed, this further work will allow flexibility in the output choice. In a case where a system is non-minimum phase and the feedback linearisation techniques analysed so far would not be valid, further analysis should be conducted to extend these limitations of feedback linearisation as demonstrated by [85].

6.6 Applying control strategies to the linearised system

To apply control strategies to the linearised system, a typical methodology would be to utilise negative state feedback. Although these typical linear controllers would have limitations in the practical application of the half-car suspension system, as they are based on gain adjustment which does not consider the complex dynamics within practical application. Therefore in this section the application of the negative state feedback is employed and compared to the slack-based optimal controller which considers the constraint transformation in a no hiden states linearised half-car suspension system.

The application of the slack variable on the linear system will lead to cheaper computational cost when compared to the non-linear control strategy due to working with a linear model with less complex dynamics. This is expected to lead to trade offs with controller application on the system. In this work we will explore the use of slack variable optimal control on the linearised system to address the limitations of state feedback.

6.6.1 Negative state feedback controller

Typical linear control methodologies such as negative state feedback utilise pole placement to design the system's control technique. The state feedback controller will be designed for the virtual inputs v_1 and v_2. The feedback control law is shown in eq. 6.82.

$$u = (r - K\mathbf{x}) \tag{6.82}$$

Where: u is the control input, K is the feedback control gain, $\mathbf{x}$: state variables and r is the reference signal. The feedback gain (K) will be obtained using the direct comparison by pole placement method. Due to the similarities in the system dynamics of the front and rear sub-systems, the controller is designed for the front quarter car sub-system and applied on both systems. Choosing poles for marginally under damped double integrator linearised system results in $K_f = K_r = [1.5\ 1.5]$.

The designed controller is used to generate the virtual inputs v_1 and v_2. After these are obtained their values are substituted into the original control input equations to obtain u_f and u_r. The controller assumes the availability of all the states. In practice it is challenging to obtain these states in a short period of time therefore the full-state observer can be used to obtain the states [6]. In the event that some of the states are available, a partial observer can be used to estimate the rest of the states.

Design procedure

The step response of the state space model suspension system was first analysed, noting the time domain characteristics. This provides a starting point and allows identification of the required dynamic behaviour. A desired behaviour was then identified through a second order stable system. A second order system is used because time domain characteristics such as rise time, overshoot, and settling time, can be directly imposed onto the system by using those characteristics to determine the parameters of a generic second order system. Through a small offset of its poles, two pole pairs can be obtained and used as desired poles for the closed loop system so as to yield a desired behaviour. Pole placement allows determination of the K matrix so that the closed loop system behaves in the desired manner with the desired poles.

Desired closed loop system

Ideally the closed loop system should have a faster rise time (T_r), faster settling time T_s and a smaller overshoot with no steady state error. The following time domain characteristics are thus specified and were seen as both realistic and feasible.

$$Ts <= 1s, Mp.5\%, Tr <= 0.5s \tag{6.83}$$

The parameters of a second order system G(s) resulting in the specifications above are calculated as follows:

$$G(s) = \frac{w_n^2}{s^2 + 2\zeta w_n s + w_2^2} \tag{6.84}$$

where:

$$\zeta = \sqrt{\frac{In(\frac{PO}{100})^2}{\Pi^2 + In(\frac{PO}{100})^2}} \tag{6.85}$$

For a percentage overshoot of 5 %, the resulting ζ is 0.69. To calculate the natural frequency w_n that achieves a settling time of 0.5 s, with a damping (ζ) of 0.69, and allowing settling time of within 1 % tolerance:

$$T_s = -\frac{In(0.01)}{\zeta \times w_n} \tag{6.86}$$

$$0.5 = -\frac{In(0.01)}{0.69 \times w_n} \tag{6.87}$$

For a settling time of 0.5 seconds, and a ζ of 0.69, the resulting w_n is 6.66 rad/s. The rise time is calculated by eq. 6.88 to be 0.29 seconds.

$$T_r = -\frac{In(1.95)}{w_n} \tag{6.88}$$

Substituting the parameters into G(s), the following poles are obtained:

$$p_1 = \text{-4.6250 + i4.7864}$$
$$p_2 = \text{-4.6250 -i 4.7864}$$

Now through pole placement, the K matrix is obtained. This was done through a Matlab command which allows for generation of K though a pole placement algorithm similar to the direct comparison method [33]. The resulting poles:

$$K = [-2741 \quad 1171 \quad 1560 \quad 1574]$$

Observer design

An observer is also necessary to be designed in order to estimate and feedback the state variables as the control law defines. However a state observer is only essential if the states of the system cannot be measured. For this design it can be argued that since the C_{matrix} does not alter the state variables and allows all of them to be fed-back as they are, then the states can be obtained. The observer is required to respond faster than the controller, thus its gain K_e was taken to be five times the closed loop poles. Since the closed loop poles were known, the K_e matrix was determined in the same procedure as for K. However a state observer is only essential if the states of the system cannot be measured. For this design it can be argued that since the C matrix does not alter the state variables and allows all of them to be fed back as they are, then the states can be obtained.

Limitations of the negative state feedback control technique

Due to the negative state feedback controller using pole placement, the resulting gains might not be dynamic and cater for state constraints. Typically as a way of handling system constraints, with feedback linearisation, tuning will take place which might result in controller poor performance based on the chosen tuning parameters by the designer therefore slack-based optimal control is proposed on the no hidden states linearised half-car suspension system.

6.6.2 Optimal control on the linearised system

This section focuses on analysing the application of a slack-based optimal control for a no hidden states linearised system at the point of equivalency for both the input-output FBL and input state FBL systems. From the linearised system, the transformed system is governed by:

$$\dot{z} = Az + Bv \tag{6.89}$$

With no hidden states feedback linearisation, the state constraints are preserved and transformed through the linearisation transformation. No hidden states linearisation is necessary since the constraints will be observable and controllable as $n = r$, whereas partial transformation leading to $n > r$ would lead to constraints being potentially hidden or eliminated, which would cause problems in the practical application of the control strategy. Also without assuring complete state transformation the state constraint equation can be be a combination of observable and controllable states and also hidden states, where it might not be sufficient to design slack-based optimal control based on the candidate states.

Constraints mapping on a complete linearised system

Since the non-linear suspension system is transformed to a linear system, it is necessary to also transform the constraints from the $\mathbf{x}$ to the $\mathbf{z}$ system. Since the constraint $g(x,t)$ was an explicit function of the original non-linear system based on states: $\mathbf{x} = [x_1 \quad x_2 \quad .. \quad x_n]^T$, in the case of complete feedback linearisation, the transformation T would meet the condition in eq. 6.90:

$$\begin{aligned} \nabla T_i \mathbf{g} = 0 \quad 1 \leq i \leq n \\ \nabla T_n g \neq 0 \end{aligned} \tag{6.90}$$

resulting in the transformed system states being modelled by:

$$z = T(x) = \begin{bmatrix} T_1 & L_f T_1 & .. & L_f^{n-1} T_1 \end{bmatrix}^T \tag{6.91}$$

Therefore the original states ($\mathbf{x}$) would be explicitly represented or mapped into the transformed system ($\mathbf{z}$). Since the original state constraint is an explicit function of one of the states in $\mathbf{x}$, therefore for a state transformation $\mathbf{x} \rightarrow \mathbf{z}$ would lead to $g(x,t) \rightarrow g(z,t)$. The state constraint will be transformed by the same invertible

matrix so that the constraint $g(z,t)$ will be an explicit function of the transformed states therefore:

$$g(z,t) + \frac{1}{2}\alpha_f^2 = 0 \tag{6.92}$$

where the constraint $g(z,t)$ is based on the direct transformation of the state constraint from f(x). The state constraint mapping results in the explicit function of the original states being mapped into the linear states.

$$\begin{bmatrix} f(x_i) \rightarrow z_1 \\ f(x_i) \rightarrow z_2 \\ ... \\ f(x_i) \rightarrow z_r \end{bmatrix} \tag{6.93}$$

where $i = 1, .., n$, since with complete feedback linearisation $n = r$, therefore $g(z,t)$ is an explicit function of the states: $[z_1 \quad L_f z_1 \quad .. \quad L_f^{n-1} z_1]^T$, based on the original constraints of the system. For the suspension system, the constraint was modelled by the suspension deflection in the original system and due to complete feedback linearisation based on the conditions for input state linearisation, all the states will be represented in the transformed front and rear suspension system. The transformed system for the half-car suspension system is characterised by:

$$\begin{bmatrix} \dot{z}_1 = z_2; & \dot{z}_2 = z_3; & \dot{z}_3 = z_4; & \dot{z}_4 = v_f \\ \dot{z}_5 = z_6; & \dot{z}_6 = z_7; & \dot{z}_7 = z_8; & \dot{z}_8 = v_r \end{bmatrix} \tag{6.94}$$

Slack variable on the linearised system

The system constraint mapped in the original system consisted of the suspension deflection $(x_3 - x_1)$. $z_1 = x_1$ and z_3 is a function of x_3, therefore the transformed suspension deflection is modelled by $z_3' - z_1$. Therefore the transformed slack variable is defined by:

$$(z_3' - z_1) - \alpha_f = 0 \tag{6.95}$$

Slack-based optimal control requires the differentiation of the slack equation until the input appears. Since z_1 is not an explicit function of the transformed input v, therefore differentiate eq. 6.95:

$$(\dot{z}_3' - \dot{z}_1) + \alpha_f \alpha_1 = 0 \tag{6.96}$$

Similarly $\dot{z}_3' = z_4'$ or $\dot{z}_1 = z_2$ is not an explicit function of v, therefore:

$$(\dot{z}_4' - \dot{z}_2) + \alpha_1^2 + \alpha_f \alpha_2 = 0 \tag{6.97}$$

z_4' is an explicit function of v, therefore the optimal control input based on the slack-based methodology is $v_2 = \alpha_2$.

Boundary Conditions

The initial conditions t_0 for the two additional states: α and α_1 and the input α_2:

$$\alpha_f = (-2(z_{sd}))^{\frac{1}{2}} = -2(z_3' - z_1)^{\frac{1}{2}} \tag{6.98}$$

And:

$$\alpha_1(t_0) = \frac{g(z_0, t0)}{z_o} \tag{6.99}$$

$$\alpha_1(t_0) = \frac{\dot{z}_3' - \dot{z}_1}{-2(z_3' - z_1)^{\frac{1}{2}}} \tag{6.100}$$

And:

$$\alpha_2(t_0) = \frac{1}{\alpha_f}[g_2(z_0)(t_0) + \alpha_1^2(t_0)] \tag{6.101}$$

$$\alpha_2(t_0) = \frac{1}{(-2(z_3' - z_1)^{\frac{1}{2}})}[(\ddot{z}_3' - \ddot{z}_1)(t_0) + \alpha_1^2(t_0)] \tag{6.102}$$

$$\alpha_2(t_0) = \frac{1}{\alpha_0}[(\ddot{z}_3' - \ddot{z}_1)(t_0) + (\frac{\dot{z}_3' - \dot{z}_1}{-2(z_3' - z_1)^{\frac{1}{2}}})^2] \tag{6.103}$$

Objective function for the linearised system

To control the linearised system, the performance index is based on the new system input v:

$$J_{opt} = \int_0^{t_f} zQ_z + \frac{1}{2}vdt \tag{6.104}$$

The control variable for the front and rear systems is represented the linearised half-car where the performance is modelled by:

$$J_{opt} = \int_0^{t_f} q_1 z_1 + \frac{1}{2}\alpha_2^2 + q_r z_5 + \frac{1}{2}\alpha_4^2 dt \tag{6.105}$$

The control variable for the front and the rear systems is represented by α_2 and α_4.

6.6.3 Performance index for the linearised system

The performance index of the transformed system on the suspension system is modelled through:

$$\begin{aligned} L(z,\alpha_p,t) =& q_f z_1^2 + \frac{1}{2}[\frac{1}{\alpha_f}(\dot{z}_4' - \dot{z}_2) - \alpha_1^2]^2 + \\ & q_r z_5^2 + \frac{1}{2}[\frac{1}{\alpha_r}(\dot{z}_8' - \dot{z}_6) - \alpha_3^2]^2 \end{aligned} \tag{6.106}$$

Therefore the performance index for the transformed half-car system is:

$$J = \int_{t_0}^{t_f} L(z,\alpha_p,t)dt \tag{6.107}$$

$$J = \int_{t_0}^{t_f} q_f z_1^2 + \frac{1}{2}[\frac{1}{\alpha_f}(\dot{z}_4' - \dot{z}_2) - \alpha_1^2]^2 + q_r z_5^2 + \frac{1}{2}[\frac{1}{\alpha_r}(\dot{z}_8' - \dot{z}_6) - \alpha_3^2]^2 dt \tag{6.108}$$

Hamiltonian and co-states

Based on the state transformation in eq. 6.109:

$$\dot{z} = F(Z,\alpha_p,t), \quad Z(t_0) = Z_0 \tag{6.109}$$

The optimal control Hamiltonian formulation is: $\mathcal{H} = L + \lambda_{(n+p)}^T F(z)$, where λ is $(n+p)$ dimensional lagrange multiplier. The Hamiltonian is then defined by:

$$\begin{aligned} \mathcal{H} =& q_f z_1^2 + \frac{1}{2}[\frac{1}{\alpha_f}(\dot{z}_4' - \dot{z}_2) - \alpha_1^2]^2 + q_r z_5^2 + \frac{1}{2}[\frac{1}{\alpha_r}(\dot{z}_8' - \dot{z}_6) - \alpha_3^2]^2 \\ & + \lambda_{(n+p)}^T[\dot{z}_1, \dot{z}_2, .., \alpha_f, \alpha_1, \alpha_r, \alpha_3] \end{aligned} \tag{6.110}$$

Slack variable methodology is limited as it cannot solve for the two control inputs (α_f) and (α_r). To address the limitation to the application of slack to the MIMO system the optimal control solution will assume weak coupling between the two sub-systems by decoupling the front and rear systems. Expanding the Hamiltonian results in function $\mathcal{H}$ as:

$$\begin{aligned} \mathcal{H} =& q_f z_1^2 + \frac{1}{2}[\frac{1}{\alpha_f}(\dot{z}_4' - \dot{z}_2) - \alpha_1^2]^2 + q_r z_5^2 + \frac{1}{2}[\frac{1}{\alpha_r}(\dot{z}_8' - \dot{z}_6) - \alpha_3^2]^2 \\ & + \lambda_1\dot{z}_1 + \lambda_2\dot{z}_2 + \lambda_3\dot{z}_3 + \lambda_4\dot{z}_4 + \lambda_5\dot{z}_5 + \lambda_6\dot{z}_6 + \lambda_7\dot{z}_7 + \lambda_8\dot{z}_8 \\ & + \lambda_9\alpha_f + \lambda_{10}\alpha_1 + \lambda_{11}\alpha_r + \lambda_{12}\alpha_3] \end{aligned} \tag{6.111}$$

The slack-based optimal control co-state equation is:

$$\dot{\lambda} = -(\frac{\partial H}{\partial z}) \tag{6.112}$$

The co-state computation for the half-car is:

$$\begin{aligned}
\dot{\lambda}_1 &= -\frac{\partial \mathcal{H}}{\partial z_1}; \quad \dot{\lambda}_2 = -\frac{\partial \mathcal{H}}{\partial z_2} \\
\dot{\lambda}_3 &= -\frac{\partial \mathcal{H}}{\partial z_3}; \quad \dot{\lambda}_4 = -\frac{\partial \mathcal{H}}{\partial z_4} \\
\dot{\lambda}_5 &= -\frac{\partial \mathcal{H}}{\partial z_5}; \quad \dot{\lambda}_6 = -\frac{\partial \mathcal{H}}{\partial z_6} \\
\dot{\lambda}_7 &= -\frac{\partial \mathcal{H}}{\partial z_7}; \quad \dot{\lambda}_8 = -\frac{\partial \mathcal{H}}{\partial z_8} \\
\dot{\lambda}_9 &= -\frac{\partial \mathcal{H}}{\partial \alpha_f}; \quad \dot{\lambda}_{10} = -\frac{\partial \mathcal{H}}{\partial \alpha_1} \\
\dot{\lambda}_{11} &= -\frac{\partial \mathcal{H}}{\partial \alpha_r}; \quad \dot{\lambda}_{12} = -\frac{\partial \mathcal{H}}{\partial \alpha 3}
\end{aligned} \tag{6.113}$$

6.6.4 Slack-based optimal control law

The resulting control law is determined from the optimality condition:

$$\frac{\partial \mathcal{H}}{\partial \alpha_p} = 0 \tag{6.114}$$

For the front and the rear parts:

$$\frac{\partial \mathcal{H}}{\partial \alpha_2} = 0; \quad \frac{\partial \mathcal{H}}{\partial \alpha_4} = 0 \tag{6.115}$$

To achieve cheaper computational costs to the optimal control problem, we utilise the linearised model and apply slack based optimal control. Optimal results for the virtual variables will be considered sufficient for the original system. The linearised optimal control problem is solved with the same procedure as the non-linear case demonstrated in the previous chapter.

6.7 Testing results

To analyse the system's performance, the slack based optimal control is applied on the completely linearised system. The controller receives mass displacement signals from the physical system and determines the required actuation force to ensure improved ride comfort and road-handling capabilities. Results were obtained from the half-car model showing the displacement and acceleration graphs for the passive and the active systems as shown in Fig. 6.4 to Fig. 6.6.

6.7.1 Simulation results on front system

Displacement (sprung:yellow, unsprung:green), velocity (sprung:purple, unsprung:red).

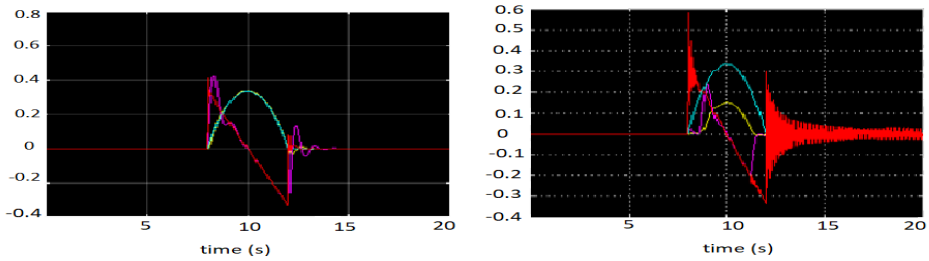

Figure 6.1: Round hump passive and active

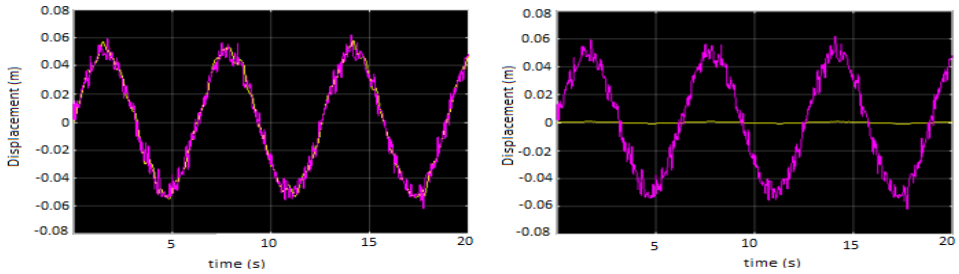

Figure 6.2: Bumpy road passive and active

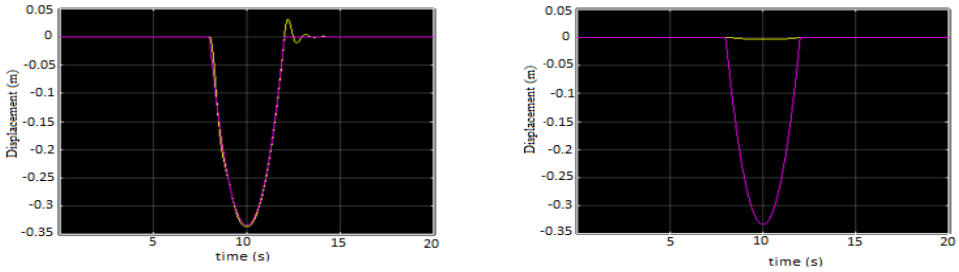

Figure 6.3: Pothole passive and active

6.7.2 Testing results on the suspension system test-rig

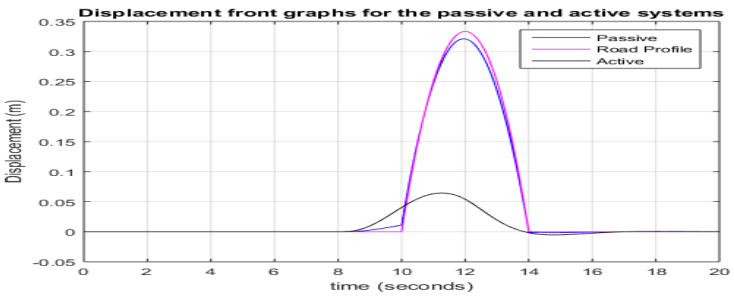

Figure 6.4: Front sprung mass displacement

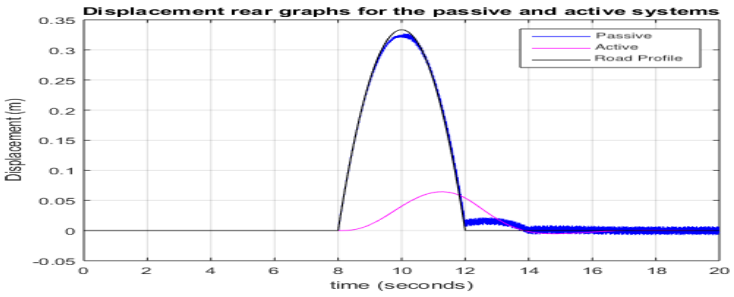

Figure 6.5: Rear sprung mass displacement

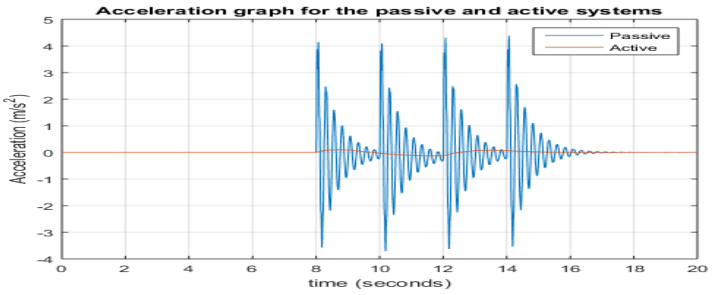

Figure 6.6: Acceleration plots for the passive and active systems

Results show that the controller achieves a displacement attenuation of 81.82 % for the front and rear sub-systems, as the passive output shows a peak displacement of 0.33m and the active suspension system has an output of 0.07m. Comparing the accelerations for the passive and the active systems shows that acceleration spikes have been reduced by 97.5 % as shown in Fig. 6.6.

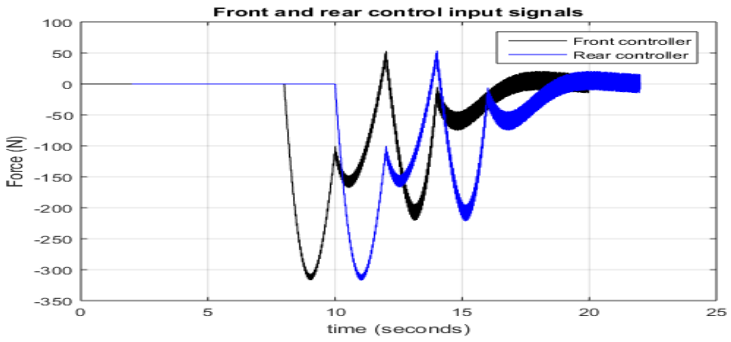

Figure 6.7: Actuation control input signal

6.8 Discussion

Linearisation at the point of equivalency ensures no hidden states, which leads to the full transformation of $n = r$ states. For the fully transformed linear system, slack-based optimal control is applied due to its computational benefits. The methodology involved ensures that the state constraints on the non-linear system are mapped and catered for when solving the optimal control problem for the linear system. The controller does achieve displacement and acceleration attenuations. The displacement plots also show that the sprung load is cushioned in the AVSS as it does not experience sharp changes in displacement. The control input signals for the front and the rear sub-systems are similar in magnitude but they have a 2s time difference as shown by Fig. 6.7. This is due to the front sub-system experiencing the road disturbance first and the rear sub-system experiences the disturbance after a time delay of 2s. Partitioning both the system and control matrix led to the necessity of computing mathematical equations in a different basis, which means that they are not the same type therefore cannot be mathematically computed.

6.9 Summary on linearisation of suspension systems

To enable the application of slack-based state constrained optimal control on the half-car linearised system, complete linearisation is explored. To achieve complete linearisation conditions for ISFBL are applied to ensure $n = r$. This ensures that the constrained states are represented on the transformed system by ensuring that the constrained states are not transformed into hidden states and dynamics. An approach for linearisation for the decoupling matrix invertibility through control

matrix re-partitioning is discussed. Hidden states and zero dynamics analysis is conducted. The linearised system is then controlled through the designed negative state feedback and the slack-based state constrained optimal control. To enhance these control techniques, adaptive properties to deal with the half-car suspension system uncertainties has to be designed to ensure overall stability.

Chapter 7

Experinmental comparison of robustness techniques

7.1 Introduction

In this chapter the developed half-car mechanical suspension system is used as a test-rig for the implemented backstepping, Proportional Integral Derivative (PID) and ASB controllers. The backstepping controller design is chosen as the primary solution due to its ability to be exploited to satisfy the conflicting concepts of ride quality and suspension travel. Sliding mode and adaptive backstepping are integrated to the backstepping technique to improve robustness and to deal with the parametric uncertainties such as measurement and sampling errors. These are associated with the system input due to the non-ideal operations of the sensors and the actuators. This section has been published in the IFAC 20^{th} world congress as presented in [61].

CONTRIBUTION 3: Applying an Adaptive Sliding Backstepping technique to a half-car suspension so as to test for robustness and adaptive properties on the constructed test-rig, through:

1. Application of backstepping control-based candidate Lyapunov function for stabilisation of the constructed half-car suspension model
2. Application of the adaptive sliding backstepping on the half-car suspension system to enhance robustness within the given boundaries
3. Comparison of the performance of the backstepping, adaptive backstepping to a general PID controller

To design the half-car backstepping controller, the front and rear designs are formulated.

7.2 Formation of backstepping controller

Backstepping is designed and implemented for the front and rear part of the suspension system. This controller stabilises the non-linear dynamic suspension system by using the Lyapunov stability theory.

7.2.1 Backstepping front controller design:

The regulating variable and the linear design filter for the front part is selected as shown in eq. 7.1 [22]. The derivative of the regulating variable is shown in eq. 7.2. The linear design filter is as shown in eq. 7.3.

$$z_1 = x_1 - \overline{x}_3 \tag{7.1}$$

$$\dot{z_1} = x_2 + \epsilon_1(x_1 - x_3) - \epsilon z_1 \tag{7.2}$$

$$\overline{x}_3 = \frac{\epsilon_1}{(s + \epsilon_1)} x_3 \tag{7.3}$$

For small values of ϵ_1, $\overline{x}_3$ is a low pass filter and $z_1 = x_1$. The oscillations are eliminated and the driver ride comfort is improved whereas the suspension deflection quality is compromised. If ϵ_1 is large high frequencies pass through and $z_1 = x_{sf} - x_{uf}$. The controller design requires the choice of the virtual control variable and error variable. In the suspension system, the first virtual control variable is x_2 and the error variable is as shown by eq. 7.4. $\phi_1(x)$ is the desired x_2 value. The derivative of the error variable is shown in eq. 7.5.

$$z_2 = x_2 - \phi_1(x) \tag{7.4}$$

$$\dot{z_2} = \dot{x_2} - \dot{\phi_1}(x) \tag{7.5}$$

$$\phi_1(x) = -\epsilon(x_1 - x_3) - c_1 z_1 \tag{7.6}$$

The candidate Lyapunov function for stabilising z_1 is shown in eq. 7.7. It is a locally positive definite function.

$$V_f(z) = \frac{1}{2}z_1^2 + \frac{1}{2}z_2^2 \tag{7.7}$$

$$\dot{V_f}(z) = -(c_1 + \epsilon_1)z_1^2 - c_2 z_2^2 \tag{7.8}$$

The coefficient c_1 and c_2 are the system's design constants and they are greater than zero to ensure that the derivative of the Lyapunov function is negative definite as shown in eq. 7.8. The remaining states are the zero dynamics, these are found to be exponentially stable for $\epsilon_1 > 0$ [15]. The resulting controller equation is shown in Fig. 7.1.

7.2.2 Backstepping rear controller design:

The regulating variable for the rear part of the suspension system is shown in eq. 7.9.

$$z_3 = x_{sr} - \overline{x}_{ur} \tag{7.9}$$

Where the linear design filter is shown in eq. 7.10 is:

$$\overline{x}_{ur} = \frac{\epsilon_2}{s + \epsilon_2} x_{ur} \tag{7.10}$$

The rear controller error state variable is shown in eq. 7.11.

$$z_4 = x_6 - \phi_2(x) \tag{7.11}$$

$$\phi_2(x) = -\epsilon_2(x_5 - x_7) - c_3 z_3 \tag{7.12}$$

The candidate Lyapunov function for stabilising z_3 is in eq. 7.13. It is a locally positive definite function. The time derivatives are negative definite as shown in eq. 7.14. The design constants are $c_1 = c_3 = 6, c_2 = c_4 = 1000$ and $\epsilon_1 = \epsilon_2 = 0.0001$.

$$V_r(z) = \frac{1}{2}z_3^2 + \frac{1}{2}z_4^2 \tag{7.13}$$

$$\dot{V_r}(z) = -(c_3 + \epsilon_2)z_3^2 - c_4 z_4^2 \tag{7.14}$$

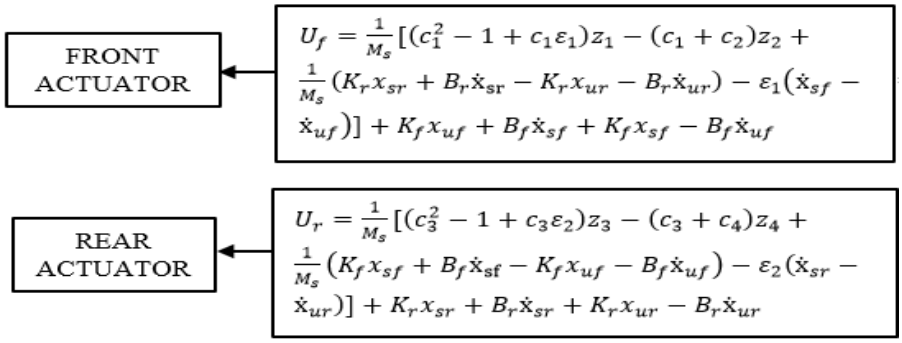

Figure 7.1: Front and rear controller inputs from the backstepping technique [61]

The rear and front controller inputs are shown in Fig. 7.1. For a robust multi-varied system, that considers the sensitivity of the un-modelled dynamics and parametric variations, the backstepping controller is augmented with the sliding mode controller and adaptive properties as per the formulation in [46].

7.3 Sliding mode controller design

The sliding mode controller is implemented to improve robustness within given bounds. The sliding mode technique is applied to ensure that z_2 is zero within finite time, as modelled in [46]. Therefore the control task is designed to obtain an input (u) that meets the defined criterion in eq. 7.15.

$$\frac{1}{2}.\frac{dz_2^2}{dt} \leq -\eta\,|z_2| \tag{7.15}$$

The sliding mode technique divides the input to the equivalent control (u_{equiv}) which ensures that for the nominal z_2 dynamics, $\dot{z_2}$ is always zero and the switching input (u_{switch}) which ensures eq. 7.15 is met. From eq. 7.5, the general expression of $\dot{z_2}$ is derived and shown in eq. 7.16.

$$\dot{z_2} = \dot{\phi_1}(x) + f(x) + gu \tag{7.16}$$

Therefore u_{equiv} is as shown in eq. 7.17 if $f(x)$ and g are unknown. The switching control is assumed to be as shown in eq. 7.18.

$$u_{equiv} = \frac{1}{g}[\dot{\phi_1}(x)] \tag{7.17}$$

$$u_{switch} = -\Upsilon(z_1, z_2) sign(z_2) \tag{7.18}$$

The full sliding backstepping control law for the front controller is in eq. 7.19.

$$U_f = \frac{1}{g_f}[\dot{\phi_1}(x)] - \Upsilon(x_1, z_1, z_2) sign(z_2) \tag{7.19}$$

Following the same procedure, the rear controller is in eq. 7.20.

$$U_r = \frac{1}{g_r}[(\dot{\phi_2}(x)] - \Upsilon(x_2, z_3, z_4) sign(z_4) \tag{7.20}$$

To enhance the performance of the sliding backstepping, adaptive properties are introduced to improve the controller robustness performance.

7.4 Adaptive back stepping controller design

Adaptive backstepping is implemented as it does not require any knowledge of the bounds of the uncertainty. Assuming there exists a positive constant d such that $\Upsilon(x_1, z_1, z_2) < d$ for all time, therefore estimation error is $\tilde{d} = d - \hat{d}$ [46]. In the previously determined U_{switch}, replace $\Upsilon(\mathbf{x})$ with the estimate $\hat{d}$ to result in the switching control eq. 7.22.

$$\upsilon(x_1, z_1, z_2) = \tilde{d} \tag{7.21}$$

$$Uswitch = -\hat{d} signz_2 \tag{7.22}$$

The candidate Lyapunov function is shown in eq. 7.23. The selected adaptive law is shown in eq. 7.26. ψ is the design constant and the $\dot{V}$ is modelled by:

$$V = \frac{1}{2} z_1^2 + \frac{\tilde{d}^2}{2\psi} \tag{7.23}$$

If there exists a function $\Upsilon(\mathbf{z})$ that satisfies the inequality:

$$\Upsilon(z) = |\frac{Af_1 g - \hat{g} u_{eq}}{g_n g}| + \epsilon \tag{7.24}$$

Therefore the derivative of the Lyapunov will be characterised by:

$$\dot{V} = z_2[Af_1 - \hat{d}signz_2] + \frac{\tilde{d}\dot{\tilde{d}}}{\psi} \tag{7.25}$$

For an adaptation law of:

$$\dot{\hat{d}} = \psi|z_2| \tag{7.26}$$

Therefore $\dot{V}$ results in a negative definite ensuring that the $z_2 = 0$, implying that the asymptotic convergence to the sliding surface is zero. The front control U_f is modelled by:

$$U_f = \frac{1}{g_f}[\dot{\phi_2}(x)] - \tilde{d}sign(z_2) \tag{7.27}$$

And similarly the rear control U_r is:

$$U_r = \frac{1}{g_r}[\dot{\phi_2}(x)] - \tilde{d}sign(z_4) \tag{7.28}$$

These control algorithms will result in chattering therefore modification of the algorithm is necessary and this is achieved by replacing the *sign* function by *tanh* similarly to the methodology used in [46] on the quad-rotor model.

7.5 PID controller

The PID gains are obtained through gain adjustment with the goal to maximise the performance on the AVSS. The K_p is choosen to improve rise time, the K_d reduces the overshoots and the K_i reduces the steady state error. The PID gains are tuned to maximise on ride comfort in the Simulink implementation. The selected K_p, K_i and K_d are 700, 30 and 10 respectively. These result in the best performance for tested road disturbances.

7.6 Experinmental testing results

The readings from the physical test-rig shown in Chapter 4 are inputs into the controller shown in Fig. 7.2. The half-car suspension model is represented by Fig. 7.2 as modelled in the simulation software. The controller outputs U_f and U_r are the input to the actuation devices that ensure the mitigation of the road disturbance. The backstepping, ASB and PID controller for the active and passive scenarios are shown in Fig. 7.3, Fig. 7.4 and Fig. 7.5 respectively. The results for backstepping, adaptive sliding backstepping and PID are obtained of two types on road disturbances: round and square hump. The designed backstepping, PID and ASB controllers are tested for the front and rear parts of the system. The sprung mass displacement results for the implemented controllers on both of the road disturbances are shown in Fig. 7.6 to Fig. 7.9. The analysis focuses on comparing the magnitude of the sprung mass displacement attenuation and not their response time as the controllers were not tested at the same time.

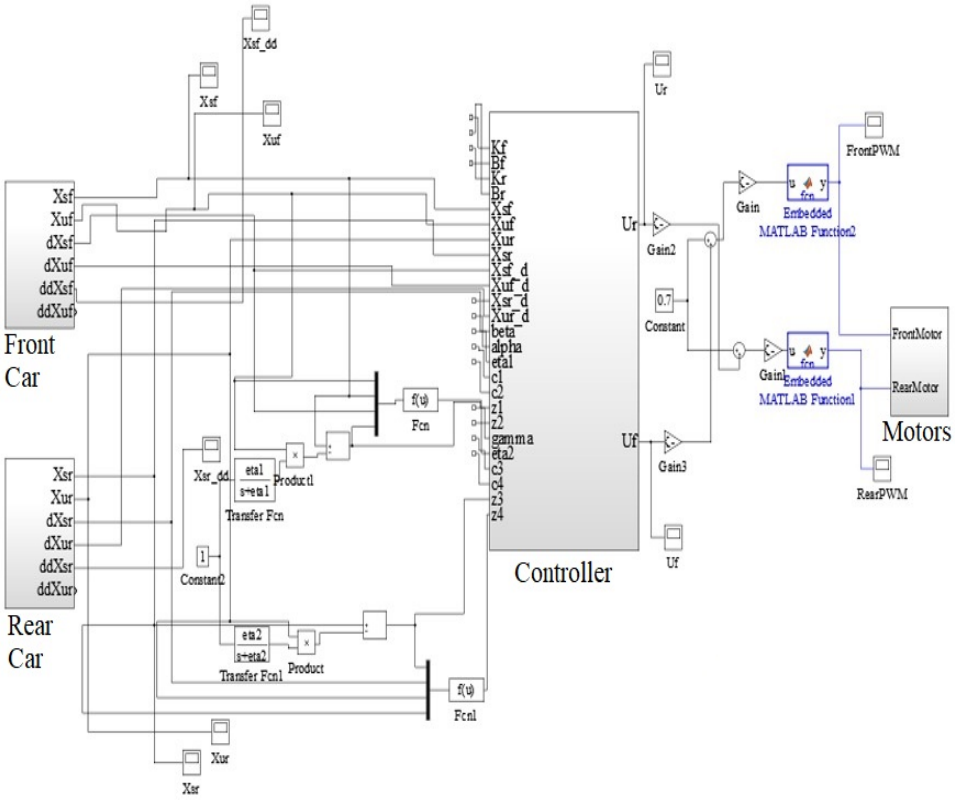

Figure 7.2: Programming environment for the half-car AVSS

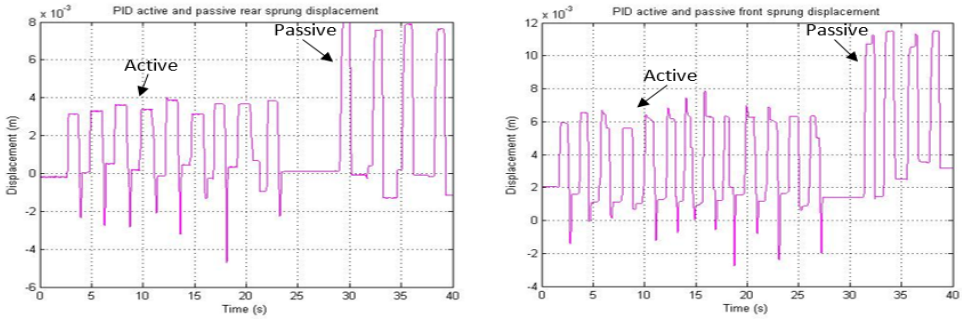

Figure 7.3: Active and passive displacement plots for the PID controller

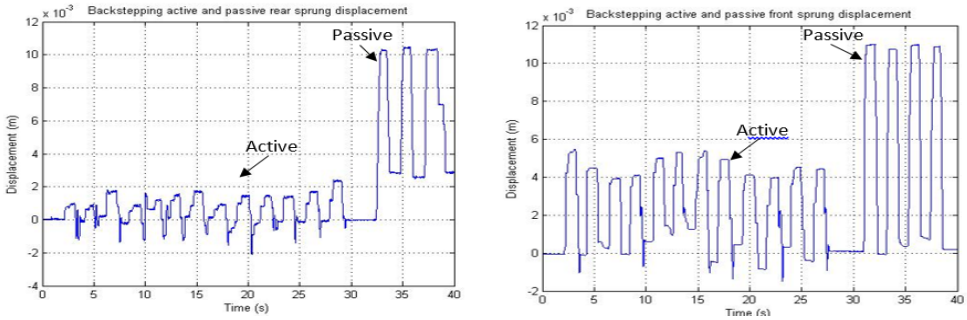

Figure 7.4: Active and passive displacement plots for the backstepping controller

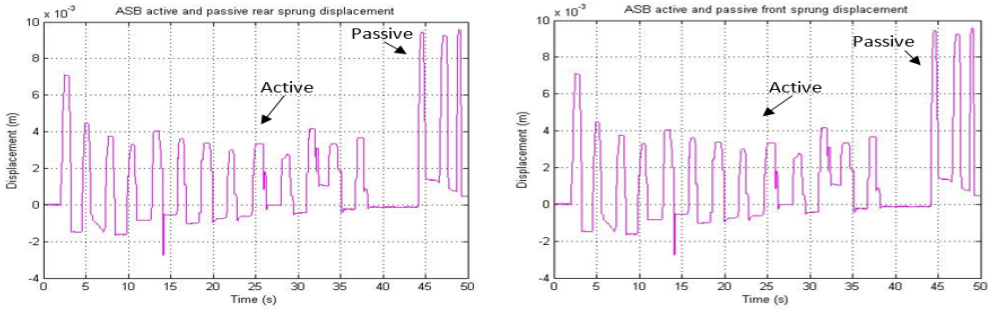

Figure 7.5: Active and passive displacement plots for the ASB controller

7.6.1 Displacement plots

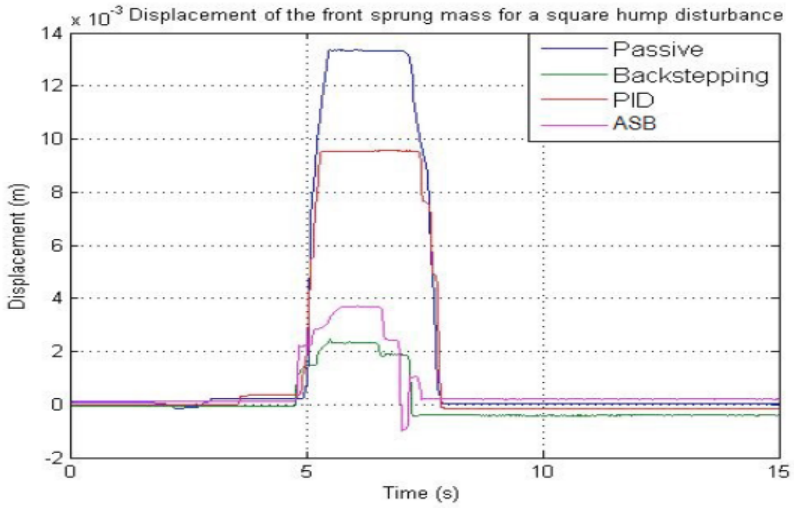

Figure 7.6: Displacement of the front sprung mass for a square hump

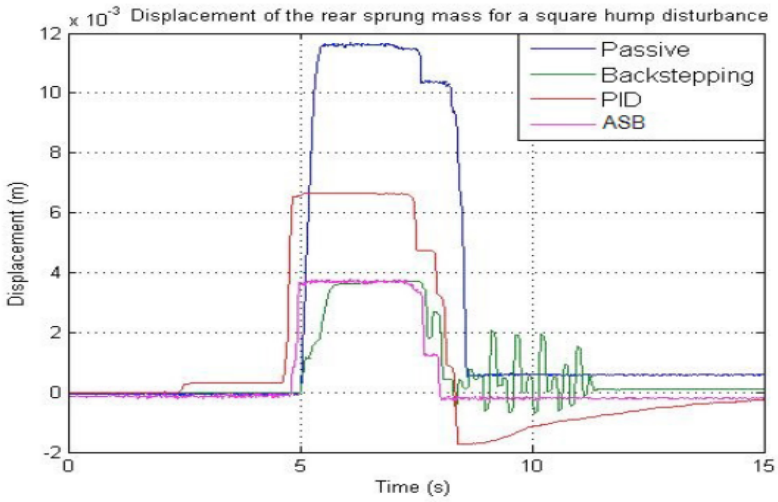

Figure 7.7: Displacement of the rear sprung mass for a square hump

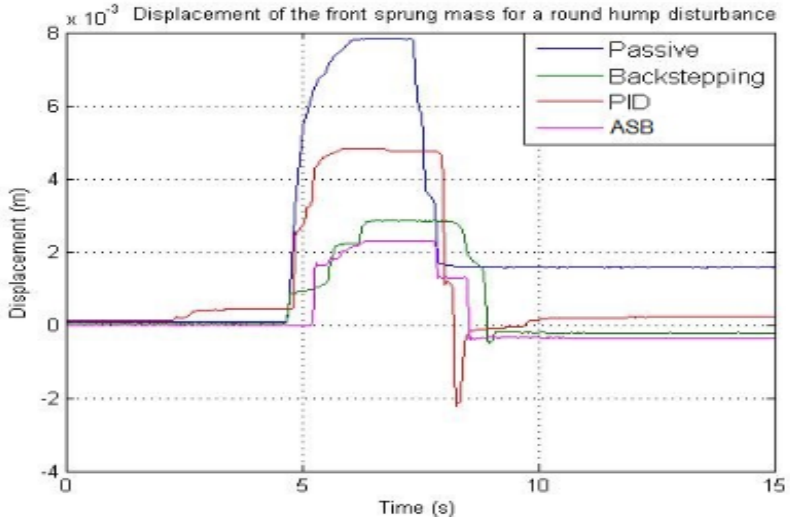

Figure 7.8: Displacement of the front sprung mass for a round hump

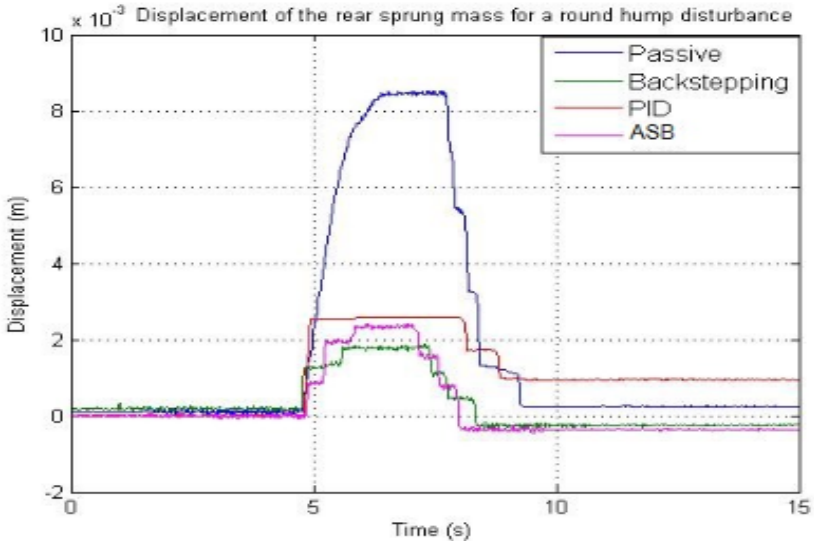

Figure 7.9: Displacement of the rear sprung mass for a round hump

7.6.2 Acceleration plots

Fig. 7.10 shows that the sprung mass does not experience much acceleration; this is due to the physical system being overdamped. However, to reduce the signal noise experienced and depicted in Fig. 7.10, filtering techniques should be implemented.

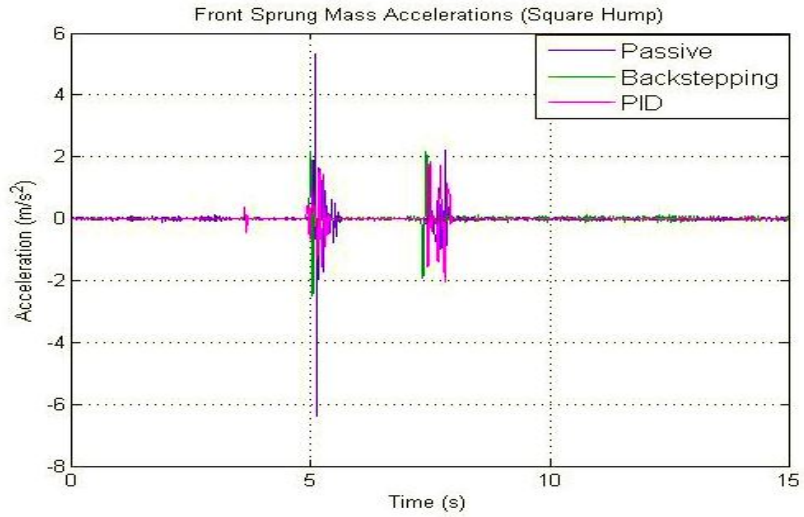

Figure 7.10: Front sprung mass acceleration for the square hump

7.6.3 Control input plots

The required control force is shown by the figure below. The control input obtained from the ASB is implemented and compared to other controllers. The ASB's limitation is that it generates a relatively high control input as shown in Fig. 7.11.

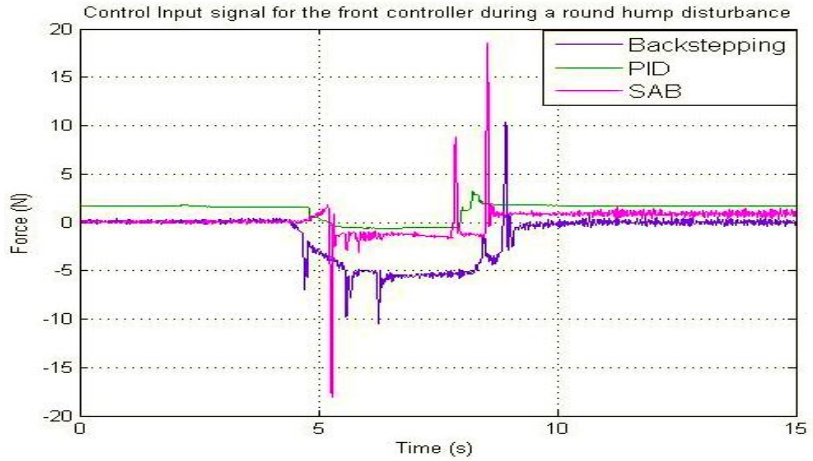

Figure 7.11: Control input during disturbance for round hump

7.6.4 Robustness plots

Robustness is demonstrated through changing parameters and observing the system behaviour. The ASB model is updated during operation, based on the measured performance as shown in Fig. 7.14.

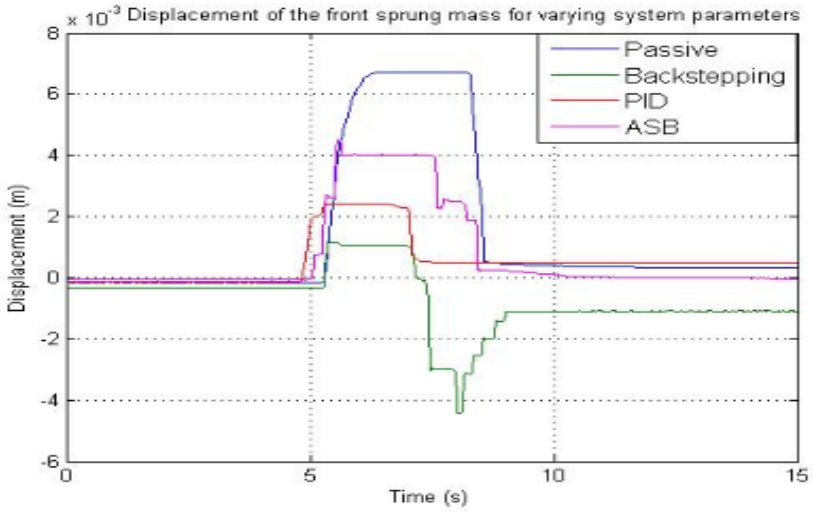

Figure 7.12: Robustness demonstration for varying parameters on front sprung mass

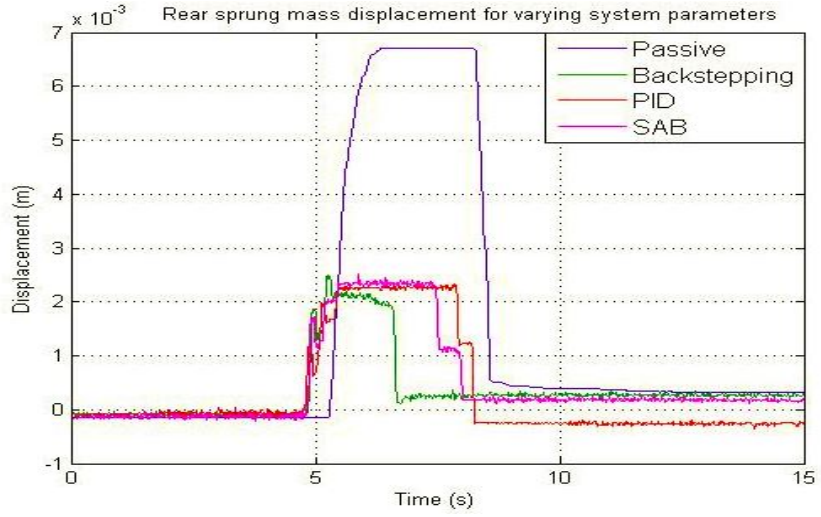

Figure 7.13: Robustness demonstration for varying parameters on rear sprung mass

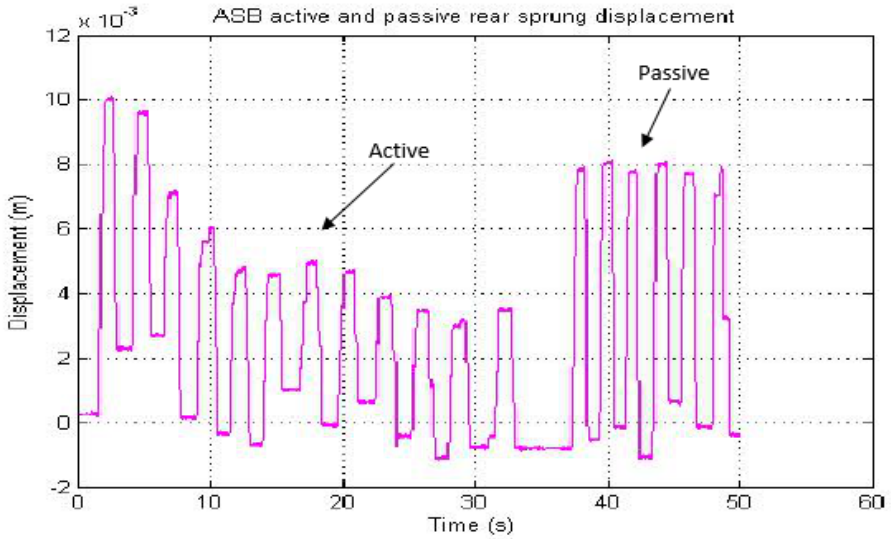

Figure 7.14: Active robustness demonstration for varying parameters

7.7 Discussion

The testing results show that the designed controllers achieve improved ride quality when compared to the performance of the passive system, which achieves less impact on the vehicle driver. The fast response is due to the choice of the sensors and motors that ensures that the actuation force can be produced and response will be fast enough to attenuate the road disturbance in real time. Since the focus of this research is not on the mechanical aspects of the test rig, the physical issues were not detailed, such as the observers and physical interventions utilised for the system inputs. The results in Fig. 7.4 show that the backstepping controller reduced the magnitude of the sprung mass displacement by 76.8 % for the rear sprung mass and by 50 % for the front sprung mass displacement. The adaptive sliding backstepping for the front and rear controllers show improvement of performance with time as shown in Fig. 7.5, which is expected as the controller is designed to adapt to the system conditions. The ASB allows up to 60 % reduction of the displacement when compared to the passive system. The back-steeping rear controller shows the best performance since it eliminates 76.8 % of the displacement that the driver would have experienced in the passive system. Table 7.1 shows a summary of the obtained results. In overall, the back stepping controller shows the best performance as compared to the PID and ASB controllers. The ASB controller performance is demonstrated when there are changes introduced to the system's spring constants.

Table 7.1: ASB, PID and backstepping comparison of attenuation results

	Square Hump		Round Hump	
	Front (%)	Rear (%)	Front (%)	Rear (%)
PID	48	35	60.9	37.5
Backstepping	68.3	73.2	76.8	62.5
ASB	68.3	63	68.2	71.3

7.8 Summary of adaptive sliding backstepping

On the constructed half-car test-rig, the backstepping, PID and ASB controllers are applied to isolate the driver from the uneven road disturbances. The PID is used as the most basic controller for benchmarking, further analysis is then conducted between the robust backstepping and Adaptive Sliding Backstepping. The experimental results show that the backstepping, ASB and the PID controllers reduce up to 76.8 %, 71.3 % and 60.9 % respectively when compared to the passive system. The software tools used are Matlab, Simulink and Dspace. The ASB controller demonstrates adaptive properties for varying road surfaces.

Chapter 8

Controller performance analysis and conclusion

8.1 Introduction

This section analyses and compares the results of the three main designed controllers for the half-car suspension test-rig. The main focus of the three controllers is to achieve road disturbance attenuation thereby achieving ride quality. The control techniques are applied to the half-car suspension model in order to analyse the different performances and trade-offs as the controllers are designed for different performance indicators. Therefore the three main control techniques target different challenges within the suspension system, such as non-linearities, energy optimisation and dealing with system uncertainties.

8.1.1 Analysis of the state constrained optimal control

Slack-based state constrained optimal control aims at modelling the half-car suspension system's front and rear rattle space as the system's additional states to ensure that the system operates within its physical constraints. The controller is designed so that it optimises for energy consumption and ride quality through the performance index. The optimal control signal is achieved through the computation of the Hamiltonian optimal condition bounded by the physical constraints of the half-car constructed model. The slack variable-based optimal control computation is conducted on the system states with additional states, involving the Hamiltonian, costates, boundary conditions and the optimality condition for the half-car model.

The half-car suspension model is perturbed by a road disturbance for the active and passive testing cases, so as to analyse the displacement attenuation, acceleration attenuation and the cost function. The results show that ride comfort and energy optimisation is achieved through reduction of the front and rear sprung mass displacement and accelerations for the case $mass = m$ and $mass = 2m$.

This analysis addressed the **first contribution:** *To investigate state constrained optimal control on the half-car suspension system by addressing the limitations of penalty function based methodology through the use of slack variable methodology to achieve energy efficiency.*

8.1.2 Analysis of the control of completely linearised systems

The main focus of this section was to address the complexities and limitations of input output feedback linearisation by addressing complexities associated with computation of hidden states analysis for the half-car suspension model. Achieving complete feedback linearisation would enable the application of state constrained optimal control, therefore the conditions for an ISFBL are applied to ensure that $n = r$. Complete linearisation is achieved for the case where the IOFBL output is equivalent to the first state for ISFBL solution. Negative state feedback and slack variable optimal control are applied to the linearised system and the results demonstrate improved attenuation of the displacement and smoother accelerations hence cushioning the sprung load. The main trade-off of this method is that the linearisation process might not cancel the full non-linearities of the half-car suspension system since only non-linearities associated with the spring and the damper are considered. The performance of this controller is enhanced by observer designs and tested in different road surfaces such as road humps, potholes and bumpy roads. Respectively 81.82 % and 97.5 % displacement and acceleration attenuation are achieved by the implemented linear controller.

This analysis addressed the **second contribution:** *To extend the application of slack variable state constrained optimal control to the completely feedback linearised half-car suspension system at the point of IOFBL and ISFBL equivalency, to enable state constraints transformation without hidden constraints.*

8.1.3 Analysis of the adaptive sliding backstepping

To achieve robustness in the half-car suspension system, the backstepping controller performance is compared to the adaptive sliding backstepping. Backstepping is utilised as the primary controller for robustness analysis due to its ability to handle non-linear systems. The backstepping controller analysis is based on Lyapunov control. The adaptive sliding backstepping controller is implemented to improve robustness and to deal with uncertainties related to varying input signals. The performance of the adaptive sliding backstepping shows strong adaptive properties when exposed to rough road surfaces. The experimental results showed that the back stepping, ASB and the PID controllers reduced the sprung mass displacement up to 76.8 %, 71.3 % and 60.9 % respectively when compared to the passive system. Although the ASB does not demonstrate the best attenuation results, it shows adaptive properties as its performance improves with time.

This analysis addressed the **third contribution:** *Applying an Adaptive Sliding Backstepping technique to a half-car suspension so as to test for robustness and adaptive properties on the constructed test-rig.*

8.2 Results comparison

The optimal control on the non-linear system achieved the best attenuation on the displacement attenuation when analysed for the $mass = m$ and $mass = 2m$. The control on the completely linearised system achieved ride quality of up to 81.82 %. The adaptive sliding backstepping showed robustness properties for varying road profiles. It has a displacement attenuation of up to 71.3 % which is lower than the standard backstepping but its main advantage is the improved robustness property. The developed controller results are compared below:

Table 8.1: Comparison of the attenuation performance for the applied controllers

	Displacement %	**Acceleration** %
Optimal control	97.5	80
Slack controller on linearised system	81.82	97.5
Backstepping	71.3	65
ASB	71.3	60
PID	60.9	20

As shown in Table 8.1, the optimal controller has the best displacement attenuation, however if robust control is a priority, the adaptive sliding backstepping controller is advantageous.

8.3 Summary of the research outputs

The developed controllers all achieve a level of ride comfort above 50 %, so the benefit for using each of the controllers is realised based on the performance parameters of interest such as robustness, suspension travel and road-handling capabilities. The adaptive sliding backstepping is recommended even though it does not achieve the highest attenuation but it has adaptive properties that allow it to perform on complex road surfaces. Therefore the research question posed for this work is answered since:

- A cost effective, rigid half-car suspension test-rig is constructed for passive and active vehicle performance analysis for varying road disturbances.
- The optimisation of the ride quality and energy efficiency is achieved by slack-based optimal control for the half-car suspension system considering the front and rear suspension travel constraints.
- The conditions for ensuring that the state transformation does not result in any hidden states are established for the half-car suspension system and the slack-based methodology is extended to the $n = r$ system.
- The performance analysis is conducted on a backstepping controller when compared to the adaptive sliding backstepping on a half-car suspension system for a varying input signal.

The objective of this section is to present the distribution of cost and time resources within the system tasks for the development of the high performance active suspension system research work. The main tasks of this research work involved the development of the suspension system physical model and the application of the developed controllers. The constructed test-rig is cost-effective when compared to similar test-rigs, as it cost R1200.

8.4 Resource management

The duration of tasks is distributed according to the work effort. The estimated project task durations are shown in Table 8.2.

Table 8.2: Duration analysis of research tasks

Task	**Duration (Percentage)**
Mechanical test-rig construction	15
System identification and modelling	5
Controller design and implementation	30
Software and hardware interface	10
Testing and evaluation	20
Results refinement	10
Performance analysis	10

The costs breakdown for constructing the half-car model with preview functionality is shown in Table 8.3.

Table 8.3: System components cost breakdown

System components	**R**ands
Displacement sensors	100
Rotational motors	300
Rack and pinion	50
Motion drill	200
Springs	100
Aluminium bolts and bars	150
Conveyor belts	100
Vehicle Wheels	100
Cables, wires and vero-board	100

The total cost of the prototype is R1200, which is cost-effective when compared to similar test-rigs in the field.

8.5 Conclusion

This document presented the design and implementation of a half-car active vehicle suspension system that aimed at reducing driver experienced vibrations. The proposed controller techniques address challenges on practical suspension systems having multi-varied inputs and outputs, non-linearities and uncertainties. The main contributions for this research work is conducting slack variable optimal control on non-linear and completely linearised models and the analysis of the application of adaptive sliding backstepping to a half-car suspension system. The three controllers for this research work are slack variable optimal control, control of the complete linearised system through slack-based optimal control and adaptive sliding backstepping for robustness which have been published in international recognised control conferences. The use of a half-car model instead of a quarter-car compromises simply chassis design and cost effectiveness but achieves a more accurate model of the mechanical vehicle. Rattle space usage and driver ride comfort are the major design trade-offs. The size of the developed test bed is portable for testing purposes. Cameras and sensors can be used for preview so that the controller can counteract the road unevenness at the right time.

The results from the optimal control, control of the completely linearised system and the adaptive sliding backstepping show respective displacement attenuation of 97.5 %, 81.82 % and 71.3 % and acceleration attenuation of 97.5 %, 80% and 65 %.Model and controller validation are conducted when the controllers are tested on the physical test-rig. The performance of these active systems show that the designed controllers perform well on the physical system, therefore validating the model and the controllers. Although the adaptive sliding backstepping controller does not achieve the best attenuation, it demonstrated robustness properties by adapting and improving its performance as it experiences uneven road surfaces.

Bibliography

[1] Ghazaly, N.M. and Moaaz, A.O., 2014. The future development and analysis of vehicle active suspension system. IOSR Journal of Mechanical and Civil Engineering, 11(5), pp.19-25.

[2] Karnopp, D., 1983. Active damping in road vehicle suspension systems. Vehicle System Dynamics, 12(6), pp.291-311.

[3] Sharp, R.S. and Hassan, S.A., 1986. The relative performance capabilities of passive, active and semi-active car suspension systems. Proceedings of the Institution of Mechanical Engineers, Part D: Transport Engineering, 200(3), pp.219-228.

[4] Poussot-Vassal, C., Savaresi, S.M., Spelta, C., Sename, O. and Dugard, L., 2010, December. A methodology for optimal semi-active suspension systems performance evaluation. In Decision and Control (CDC), 2010 49th IEEE Conference on (pp. 2892-2897). IEEE.

[5] Shirahatti, A., Prasad, P.S.S., Panzade, P. and Kulkarni, M.M., 2008. Optimal design of passenger car suspension for ride and road holding. Journal of the Brazilian Society of Mechanical Sciences and Engineering, 30(1), pp.66-76.

[6] Trachtler, A., 2004. Integrated vehicle dynamics control using active brake, steering and suspension systems. International Journal of Vehicle Design, 36(1), pp.1-12.

[7] Alleyne, A., 1997. Improved vehicle performance using combined suspension and braking forces. Vehicle System Dynamics, 27(4), pp.235-265.

[8] Karnopp, D., Crosby, M.J. and Harwood, R.A., 1974. Vibration control using semi-active force generators. Journal of Engineering for Industry, 96(2), pp.619-626.

[9] Liao, W.H. and Wang, D.H., 2003. Semiactive vibration control of train suspension systems via magnetorheological dampers. Journal of Intelligent Material Systems and Structures, 14(3), pp.161-172.

[10] Nakano, K., Ohori, M. and Tagaya, A., 2010, April. Feasibility study on self-powered active vibration control using a piezoelectric actuator. In Active and Passive Smart Structures and Integrated Systems 2010 (Vol. 7643, p. 76432Y). International Society for Optics and Photonics.

[11] Kawamoto, Y., Suda, Y., Inoue, H. and Kondo, T., 2007. Modeling of electromagnetic damper for automobile suspension. Journal of System Design and Dynamics, 1(3), pp.524-535..

[12] Singal, K. and Rajamani, R., 2011, June. Simulation study of a novel self-powered active suspension system for automobiles. In American Control Conference (ACC), 2011 (pp. 3332-3337). IEEE.

[13] Wang, J., Wang, W., Atallah, K. and Howe, D., 2009, May. Design of a linear permanent magnet motor for active vehicle suspension. In Electric Machines and Drives Conference, 2009. IEMDC'09. IEEE International (pp. 585-591). IEEE.

[14] Sahin, H., Fukushima, N., Mochizuki, T. and Hagiwara, I., 2010, March. HIL simulation evaluation of a novel hybrid-type self-powered active suspension system. In Industrial Technology (ICIT), 2010 IEEE International Conference on (pp. 1123-1130). IEEE.

[15] Lin, J.S. and Kanellakopoulos, I., 1997. Nonlinear design of active suspensions. IEEE Control Systems, 17(3), pp.45-59.

[16] Popovic, V., Vasic, B., Petrovic, M. and Mitic, S., 2011. System approach to vehicle suspension system control in CAE environment. Strojniški vestnik-Journal of Mechanical Engineering, 57(2), pp.100-109.

[17] Necsulescu, D., Pruner, E., Sasiadek, J. and Kim, B., 2010, August. Control of nonholonomic autonomous vehicles and their formations. In 2010 15th International Conference on Methods and Models in Automation and Robotics (pp. 37-42). IEEE.

[18] Pusadkar, U.S., Chaudhari, S.D., Shendge, P.D. and Phadke, S.B., 2019. Linear disturbance observer based sliding mode control for active suspension systems with non-ideal actuator. Journal of Sound and Vibration, 442, pp.428-444.

[19] Venkateswarulu, E., Ramesh raju N. and Seshadri G., 2014, The active suspension system with hydraulic actuator for half car model analysis and self-tuning with PID controllers. International Journal of Research in Engineering and Technology, 3, pp.415-421.

[20] Hyniova, K., Stribrsky, A., Honcu, J. and Kruczek, A., 2009, January. Active suspension system-energy control. In ICONS (pp. 146-152).

[21] Lu, J. and DePoyster, M., 2002. Multiobjective optimal suspension control to achieve integrated ride and handling performance. IEEE Transactions on Control Systems Technology, 10(6), pp.807-821

[22] Lin, J.S. and Huang, C.J., 2004. Nonlinear backstepping active suspension design applied to a half-car model. Vehicle system dynamics, 42(6), pp.373-393.

[23] Pedro, J.O., Dahunsi, O.A. and Nyandoro, O.T., 2012. Direct adaptive neural control of antilock braking systems incorporated with passive suspension dynamics. Journal of Mechanical Science and Technology, 26(12), p.4115.

[24] Velenis, E., Frazzoli, E. and Tsiotras, P., 2009, December. On steady-state cornering equilibria for wheeled vehicles with drift. In Decision and Control, 2009 held jointly with the 2009 28th Chinese Control Conference. CDC/CCC 2009. Proceedings of the 48th IEEE Conference on (pp. 3545-3550). IEEE.

[25] Qing-Nian, W., Huan-Huan, Z. and Li-qing, J., 2007. Torque co-ordinated control of four-wheel independent drive electric vehicles in cornering. Journal of Jilin University (Engineering and Technology Edition), 5, p.003.

[26] Huang, C.J., Li, T.H.S. and Chen, C.C., 2009. Fuzzy feedback linearization control for MIMO nonlinear system and its application to full-vehicle suspension system. Circuits, Systems and Signal Processing, 28(6), p.959.

[27] Gobbi, M., Levi, F. and Mastinu, G., 2006. Multi-objective stochastic optimisation of the suspension system of road vehicles. Journal of Sound and Vibration, 298(4-5), pp.1055-1072.

[28] Pop, C.I. and Dulf, E.H., 2011. Robust feedback linearization control for reference tracking and disturbance rejection in nonlinear systems. In Recent Advances in Robust Control-Novel Approaches and Design Methods. InTech.

[29] Zhen, C., Jiffri, S., Li, D., Xiang, J. and Mottershead, J.E., 2018. Feedback linearisation of nonlinear vibration problems: A new formulation by the method of receptances. Mechanical Systems and Signal Processing, 98, pp.1056-1068.

[30] Chingozha, T., Nyandoro, O.T., van Wyk, A. and Ekoru, J.E., 2016. The zero dynamics of feedback linearisation and Ehresmann connections. arXiv preprint arXiv:1606.03327.

[31] Guemghar, K., Srinivasan, B., Mullhaupt, P., and Bonvin, D., 2005. Analysis of cascade structure with predictive control and feedback linearisation. IEE Proceedings-Control Theory and Applications, 152(3), pp.317-324.

[32] Nyandoro, O.T., Pedro, J.O., Dwolatzky, B. and Dahunsi, O.A., 2011. State feedback based linear slip control formulation for vehicular antilock braking system. In Proceedings of the World Congress on Engineering (Vol. 1).

[33] Burns, R., 2001. Advanced control engineering. Elsevier.

[34] Hippe, P. and Deutscher, J., 2009. Design of observer-based compensators: From the time to the frequency domain. Springer Science and Business Media.

[35] Lewis, F.L., Vrabie, D. and Syrmos, V.L., 2012. Optimal control. John Wiley and Sons.

[36] Krtolica, R. and Hrovat, D., 1990, December. Optimal active suspension control based on a half-car model. In 29th IEEE Conference on Decision and Control (pp. 2238-2243). IEEE.

[37] Nekoui, M.A. and Hadavi, P., 2010, September. Optimal control of an active suspension system. In Power Electronics and Motion Control Conference (EPE/PEMC), 2010 14th International (pp. T5-60). IEEE.

[38] Meng, J., Chen, Q. and He, R., 2014. Research on optimal control for the vehicle suspension based on the simulated annealing algorithm. Journal of Applied Mathematics, 2014.

[39] Ismail, M.F., Peng, K., Hamzah, N., Sam, Y.M., Aripin, M.K. and Hasan, M.H.C., 2012, December. A linear model of quarter car active suspension system using composite nonlinear feedback control. In Research and Development (SCOReD), 2012 IEEE Student Conference on (pp. 98-103). IEEE.

[40] Kumar, M.S. and Vijayarangan, S., 2006, June. Design of LQR controller for active suspension system. Indian Journal of Engineering and Material Sciences Vol 13.

[41] Kruezek, A. and Stribrsky, A., 2005. H-infinity control of automotive active suspension with linear motor. In Mechatronic Systems 2004: A Proceedings Volume from the 3rd IFAC Symposiun, Sydney, Australia, 6-8 September 2004 (Vol. 1). Elsevier.

[42] Vocking, H. and Trachtler, A., 2008, October. Self-optimization of an active suspension system regarding energy requirements. In Control, Automation and Systems, 2008. ICCAS 2008. International Conference on (pp. 569-574). IEEE.

[43] Snyman, J.A., Frangos, C. and Yavin, Y., 1992. Penalty function solutions to optimal control problems with general constraints via a dynamic optimisation method. Computers Mathematics with Applications, 23(11), pp.47-55.

[44] Wu, X., Zhang, K. and Cheng, M., 2019. Sensitivity analysis for an optimal control problem of chemical processes based on a smoothing cost penalty function approach. Chemical Engineering Research and Design, 146, pp.221-238.

[45] Basari, A.A., Sam, Y.M. and Hamzah, N., 2007, May. Nonlinear active suspension system with backstepping control strategy. In Industrial Electronics and Applications, 2007. ICIEA 2007. 2nd IEEE Conference on (pp. 554-558). IEEE.

[46] Chingozha, T. and Nyandoro, O., 2014. Adaptive sliding backstepping control of quadrotor UAV attitude. IFAC Proceedings Volumes, 47(3), pp.11043-11048.

[47] Slotine, J.J. and Coetsee, J.A., 1986. Adaptive sliding controller synthesis for non-linear systems. International Journal of Control, 43(6), pp.1631-1651.

[48] Deshpande, V.S., Bhaskara, M. and Phadke, S.B., 2012, January. Sliding mode control of active suspension systems using a disturbance observer. In Variable Structure Systems (VSS), 2012 12th International Workshop on (pp. 70-75). IEEE.

[49] Patil, K.S., Jagtap, V., Jadhav, S., Bhosale, A. and Kedar, B., 2013. Performance evaluation of active suspension for passenger cars using Matlab. In Second National Conference on Recent Developments in Mechanical Engineering, IOSR Journal of Mechanical and Civil Engineering (pp. 06-14).

[50] Ekoru, J.E., Dahunsi, O.A. and Pedro, J.O., 2011, September. PID control of a nonlinear half-car active suspension system via force feedback. In AFRICON, 2011 (pp. 1-6). IEEE.

[51] Hedrick, M.D.J., 2001. Implementation of an active suspension, preview controller for improved ride comfort. The University of California at Berkeley.

[52] Yan, L. and Shaojun, L., 2009, October. Preview control of an active vehicle suspension system based on a four-degree-of-freedom half-car model. In 2009 Second International conference on Intelligent Computation Technology and Automation (Vol. 1, pp. 826-830). IEEE.

[53] Ahmed, F. and Purdy, D., 2012. Controller design of active suspension system with terrain preview using evolutionary multi-objective algorithms. In Proceedings of the International Conference on Soft Computing for Problem Solving (SocProS 2011) December 20-22, 2011 (pp. 865-876). Springer, India.

[54] HAĆ, A., 1992. Optimal linear preview control of active vehicle suspension. Vehicle system dynamics, 21(1), pp.167-195.

[55] Ismail, M.F., Peng, K., Hamzah, N., Sam, Y.M., Aripin, M.K. and Hasan, M.H.C., 2012, December. A linear model of quarter car active suspension system using composite nonlinear feedback control. In 2012 IEEE Student Conference on Research and Development (SCOReD) (pp. 98-103). IEEE.

[56] Mohite, A.G. and Mitra, A.C., 2018. Development of linear and non-linear vehicle suspension model. Materials Today: Proceedings, 5(2), pp.4317-4326.

[57] Shelke, G.D., Mitra, A.C. and Varude, V.R., 2018. Validation of simulation and analytical model of nonlinear passive vehicle suspension system for quarter car. Materials Today: Proceedings, 5(9), pp.19294-19302.

[58] Yu, M., Evangelou, S.A. and Dini, D., 2017. Model identification and control for a quarter car test rig of series active variable geometry suspension. IFAC-PapersOnLine, 50(1), pp.3376-3381.

[59] Nkomo, L.I., Dove, A., Ngwako, M.T. and Nyandoro, O.T., 2017. Heaviside based optimal control for ride comfort and actuation energy optimisation in half-car suspension systems. IFAC-PapersOnLine, 50(2), pp.259-264.

[60] Nkomo, L.I. and Nyandoro, O.T., 2019. Conditions for complete feedback linearisation on active suspension systems for mining trucks. IFAC-PapersOnLine, 52(14), pp.189-194.

[61] Nkomo, L.I., Nyandoro, O.T. and Dove, A., 2017. Comparison of backstepping and sliding mode control techiniques for a high performance active vehicle suspension System. IFAC-PapersOnLine, 50(1), pp.12604-12610.

[62] Eret, P. and Meskell, C., 2008. A practical approach to parameter identification for a lightly damped, weakly nonlinear system. Journal of Sound and Vibration, 310(4-5), pp.829-844.

[63] Li, S., Yang, J., Chen, W.H. and Chen, X., 2016. Disturbance observer-based control: Methods and applications. CRC Press.

[64] Malisani, P., Chaplais, F. and Petit, N., 2011, December. Design of penalty functions for optimal control of linear dynamical systems under state and input constraints. In 2011 50th IEEE Conference on Decision and Control and European Control Conference (pp. 6697-6704). IEEE.

[65] Kirk, D.E., 2004. Optimal control theory: An introduction. Courier Corporation.

[66] Naidu, D.S., 2002. Optimal control systems. CRC Press.

[67] Feehery, W.F. and Barton, P.I., 1998. Dynamic optimization with state variable path constraints. Computers and Chemical Engineering, 22(9), pp.1241-1256.

[68] Clarke, F.H. and Loewen, P.D., 1987. State constraints in optimal control: A case study in proximal normal analysis. SIAM Journal on Control and Optimization, 25(6), pp.1440-1456.

[69] Redfern, D.A. and Goh, C.J., 1996. Feedback control of state constrained optimal control problems. In System Modelling and Optimization (pp. 442-449). Springer, Boston, MA.

[70] Jacobson, D. and Lele, M., 1969. A transformation technique for optimal control problems with a state variable inequality constraint. IEEE Transactions on Automatic Control, 14(5), pp.457-464.

[71] Fikar, M., 2001. On inequality path constraints in dynamic optimisation. Technical Report mf0102, Laboratoire des Sciences du Génie Chimique, CNRS, Nancy, France, 2001. 46.

[72] Slotine, J.J.E. and Li, W., 1991. Applied nonlinear control (Vol. 199, No. 1). Englewood Cliffs, NJ: Prentice Hall.

[73] Garcia, P., Albertos, P. and Hagglund, T., 2006. Control of unstable non-minimum-phase delayed systems. Journal of Process Control, 16(10), pp.1099-1111.

[74] Matousek, R., Svarc, I., Pivoňka, P., Osmera, P. and Seda, M., 2009. Simple methods for stability analysis of nonlinear control systems. In 13th WSEAS International Conference on Systems.

[75] Isidori, A. ed., 2014. Nonlinear control systems design 1989: Selected papers from the IFAC Symposium, Capri, Italy, 14-16 June 1989. Elsevier.

[76] Talpaert, Y., 2000. Differential geometry with applications to mechanics and physics. CRC Press.

[77] Levine, J., 2009. Analysis and control of nonlinear systems: A flatness-based approach. Springer Science and Business Media.

[78] Coogan, S., 2019. A contractive approach to separable Lyapunov functions for monotone systems. Automatica, 106, pp349-357.

[79] Isidori, A., 2013. The zero dynamics of a nonlinear system: From the origin to the latest progresses of a long successful story. European Journal of Control, 19(5), pp.369-378.

[80] Sarma, P. and Bandyopadhyay, B., 2009. Nonlinear zero dynamics in control systems. CONTROL SYSTEMS, ROBOTICS AND AUTOMATION- Volume XIII: Nonlinear, Distributed, and Time Delay Systems-II, p.24.

[81] Zietkiewicz, J., 2015. Linear quadratic control with feedback linearized models. Studies in Automation and Information Technology, 40, pp.37-49.

[82] Chen, C.C. and Lin, Y.F., 2006. Application of feedback linearisation to the tracking and almost disturbance decoupling control of multi-input multi-output nonlinear system. IEE Proceedings-Control Theory and Applications, 153(3), pp.331-341.

[83] Shin, H.S., Choi, H.L. and Lim, J.T., 2006. Feedback linearisation of uncertain nonlinear systems with time delay. IEE Proceedings-Control Theory and Applications, 153(6), pp.732-736.

[84] Baibeche, K. and Moog, C.H., 2014, June. Input-state feedback linearization of single-input nonlinear time-delay systems. In 2014 European Control Conference (ECC), (pp. 460-465). IEEE.

[85] Hauser, J., Sastry, S. and Meyer, G., 1992. Nonlinear control design for slightly non-minimum phase systems: Application to V/STOL aircraft. Automatica, 28(4), pp.665-679.